REPORT DOCUMENTATION PAGE

Form Approved
OMB No. 0704-0188

PLEASE DO NOT RETURN YOUR FORM TO THE ABOVE ORGANIZATION.

1. REPORT DATE *(DD-MM-YYYY)*	2. REPORT TYPE	3. DATES COVERED *(From - To)*
08/17/2017	Dissertation	

4. TITLE AND SUBTITLE
Efficacy of Real-Time Functional Magnetic Resonance Imaging Neurofeedback Training (fMRI-NFT) in the Treatment of Tinnitus

5a. CONTRACT NUMBER

5b. GRANT NUMBER

5c. PROGRAM ELEMENT NUMBER

6. AUTHOR(S)
Matthew S. Sherwood

5d. PROJECT NUMBER

5e. TASK NUMBER

5f. WORK UNIT NUMBER

7. PERFORMING ORGANIZATION NAME(S) AND ADDRESS(ES)
59th Clinical Research Division
1100 Willford Hall Loop, Bldg 4430
JBSA-Lackland, TX 78236-9908
210-292-7141

8. PERFORMING ORGANIZATION REPORT NUMBER
17308

9. SPONSORING/MONITORING AGENCY NAME(S) AND ADDRESS(ES)
59th Clinical Research Division
1100 Willford Hall Loop, Bldg 4430
JBSA-Lackland, TX 78236-9908
210-292-7141

10. SPONSOR/MONITOR'S ACRONYM(S)

11. SPONSOR/MONITOR'S REPORT NUMBER(S)

12. DISTRIBUTION/AVAILABILITY STATEMENT
Approved for public release. Distribution is unlimited.

13. SUPPLEMENTARY NOTES

14. ABSTRACT

15. SUBJECT TERMS

16. SECURITY CLASSIFICATION OF:			17. LIMITATION OF ABSTRACT	18. NUMBER OF PAGES	19a. NAME OF RESPONSIBLE PERSON
a. REPORT	b. ABSTRACT	c. THIS PAGE			Clarice Longoria
					19b. TELEPHONE NUMBER *(Include area code)* 210-292-7141

A Dissertation

Efficacy of Real-Time Functional Magnetic Resonance Imaging Neurofeedback Training (fMRI-NFT) in the Treatment of Tinnitus

By: Matthew S. Sherwood
Ph.D. Candidate

Department of Biomedical, Industrial and Human Factors Engineering
Wright State University, Dayton, OH 45435

Submitted to:

Subhashini Ganapathy
Frank Ciarallo
Jaime Ramirez-Vick
Curtis Tatsuoka
Jason Parker

Submitted on:

Submitted in Partial Fulfillment for the Degree of Doctor of Philosophy

Table of Contents

List of Figures

List of Tables

List of Abbreviations

^{1}H	Hydrogen
A1	Primary Auditory Cortex
A2	Secondary Auditory Cortex
ACC	Anterior Cingulate Cortex
ACS	Attentional Control Scale
ADP	Adenosine Diphosphate
AE	Attention to Emotion Task
ASL	Arterial Spin Labeling
ATP	Adenosine Triphosphate
BA	Brodmann Area
BOLD	Blood Oxygen Level-Dependent
BRAVO	Brain Volume Imaging
CBF	Cerebral Blood Flow
cm	Centimeters
CON	Control Group
CPT	Continuous Performance Task
CPT-X	Continuous Performance Task Vigilance Variant
dB	Decibels
DMN	Default Mode Network
EEG	Electroencephalography
EPI	Echo Planar Imaging
EV	Explanatory Variable
EXP	Experimental Group
FDG	^{18}F-Deoxyglucose

fMRI	Functional Magnetic Resonance Imaging
fMRI-NFT	Real-Time fMRI Neurofeedback Training
fNIRS	Functional Near-Infrared Spectroscopy
FSL	FMRIB Software Library
FSPGR	Fast Spoiled Gradient-Echo
FWHM	Full-Width Half-Maximum
GLM	General Linear Model
GRE	Gradient Recalled Echo
HRF	Hemodynamic Response Function
Hz	Hertz
IC	Inferior Colliculus
ICA	Independent Component Analysis
IRB	Institutional Review Board
ITI	Inter-Trial Interval
LTP	Long Term Potentiation
MeFG	Medial Frontal Gyrus
MEG	Magnetoencephalography
min	Minute
mm	Millimeters
MRI	Magnetic Resonance Imaging
ms	Milliseconds
NADH	Nicotinamide Adenine Dinucleotide
NFT	Neurofeedback Training
NMR	Nuclear Magnetic Resonance
PET	Positron Emission Tomography
ppm	Parts Per Million

RF	Radio Frequency
ROI	Region of Interest
rTMS	repetitive Transcranial Magnetic Stimulation
s	Seconds
SDT	Signal Detection Theory
SLF	Spontaneous Low-Frequency Signal Fluctuations
SLT	Sound Level Tolerance
STG	Superior Temporal Gyrus
T	Tesla
TE	Echo Time
TFCE	Threshold-Free Cluster Enhancement
TI	Inversion Time
vmPFC	ventro-medial Prefrontal Cortex

I. Executive Summary

There is a growing interest in the application of real-time (fMRI) with neurofeedback training (NFT) to the treatment of disorders associated with abnormal brain function. Chronic tinnitus is one such disorder that is often characterized by hyperactivity of the primary auditory cortex (A1) and decreased activity of the ventromedial prefrontal cortex (vmPFC). The overall objective of the proposed study is to determine the efficacy of fMRI-NFT for the treatment of tinnitus with the following hypotheses:

> *Hypothesis 1:* The experimental group will achieve significantly greater control over the region targeted for neurofeedback training, measured as deactivation magnitude during neurofeedback, than the control group.
>
> *Hypothesis 2:* Behavioral measures of attentional control, measured from self-report questionnaires and simple laboratory tasks, will show significantly greater improvement in the experimental group.
>
> *Hypothesis 3:* A1 activity, measured as the activation in response to auditory stimulation, will show a significantly greater reduction following fMRI-NFT for the experimental group compared to the control group.
>
> *Hypothesis 4:* Functional connectivity between the auditory and limbic regions, measured as resting-state connectivity, will be reduced significantly more in the experimental group than the control group.
>
> *Hypothesis 5:* Steady-state perfusion, measured as interhemispheric asymmetry in cerebral blood flow (CBF; mL/100 mg/min), will decrease significantly more in the experimental group when compared with the control group.

Healthy participants were separated into two groups: the experimental group received real feedback regarding activity in the A1 while control group was supplied sham feedback yoked from a random participant in the experimental group and matched for fMRI-NFT experience. Twenty-seven healthy volunteers with normal hearing (defined as no more than 1 frequency < -40 dB on a standard audiogram) underwent five fMRI-NFT sessions, each consisting of 1 auditory fMRI to functionally localize the A1, and 2 closed-loop neuromodulation runs using feedback from A1. FMRI data were acquired at 3T using 2D, single-shot echo planar imaging (EPI) during all three runs. The auditory fMRI was comprised of alternating blocks without and with auditory stimulation (continuous white noise delivered at 90 dB via in-ear headphones). During each closed-loop neuromodulation run, subjects completed alternating blocks identified as a "relax" period (*i.e.*, watch the bar) or a "lower" period (*i.e.*, lower the bar). Auditory stimulation (same as for the auditory fMRI) was supplied during both sets of blocks. A1 activity was continuously presented using a simple bar plot during the closed-loop neuromodulation runs and updated with each EPI volume. A set of 4 simple directed attention strategies were suggested before each scan session to provide examples of brain control techniques to lower the bar, but the subjects were explicitly instructed to use any mental strategy they preferred. Average A1 deactivation was extracted from each closed-loop neuromodulation run and used to quantify the control over A1 (A1 control). Additionally, behavioral testing was completed outside of the MRI on sessions 1 and 5, and at a 2-week follow-up. This consisted of a subjective questionnaire to assess

attentional control (attentional control scale; ACS) and two quantitative tests: the attention to emotion task (AE) and a vigilance variant of the continuous performance task (CPT-X). The ACS total was computed according to the associated literature. The AE task was assessed for the impact of emotion on attention by computing the percentage change between the average latency for emotional and neutral trials. A sensitivity index (d') was computed from the CPT-X using signal detection theory. In this work, we investigated the use of fMRI-NFT to teach self-regulation of A1 using directed attention strategies. A 2x5x2 (group by session and run) mixed-model ANOVA was performed on A1 control followed by *post hoc,* Bonferroni-corrected pairwise comparisons the evaluate the session by group interaction. It was determined that A1 control improved with training (p =), and that sessions 5 and 2 were significantly increased compared to session 1 only for the experimental group (p = , p = , respectively). Behavior was assessed by 2x2 and 2x3 (group by session) mixed-model ANOVAs were conducted on each test score to assess the effects. Separate ANOVAs were conducted due to three participants that did not complete the follow-up behavioral assessment. The control group showed a markedly reduced impact of emotion on attention on average (p =). However, no other effects were observed. Additionally, the change in A1 deactivation and the impact of emotion on attention were negatively correlated (r = , p =). A neural assessment consisting of measures of brain activity in response to auditory stimulation, resting-state networks, and steady-state perfusion was also conducted on sessions 1 and 5 inside the MRI. Average activation was extracted from the A1 during the auditory fMRI. Auditory, default mode, and executive control networks were assessed from resting-state fMRI. Average CBF was extracted from the auditory cortex (A1 and superior temporal gyrus) and attentional regions (anterior cingulate cortex and medial frontal gyrus). Averaging across groups, A1 activity in response to continuous noise stimulation across training (p =) and functional reorganization in the auditory and default mode networks were observed in brain regions implicated in auditory processing, sustained attention, and executive functions. This work suggests that fMRI-NFT can be used to teach control over A1 and that this enhanced control can reduce the impact of emotion on attention. However, there were improvements observed across training when averaging across groups which implies attempted A1 control may be effective at producing behavioral and neural effects. This may be useful in translating a therapy outside of the MRI and to home-based solutions. Furthermore, the effects of emotion and attention may be useful in developing therapies for other neurologic disorders with abnormal attentional and emotional states such as chronic pain.

II. Background

Humans have five traditional senses: sight, sound, smell, taste and touch. Each of these senses begin with receptor cells sensitive to particular stimuli. These receptor cells send signals to the brain which translates and interprets the signals, resulting in perceptions of the world. The sensory pathway from these receptor cells to the cerebral cortex is unique to each sense and fundamental in the study of perception.

Psychophysical analysis, the correlation of aspects of physical stimuli with the evoked sensation, has led to the basic understanding of the alteration of brain activity from various stimuli. Specific neurons within the sensory system encode the critical attributes of stimuli. Populations of sensory neurons encode other attributes through patterns of activity. Aspects of perception may be carried and processed in parallel by different components of the particular sensory system. Abstracts of perception are represented in pathways and central regions through feature detection and pattern of firing. These central regions then interact to reconstruct the components into a perception (Kandel, Schwartz, & Jessell, 1991).

A. Auditory System

The auditory system is responsible for the sense of sound. In short, sounds are produced by vibrations. Vibrations produce alternating compression and rarefaction of the surrounding air radiating outward from the source. The frequency of these pressure waves determines the pitch of the sound produced. The human ear can sense a range of frequencies from 20 to 20,000 Hz. The amplitude of the wave, measured in decibels (dB), determines the loudness of the sound:

$$\mathrm{d}B = 20 \cdot log_{10} \frac{P_t}{P_T} \qquad (1)$$

where P_t is the test pressure and P_T is a reference pressure (20 $\mu N/m^2$). Alexander Graham Bell devised this scale as he found that the Weber-Fechner law, which describes the sensation intensity as proportional to the logarithm of the ration of the stimulus to a threshold (Kelly, 1991), applies to hearing. Sound pressures greater than 100 dB can result in damage to the human auditory system, depending upon the intensity, frequency and duration of the sound (Kelly, 1991).

Sound pressure waves reaching the ear may be perceived. The ear consists of three parts: outer, middle, and inner ear (Figure 1). The inner ear contains the cochlea, a spiral bony canal that is filled with fluid. The cochlea also contains the organ of Corti, the sensory transduction apparatus.

Sound travels through the external ear canal, or external auditory meatus, continuing to the middle ear (Figure 1). The pressure waves reaching the middle ear cause the tympanic membrane to vibrate. This vibration is transferred through the middle ear to the inner ear by three small bones (ossicles; Figure 2). A single ossicle, the malleus, is physically attached to the tympanic membrane. The vibration is then transmitted to an opening in the cochlea, the oval window, by the other two ossicles (the incus and stapes). This process is required to ensure efficient transmission to the cochlea. Without this process, the sound would be reflected and not sensed due to the higher acoustic impedance

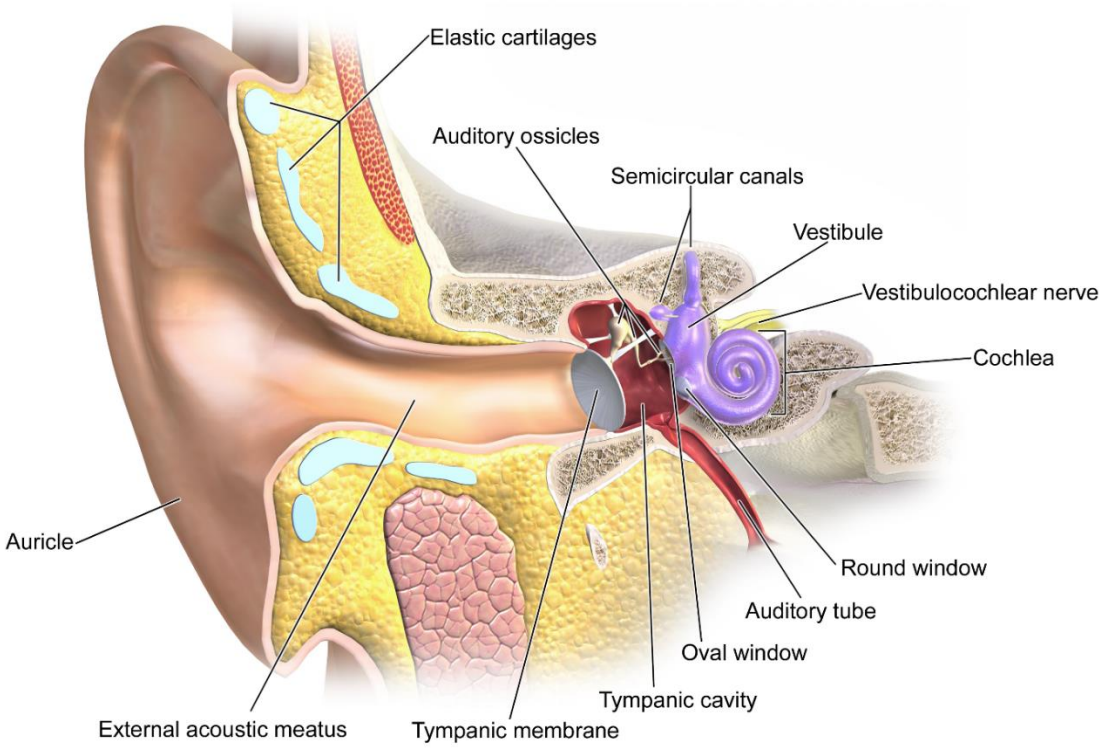

Figure 1. The ear consists of the outer, middle, and inner ear. This figure was taken from https://upload.wikimedia.org/wikipedia/commons/c/c8/Outer%2C_middle_and_inner_ear.jpg with permission.

of the cochlear fluid than air. Further, the arrangement of these components are such to reduce inertial motion resulting from body or head movements.

The cochlea (Figure 3) spirals around a central pillar, the modiolus. Three fluid-filled chambers, or scalae, are contained within the cochlea. One, the scala tympani, follows the outer contours of the cochlea. Another, the scala vestibuli, follows the inner contours and is continuous with the scale tympani at the apex of the cochlea, referred to as the helicotrema. The third, the scala media, lies between the others extending like a finger into the cochlea channel and ends near the helicotrema.

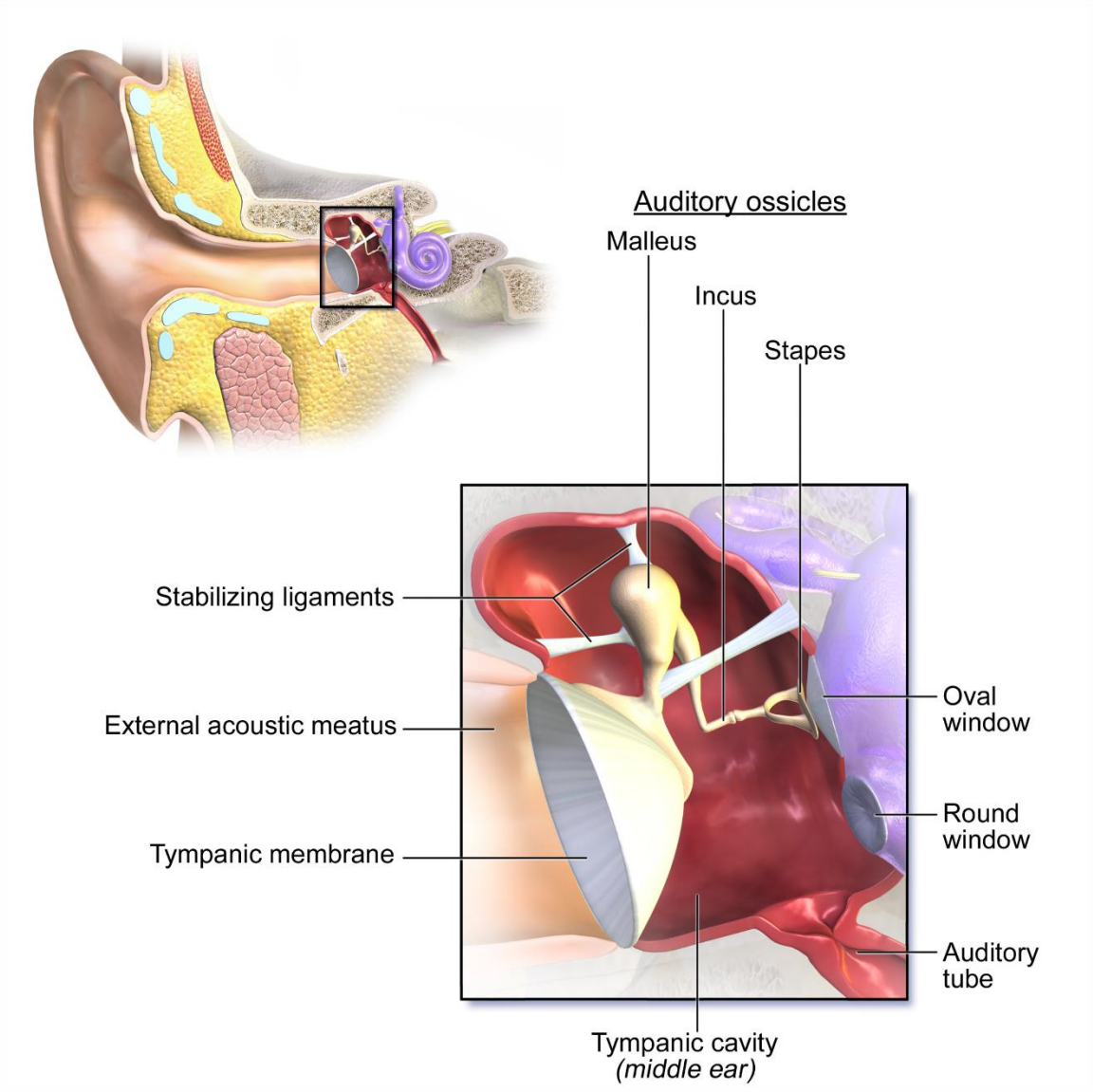

Figure 2. The middle ear contains three small bones (ossicles) which transfers sound pressure waves vibrating the tympanic membrane to an opening in the cochlea. This figure was taken with permission from https://commons.wikimedia.org/wiki/File:Blausen_0330_EarAnatomy_MiddleEar.png.

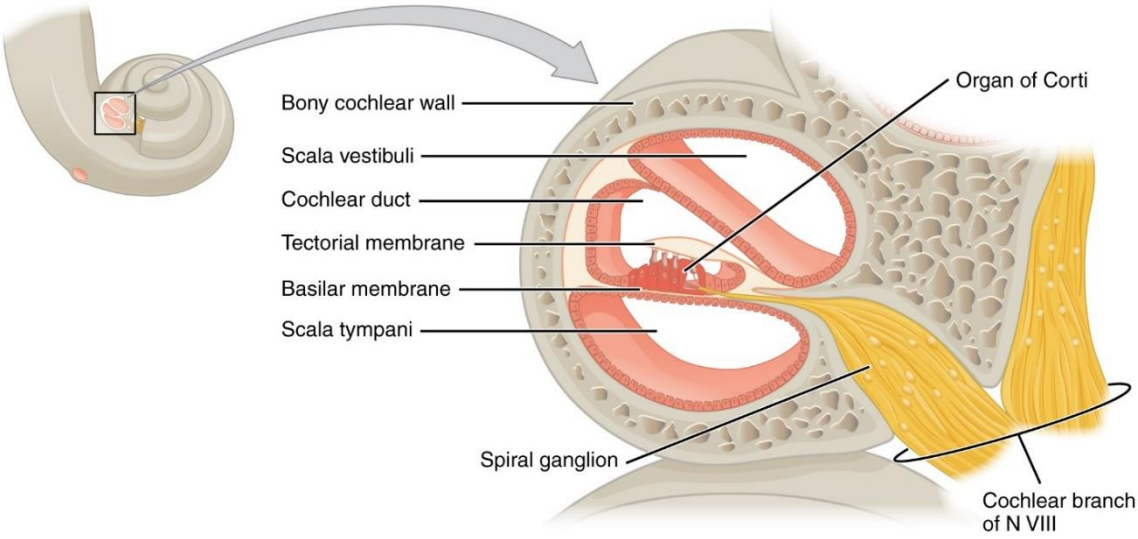

Figure 3. The cochlea contains the organ of Corti, the sensory transduction apparatus. The cochlea contains three fluid-filled chambers which are used to transmit oscillations of the stapes. This figure was taken with permission from https://commons.wikimedia.org/wiki/File:1406_Cochlea.jpg.

Energy from the vibrating stapes is transmitted to the fluid in the scala vestibuli (perilymph). The stapes pushes in and out of the cochlea as it oscillates, applying variable pressure on the perilymph. The incompressible nature of the perilymph causes an alternating outward and inward movement of the round window membrane of the scala tympani, located near the middle ear cavity. The differential pressure between the scala vestibuli and scala tympani are converted into oscillating movements of the fluid within scala media (endolymph). The movement of the endolymph will stimulate movement of the basilar membrane in which the organ of Corti, the sensory transducer in the scala media, rests. This movement results in slight vibrations in the tectorial membrane of the organ of Corti. The differential movement between the tectorial and basilar membranes excite and inhibit the sensory receptor cells in the organ of Corti.

The sensory receptor cells of the inner ear, residing in the organ of Corti, are called hair cells (Figure 4). On the apical surface of each hair cell is a bundle of stereocilia, filled with stiff parallel arrays of cross-bridged actin filaments. The stereocilia project into the overlying tectorial membrane. The stereocilia will be displaced if the tectorial membrane and the basilar membrane move with respect to one another. This occurs when the basilar membrane vibrates moving the body of the hair cell causing the stereocilia to bend in relation to the hair cell body.

The motion of the stereocilia in one direction depolarizes the cell by opening K^+ channels producing an inward current (Figure 5). This inward current activates voltage-sensitive Ca^{2+} ion channels. Motion in the opposite direction hyperpolarizes the cell by closing the K^+ channels. Thus, oscillations of the basilar membrane produce back-and-forth angular displacements of the stereocilia resulting in sinusoidal potential changes at the frequency of the sound.

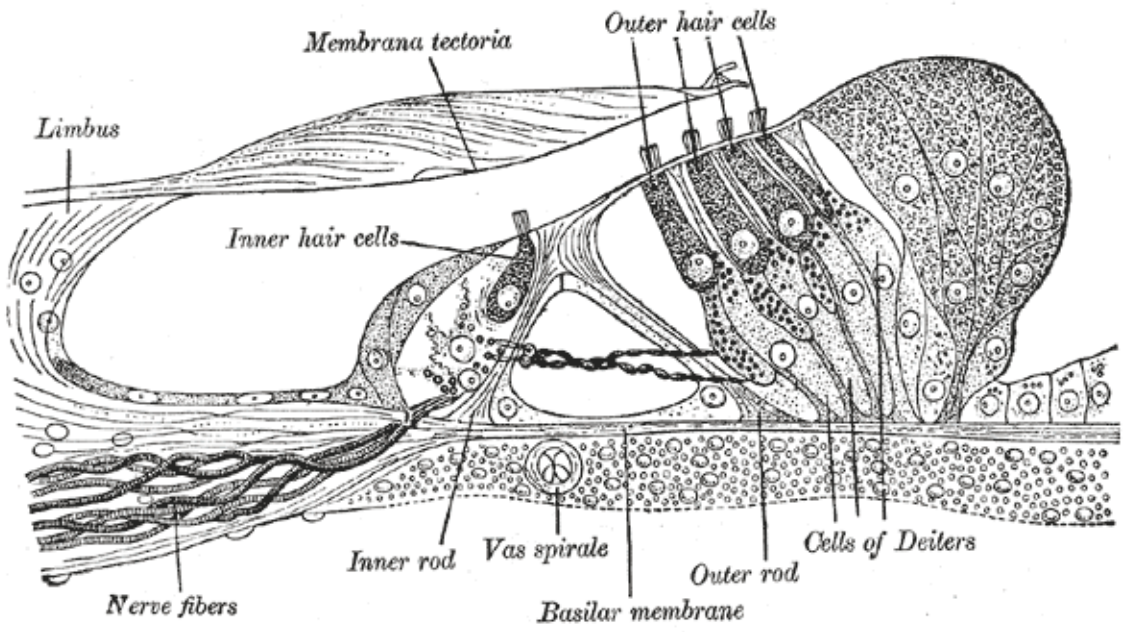

Figure 4. Hair cells reside in the organ of Corti. Hair cells are sensory receptors of the inner ear. This figure was taken with permission from https://commons.wikimedia.org/wiki/File:Gray931.png.

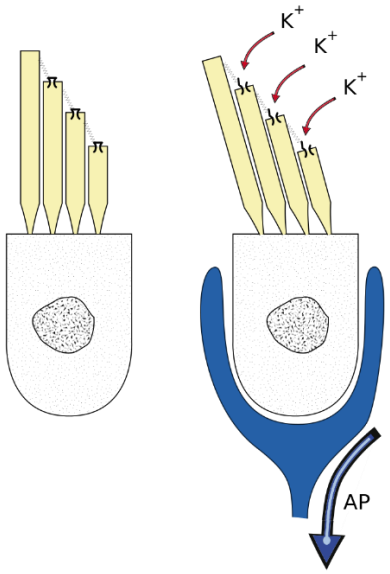

Figure 5. Motion of stereocilia can cause depolarization or hyperpolarization of hair cells by opening or closing K^+ channels. This figure was taken with permission from https://commons.wikimedia.org/wiki/File:HairCell_Transduction.svg.

Hair cells also are capable of releasing chemical transmitters at their basal end. At the basal end, hair cells are contacted by peripheral branches of bipolar neuron axons. A single auditory nerve

cell will only innervate a single inner hair cell. Each inner hair cell is innervated by approximately 10 auditory nerves. Some auditory nerve fibers innervate many outer hair cells. The cell bodies of these auditory neurons lie in the spiral ganglion and the central axons constitute the auditory nerve. A neurotransmitter (glutamate) is released at the base of hair cells when depolarized as a product of the increase in intracellular Ca^{2+}, exciting the peripheral terminal of the sensory neuron. Summation of sensory neuron excitation can result in action potentials initiated in the auditory nerve cell's central axon. The oscillation in the potential of the hair cell causes oscillatory release of neurotransmitters and alternating the firing of axons in the auditory nerve.

Auditory nerve cells enter the brain stem just under the cerebellum, and terminate in the cochlear nucleus of the brain stem (Figure 6). Most axons of cochlear nucleus cells cross to the contralateral side of the brain; the majority of auditory information processed by one half of the brain comes from the ear on the opposite side of the head. Ventral cochlear nuclei project to the superior olivary complex located in the brainstem. The superior olivary complex receives axons that both cross and do not cross the midline. It is the first location in the ascending auditory system which receives inputs from both ears (although the majority come from the contralateral ear). Fibers leaving the superior olivary complex project along two pathways. Some synapse in the nucleus of the lateral lemniscus while the majority travel to the inferior colliculus (IC) directly. The central cochlear nuclei axons projecting to the superior olivary complex is thought to play a role in localizing sound.

In contrast to the ventral pathway, dorsal cochlear nuclei project directly to the contralateral IC. Both direct ventral and dorsal pathways to the IC are important in other aspects of auditory perception. A major pathway in the IC allows information to cross the midline, enabling information from both ears to be almost equally represented in both hemispheres of the brain in further ascending pathways. Axons leaving the IC project to the medial geniculate nucleus located in the thalamus. Medial geniculate fibers project to the primary auditory cortex (A1) in the superior temporal gyrus (STG). Most cells within the auditory cortex receive input from both ears. These cells are ordered in such a way that

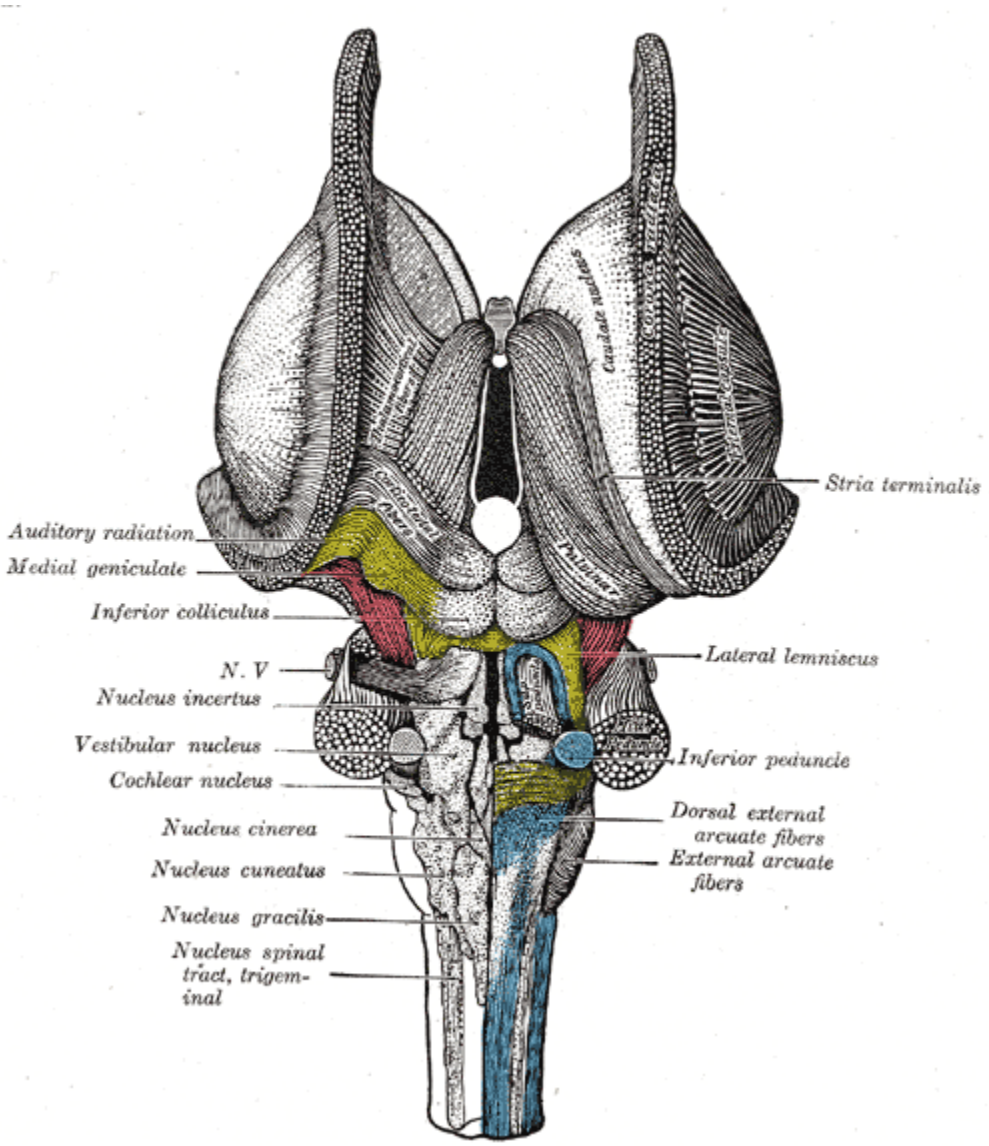

Figure 6. Auditory nerve cells terminate in a small portion of the brain stem. This figure was replicated with permission from https://commons.wikimedia.org/wiki/File:Gray691.png.

a relationship exists between the spatial position of the cells within the cortex and the frequencies of sounds which they are sensitive. A1 is surrounded by higher order cortical auditory areas located on both superior and lateral surfaces of the temporal lobe in the STG. The left cerebral hemisphere, which has a longer lateral sulcus, is specialized for linguistic function and interpretive speech mechanisms. The right hemisphere is involved in non-linguistic function such as motor speech.

A1 contains several distinct tonotopic maps of the frequency spectrum. Different layers within the auditory cortex form connections with other cortical areas and are functionally organized into columns. Binaural cells are clustered into two alternating columnar groups, summation and suppression columns, running from the pial surface to the underlying white matter. Summation

columns respond greater to binaural input than monaural while suppression columns respond the greatest to monaural input. Functional divisions (Figure 7) in the frontal and temporal lobes are utilized for the perception of speech sounds (Broca's area and Wernicke's area). Separate areas are also utilized to map the timing, intensity, and frequency of the sound to generate a perception of location, loudness, and pitch.

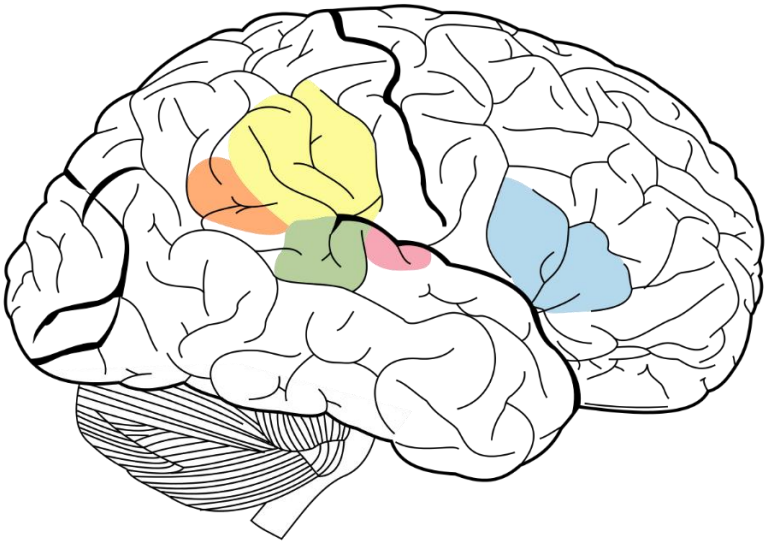

Figure 7. Different divisions of the frontal and temporal lobes are utilized in the perception of sound. Angular Gyrus, orange; Supramarginal Gyrus, yellow; Broca's area, blue; Wernicke's area, green; and A1, pink. This figure was replicated with permission from https://commons.wikimedia.org/wiki/File:Brain_Surface_Gyri.SVG.

B. Tinnitus

There are two main categories of hearing loss. The first is caused by inner ear damage, usually resulting in permanent deficits. The second results when sound waves do not traverse to the inner ear, the effects of which are most likely reversible. In 2012, the World Health Organization estimated 360 million people (5.3% of the world population) suffered from disabling hearing loss (World Health Organization, 2012). Certain conditions such as age, illness, and genetics may contribute to hearing loss, although the most common cause is repeated exposure to loud noises (Vio & Holme, 2005). Noise-induced hearing loss is thought to cost between 0.2 and 2 percent GDP (Vio & Holme, 2005).

Tinnitus, formally known as chronic subjective tinnitus, is the phantom perception of sound (*e.g.* ringing, buzzing, roaring, clicking, or hissing): individuals perceive sound in the absence of a physical sound wave. Tinnitus is not a condition itself but rather a symptom of an underlying condition such as age-related hearing loss, ear injury, or a circulatory system disorder. Tinnitus is one of the first signs of damage to the auditory system (Vio & Holme, 2005). The phantom noise is highly variable in both pitch and intensity across individuals. Further, the phantom noise can manifest itself laterally, appearing dominant in the left or right, or bilaterally, appearing as if perceived both ears.

It has been reported that tinnitus affects 5-30% of the population (Axelsson & Ringdahl, 1989; de Ridder et al., 2007; Fabijanska, Rogowski, Bartnik, & Skarzynski, 1999; Heller, 2003; Henry, Dennis, & Schechter, 2005; Mühlnickel, Lutzenberger, & Flor, 1999; Vio & Holme, 2005; Weissman & Hirsch, 2000; Wunderlich et al., 2010). In a recent study by the U.S. Centers for Disease Control, 7.3% of the 9364 people questioned reported they have been bothered by ringing, roaring, or buzzing for more than five minutes within the previous year. 41.4% of these individuals reported the ringing, roaring, or buzzing has been perceived for more than five years, and 67.3% reported more than one year (U.S. Centers for Disease Control, 2013).

It was previously reported that 6-25% report interference with their daily lives causing considerable distress (Baguley, 2002; Eggermont & Roberts, 2004; Heller, 2003; Smits et al., 2007), and that tinnitus causes severe disabilities in 0.2-1% of the population which restrict the performance of daily functions (Andersson & Kaldo, 2004; Axelsson & Ringdahl, 1989; Coles, 1984; Davis & Rafaie, 2000; de Ridder et al., 2007; Leske, 1981; Meyershoff, 1992; Mühlnickel et al., 1999; Vio & Holme, 2005). From the same U.S. Centers for Disease Control study, 16.8% of those reporting a tinnitus percept indicated that it was bothersome. Further, 3.3% classified the tinnitus percept as being a very big problem, and 30.6% indicated it was a moderate problem or worse (U.S. Centers for Disease Control, 2013). An American Tinnitus Association report suggests approximately 20 million people are dealing with burdensome tinnitus on a regular basis. More importantly, nearly 2 million people struggle with severe, potentially debilitating, tinnitus (American Tinnitus Association, 2015).

In the majority of tinnitus cases, there is no obvious source (*i.e.* blood vessel problems, an inner ear bone condition, or muscle contractions) for the phantom sound (Fowler, 1944; Penner, 1990; Sismanis & Smoker, 1994). It can interfere with everyday tasks by decreasing concentration or interfering with the perception of actual sound. Furthermore, individuals affected by tinnitus may also experience fatigue, stress, sleep problems, memory problems, depression, anxiety, and irritability (Vanneste et al., 2010). Interestingly, psychometric quantities cannot accurately predict the distress one may encounter (Golm, Schmidt-Samoa, Dechent, & Kröner-Herwig, 2013). The Neurophysiological Model (Jastreboff, Gray, & Gold, 1996) proposes distress emerges if initial perception is associated with a negative evaluation.

In the U.S. military, tinnitus is the number one service-connected disability in Gulf War Era (1990 – present) veterans. In 2014, almost half of new compensation recipients of service-connected disability payments had tinnitus, and almost 1.3 million veterans received compensation for service-connected tinnitus disability. This was the most prevalent disability among new compensation recipients and all recipients, with more than 300,000 more cases than hearing loss and more than 500,000 cases than post-traumatic stress disorder. Almost half of new and a third of total compensation recipients receive disability for tinnitus, representing 9.5% and 7.2% of total disabilities, respectively. Both proportions are higher than any other disability. With an average annual payout of $13,732, service-connected tinnitus disability payments are estimated at $3.9 billion. Although the average recipient has 4.5 disabilities (U.S. Department of Veterans Affairs, 2014), the cost due solely to tinnitus is difficult to determine. The delivery of tinnitus-related healthcare services to these individuals is estimated to be much higher (American Tinnitus Association, 2015). In summation, tinnitus has a major impact in the effectiveness of the U.S. military, from personnel issues to degraded mission success rates caused by lower situational

awareness or reduced performance (Hearing Center of Excellence, 2013), and major economic and social impacts.

C. Biomarkers of Tinnitus

The neural underpinnings of tinnitus are currently unknown. With tinnitus being a symptom of an underlying condition, it is difficult to study and isolate the causes and effects due to tinnitus. However, evidence supports a central mechanism for the tinnitus percept, as it remains following complete dissection of the auditory nerve (Folmer, Griest, & Martin, 2001). In the following sections, the current state of the art in the study of tinnitus using MR methods will be presented.

1. Brain Activity

Several imaging modalities can acquire measurements of functional brain activity including electroencephalography (EEG), functional near infrared spectroscopy (fNIRS), magnetoencephalography (MEG), positron emission tomography (PET), and functional magnetic resonance imaging (fMRI). External sensors, like those used in fNIRS, EEG, and MEG, only allow the source of the events to be estimated. FMRI and PET enable accurate localization of metabolic changes following neural activity. FMRI provides slightly higher spatial resolution than PET without any known health risks. Table 1 outlines the advantages and disadvantages of each modality. Of these imaging modalities, fMRI provides adequate temporal resolution while maintaining the spatial resolution necessary to investigate whole-brain effects of tinnitus without the use of ionizing radiation. Therefore, fMRI is optimal to study deep and cortical structures for neural correlates of tinnitus.

Table 1. Advantages and disadvantages of functional brain imaging modalities.

Technology	Advantages	Disadvantages
Magnetoencephalography	• Direct measure of neural activity • Non-invasive • No side effects	• Expensive • Low availability • Low spatial resolution • Limited to cortical activity
Positron Emission Tomography	• High spatial resolution	• Requires radioactive nuclei • Low temporal resolution • High cost • Indirect measure of neural activity
Electroencephalography	• Direct measure of neural activity • High temporal resolution • Low cost • Non-invasive • No side effects	• Small signal-to-noise ratio • Low spatial resolution • Signal can contain artifacts from muscle activity, eye movements, and blinking • Long set-up time
Functional Magnetic Resonance Imaging	• High spatial resolution • No side effects • Non-invasive	• High cost • Low temporal resolution • Indirect measure of neural activity
Functional Near-Infrared Spectroscopy	• High temporal resolution • Non-invasive • No side effects • Low cost	• Low spatial resolution • Indirect measure of neural activity

a. Background on Functional Magnetic Resonance Imaging

i. Physics

FMRI was developed from nuclear magnetic resonance (NMR). NMR exploits the magnetic properties of atomic nuclei to measure signals from protons and neutrons of atomic nuclei. Protons and neutrons possess an intrinsic angular momentum referred to as the "spin". This angular momentum cannot be changed, but the axis of spin can be manipulated. When a nucleus has an even number of protons and neutrons, the nucleus has no net spin and is not magnetic (*i.e.* cannot be detected using NMR). However, when a nucleus has an odd number, there is a net spin and NMR can be used to alter the spins.

Along with an angular momentum, each spin has a magnetic dipole moment. This allows a magnetic field to exert a torque on protons capable of rotating the dipole into alignment with the field. During this rotation, the angular moment causes the spins to precess around the field axis. The frequency of precession, referred to as the Larmor frequency, is unique to every atom. This frequency is directly proportional to the strength of the magnetic field:

$$\omega = -\gamma\beta_0 \quad (2)$$

where β_0 is the strength of the magnetic field and γ is the magnetogyro ratio represented as a function of the magnetic moment μ and spin angular momentum J:

$$\gamma = \mu/J. \qquad (3)$$

Once placed in a large magnetic field, created by a superconducting magnet, dipoles gradually tend to align with the magnetic field. This alignment occurs exponentially with a time constant T1 (Figure 8; longitudinal relaxation). Exchanges of energy between the orientation of the dipole and thermal motions prevent dipoles from settling in their lowest energy state – parallel to the magnetic field B_0. Therefore, at equilibrium there is an approximate difference of 10 ppm between spins which align parallel and antiparallel to the magnetic field. The total magnetic moment, net magnetization M_0, represents the sum of the magnetization of all spins, which always is parallel to the magnetic field (Figure 9). This magnitude is directly proportional to the local spin density.

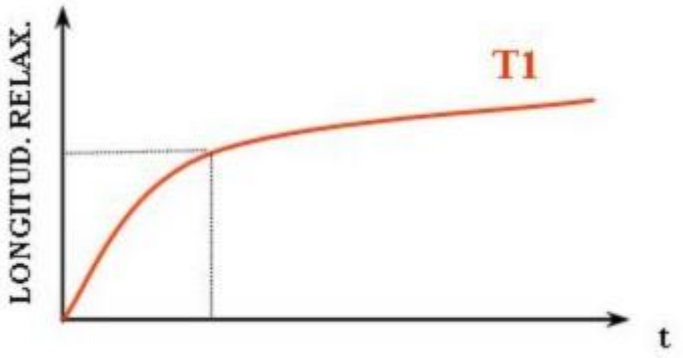

Figure 8. T1 characterizes the exponential recovery of the z-component (longitudinal) toward thermodynamic equilibrium. T1 is measured at 67% recovery. Figure taken with permission from https://commons.wikimedia.org/wiki/File:T1_relaxation.jpg.

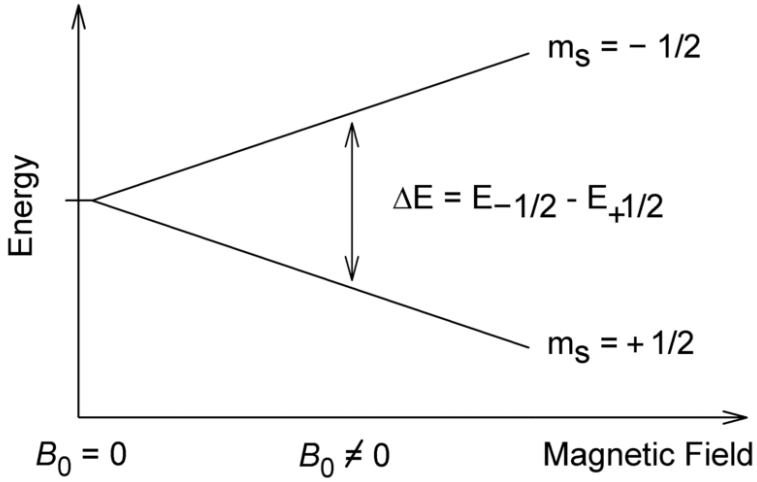

Figure 9. Spins inside of a magnetic field can align parallel (lower energy state) or anti-parallel (higher energy state) to the direction of the magnetic field. The resultant net magnetization is

aligned with the magnetic field. This figure was replication with permission from https://commons.wikimedia.org/wiki/File:NMR_splitting.gif.

A measurable, transient signal can be produced by using a radiofrequency (RF) pulse to tip the dipoles which contribute to M_0. The RF pulse is delivered by passing a current through a coil perpendicular to the magnetic field. The RF pulse sends electromagnetic waves which resonate at particular frequencies. These pulses perturb the equilibrium state which exists inside the magnetic field. A specific RF can be selected to match a Larmor frequency to excite specific spins. The target spins absorb the energy in the electromagnetic wave, energy that is released when the RF pulse is turned off. Current is induced from the energy released from the excited spins in the coils which produce the RF pulse. The measured current is proportional to the magnitude of the precessing magnetization. Once the RF pulse ends, the net precession magnetization decays exponentially with a time constant T2 (Figure 10; transverse relaxation). This delay occurs as the phase between precessions across spins increases and no longer add coherently. Both T1 and T2 vary between tissue types, developing contrast between various tissues in the constructed images.

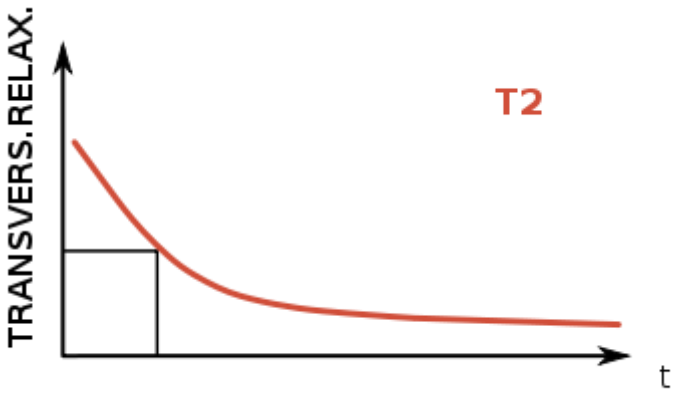

Figure 10. T2 characterizes the exponential decay of the transverse component of the magnetization vector, measured at 37%. Figure taken with permission from https://commons.wikimedia.org/wiki/File:T2_relaxation.svg.

Images can be created by applying gradients to the magnetic field. Three orthogonal coils are used to create linear gradients in each dimension. Equation 2 specifies the resonant frequency of protons is directly proportional to the magnetic field. Therefore, once a gradient is created, protons in different spatial locations will resonate at different frequencies. The strength of these gradients are small compared to B_0, and are usually expressed in units of the resonant frequency change they produce per unit length (cm). RF pulses are shaped to produce only a narrow band of frequencies centered on a particular frequency. Only the protons resonating within this band will be excited by the RF pulse, and these protons should reside in a specific, known slice relative to the magnetic field gradient (Figure 11). Information can be encoded about the remaining two dimensions of each signal allowing the image of the distribution in this plane to be reconstructed (Buxton, 2009; Hendee & Ritenour, 2002; Huettel, Song, & McCarthy, 2004).

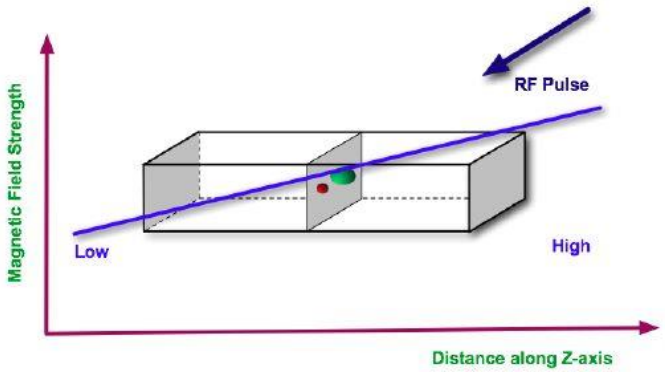

Figure 11. Gradients in the magnetic field cause the frequency of precession to vary throughout the field. The input RF frequency can be tuned to target spins from a specific location in the gradient field and, therefore, specific spatial locations. This figure was taken from with permission from https://commons.wikimedia.org/wiki/File:Tomographic_imaging_slice_selection.jpg.

ii. Neurophysiology

The physical laws of thermodynamics state any chemical system that is not at equilibrium has the capacity to do "work". The capacity is called the free energy of the system. Neurons at steady-state are not in equilibrium due to an imbalance between intra- and extra-cellular ionic concentrations and, therefore, have the ability to do work. This work is referred to as an action potential: the opening and closing of ion channels along the axon which produces a current along the cell membrane and the release of neurotransmitters at the synapse. The available free energy of neurons is reduced with each action potential and neurotransmitter release. Energy metabolism is required to restore the free energy and return the neuron to its state prior to the action potential. This process involves the conversion of adenosine triphosphate (ATP) to adenosine diphosphate (ADP) coupled to other reactions referred to as ATPase (Buxton, 2009). Glucose and oxygen are used to restore the ATP/ADP ratio following the free energy recovery.

The mechanism for free energy recovery from glucose and oxygen is completed in four stages. In the first stage, glycolysis, glucose is broken down into two pyruvate molecules. Next, the citric acid cycle (Kreb's cycle) breaks pyruvate down to form carbon dioxide in the mitochondria. Energy is stored in the form of reduced nicotinamide adenine dinucleotide (NADH). In the third stage, the electron transfer chain in the mitochondria transfers electrons from NADH to oxygen to form water. Coupled with this is the pumping of H+ across the inner membrane of mitochondria against is gradient, thus storing energy. The final stage moves H+ across the gradient coupled with the combination of ADP and pyruvate form ATP. The product of this metabolism is carbon dioxide and heat, which is carried away by venous blood.

The human brain requires a high level of energy metabolism. To fuel the brain, it is supplied with approximately 15% of total cardiac output (Buxton, 2009). Blood flow is used to deliver glucose and oxygen to the brain, which requires a continuous supply of glucose and oxygen as it contains virtually no reserve storage of oxygen. Glucose diffuses out of the blood down its gradient through channels in the capillary wall. Directional preference does not exist for these channels; therefore, this method is also used to return unmetabolized glucose to the blood stream. Glucose

is delivered in excess to the required amount at rest. Approximately 15% of glucose delivered to the capillary bed is metabolized (Buxton, 2009).

Oxygen, however, is carried in the blood by hemoglobin but a small fraction exists as dissolved gas in the plasma. Oxygen is transported down a concentration gradient between dissolved gas in capillary plasma and dissolved gas in tissue. When oxygen diffuses out of the capillary it is replenished by the release of oxygen bound to hemoglobin, or oxyhemoglobin. Hemoglobin which loses the oxygen it carries becomes deoxyhemoglobin, and the magnetic properties change in a subtle way. These changes alter the NMR signal slightly: the magnitude of the signal from protons within oxyhemoglobin is slightly higher than that from deoxyhemoglobin. When an area of the brain becomes active, blood flow to this area increases much more than the oxygen metabolic rate leading to a reduction in the oxygen extraction fraction – the fraction of oxygen leaving the blood and metabolized in cells. These two phenomena sum to create local, measurable increases in the NMR signal called the blood oxygen-level dependent (BOLD) effect. The hemodynamic response function (HRF) describes how the BOLD effect responds to neural activation (Figure 12).

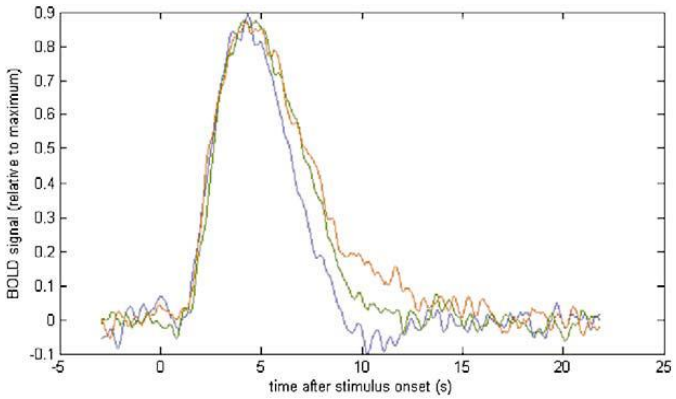

Figure 12. Group average HRFs. HRFs were the averaged BOLD signal from the 10 voxels which responded most robustly to a flashing monochrome checkerboard stimulus. The HRFs were then averaged across individuals and trials. The blue line indicates children (aged 7 to 20), the green line indicates young adults (aged 21 to 27), and the yellow line indicated older adults (aged 30+). Reprinted from Richter and Richter (2003) with permission from Elsevier.

The classical understanding of the relationship between neural activity and changes in blood flow is described with a chain of events. First, neural activity increases the local rate of energy metabolism. To fuel the metabolism, blood flow must be increased to deliver glucose and oxygen to the active area. However, recent views seem to contradict this classical theory. New principles hypothesize changes in blood flow are driven directly by aspects of neuronal activity. Multiple neuronal signaling pathways seem to drive modifications of blood flow. Astrocytes, which make contact with blood vessels and neurons, have a complex signaling method and may create a bridge between neuronal signaling and changes in blood flow. Therefore, these astrocytes may play an important role in driving changes in blood flow following neural activity (Buxton, 2009). In either case, changes in blood flow are a correlate of neural activity.

b. FMRI-based Correlates of Tinnitus

A growing theory, the Global Brain Model (Schlee et al., 2011), builds upon the Neurophysiological Model describing tinnitus as a result from abnormal brain activity arising at points along the auditory pathway. Reduced sensory input due to a damaged hearing system decreases inhibitory mechanisms in the central auditory system and enhances excitability of the auditory cortices. This aberrant activity creates the perception of a sound although no sound is present (Eggermont & Roberts, 2004; Giraud et al., 1999; Jastreboff, 1990). Such neural correlates of tinnitus may arise due to neuroplastic mechanisms engaged in response to total or partial deafferentation somewhere in the auditory tract (de Ridder et al., 2004; Kaltenbach, 2000; Mühlnickel, Elbert, Taub, & Flor, 1998). It has been suggested that these changes may be driven by a compensatory mechanism to enhance excitability of auditory cortices in response to reduced sensory input caused by damage to the mechanical system of the ear (Golm et al., 2013).

i. Assessment of Tinnitus from Continuous Noise Stimulation

In most individuals, the tinnitus percept can be masked by an acoustic stimulus (Feldmann, 1971; Fowler, 1944; Penner, Brauth, & Hood, 1981). Melcher, Sigalovsky, Guinan, & Levine. (2000) proposed auditory stimulation (continuous, broadband noise) in a block design[1] will alternate the loudness of the tinnitus percept, thus revealing tinnitus-related abnormalities. Participants were separated into subpopulations experiencing either lateralized or non-lateralized tinnitus, and compared to a group of healthy individuals who do not have tinnitus or whose tinnitus was masked completely by the acoustic noise in the imaging environment. Four of the thirteen participants had some hearing loss, two from the non-lateralized group and two from the healthy controls. Auditory stimulation was performed binaurally or monaurally, dependent upon the run, at 55 dB sensation level, established inside the MRI, except in the first four experiments which used 35, 40, or 60 dB. The noise was alternated with periods with no stimulation. Activity in the IC was assessed using fMRI. IC activity did not significantly vary between the control and non-lateralized groups, and were grouped into a single reference group. For this reference group, binaural noise produced comparable levels of activation in the left and right IC. In lateralized tinnitus participants, binaural noise produced abnormally low activation in the IC contralateral to the tinnitus percept. Activity in the IC ipsilateral to the tinnitus percept did not significantly vary from the reference group. Monaural noise produced greater activation in the IC contralateral to the stimulus in the reference group. Left stimulation in the IC contralateral to the tinnitus percept resulted in decreased activity in the lateralized tinnitus group than the reference group. Further, activation in the left IC for right stimulation was less than activation in the right IC for left stimulation for all lateralized tinnitus participants. These phenomena only appeared in 2 of the 6 in the reference participants.

Gu, Halpin, Nam, Levine, & Melcher (2010) explained that hyperacusis, increased perception of sound loudness, can accompany tinnitus. Hyperacusis, like tinnitus, is thought to arise from abnormal gain in the auditory pathway (Levine & Kiang, 1995; Salvi, Wang, & Ding, 2000). They suggest that hyperacusis must be controlled in the experimental population to determine if

[1] In block design experiments, two or more conditions are alternated in distinct blocks only useful for determining which voxels show differential signals between conditions.

the previously observed abnormal activity (*e.g.* Melcher et al., 2000) were attributable solely to tinnitus. In their study, sound-level tolerance (SLT) was measured from each participant to address whether tinnitus, abnormal SLT, or both contribute to aberrant brain activity. During fMRI acquisition broadband noise was delivered binaurally at 50, 70, and 80 dB sound pressure level alternated periods of no auditory stimulation. Their region of interest (ROI) based analysis revealed elevated activity in the auditory midbrain, thalamus, and A1 in participants with hyperacusis. They did not report any subcortical region with abnormal activity in participants with tinnitus, however, elevated activity in A1 was observed. This elevated activity was more prominent with the 50 dB stimulation than the 70 dB. The lack of subcortical hyperactivity in tinnitus patients leads to the hypothesis that elevations of activity in cortical structures (*e.g.* A1) may be driven by attention drawn to the auditory system as subcortical activity is less likely modulated by attentional state, although their analysis did not include any attentional regions which could have supported this theory.

Seydell-Greenwald et al. (2012) add to this body of research. Their study involved auditory stimulation of tinnitus patients and age/sex matched controls. Binaural stimulation consisted of trains of short noise bursts centered around 375, 1500, and 6000 Hz. For each tinnitus patient, the noise nearest the tinnitus frequency, determined through subjective pitch and tone matching, was replaced with a stimulus centered at the tinnitus frequency. Stimuli were delivered at a constant level 15 to 30 dB above SLT, determined inside the scanner, depending upon the highest intensity that did not induce sound artifacts. In a whole-brain analysis, two clusters were identified with a significant group difference between tinnitus patients and healthy controls for trials with stimulation at the tinnitus frequency compared to trials without auditory stimulation. These clusters were centered in the right ventro-medial prefrontal cortex (vmPFC) and right STG. They did not find any significant group differences with stimulation of frequencies which were not near the tinnitus frequency compared to trials without auditory stimulation. For the group of tinnitus patients, the BOLD response in the vmPFC was strongly correlated with subjective measures of tinnitus: general loudness ratings and tinnitus awareness. These correlations were strongest on trials with stimulation at the tinnitus frequency. They propose the vmPFC provides input for a thalamic auditory gating mechanism that can suppress the tinnitus percept. Tinnitus patients likely engaged their inhibitory gating mechanism to drive attention away from the tinnitus percept while control participants were not likely engaging this system.

ii. Other Methods to Assess Tinnitus-related Abnormalities

Alternative methods have been proposed for the investigation of tinnitus-related abnormalities in brain activity. These methods are based upon assessing the interaction between activity and external stimuli such as sound, instead of the aforementioned method which attempts to alter the tinnitus percept. Smits, Kovacs, de Ridder, Peeters, van Hecke, & Sunaert (2007) binaurally presented lyrical pop music to lateralized and non-lateralized tinnitus patients in addition to healthy volunteers. Asymmetrical activation was observed in the auditory cortices (A1, IC, and medial geniculate body) in patients with lateralized tinnitus, with reduced activity in cortices contralateral to the tinnitus percept. Although it is possible the stimuli masked the tinnitus percept which could lead to lower activity on the affected side. For those with non-lateralized tinnitus this activation was symmetrical. Activation was also symmetrical for healthy controls for auditory cortices, except A1 which was left-lateralized as anticipated for linguistic and nonlinguistic

stimuli. The researchers suggest this indicates increased spontaneous activity of the affected brain areas in tinnitus patients during rest.

Wunderlich et al. (2010) recruited tinnitus patients and healthy controls to perform a pitch discrimination task. Activation in the caudate nucleus, superior frontal gyrus, and cingulate cortex was increased in the tinnitus patients when compared to healthy controls. This suggests tinnitus enhances the emotional response to auditory stimuli. Using the theory that distress heightens tinnitus perception and attentional focus on the percept, Golm, Schmidt-Samoa, Dechent, & Kröner-Herwig (2013) used an emotional sentence task to evaluate high- and low-distressed tinnitus patients in addition to healthy controls. High-distressed tinnitus patients showed stronger activity compared to healthy controls in parts of the cingulate gyrus, insula, dorsolateral prefrontal cortex, orbitofrontal cortex, and left middle frontal gyrus when contrasting tinnitus-related sentences to neutral ones. Activity in the left middle frontal gyrus was also enhanced in the high-distressed group compared with the low-distressed. Correlations between a seed region of the left middle frontal gyrus and limbic, frontal, and parietal regions were stronger for the high-distressed group.

iii. Summary

Several different paradigms utilizing various designs have reported variations between healthy individuals and those affected by tinnitus. This evidence supports a central mechanism for the tinnitus percept and not the subcortical structures originally identified, but suggests this effect further extends to areas involved in the processing of emotion and attentional state. Variations in activity between tinnitus patients and healthy counterparts were described. Also, differences in lateralized and non-lateralized tinnitus patients as well as between low- and high-distressed groups were reported.

2. Resting-State Networks

Neural networks can be described in two ways: anatomical and functional. Anatomical networks define the physical connections between brain regions made by single axons or white matter tracts. In contrast, functional networks are defined by the interactions between brain regions in the execution of cognitive functions. The fundamental principle of functional connectivity is that individual regions within the network have activity which temporally co-vary, allowing for emergent functions and cognitive processing (Guo & Blumenfeld, 2014).

a. Background on Resting-State fMRI

Functional networks are characterized by systematic, spontaneous low-frequency (<0.1 Hz) signal fluctuations (SLFs). SLFs from regions which are functionally connected appear to fluctuate synchronously. FMRI is well-suited to derive measures functional connectivity given its good spatial resolution and temporal resolution fair enough to capture SLFs. In traditional fMRI, specific variables are intentionally modulated to detect corresponding changes in the measured BOLD signal. To detect SLFs, fMRI data is acquired when individuals are at rest (*i.e.* resting-state fMRI), diverging from the traditional methods of fMRI. Biswal, Zerrin Yetkin, Haughton, & Hyde (1995) first applied resting-state fMRI to study functional connectivity in individuals at rest. They found a high degree of correlation between SLFs of regions associated with motor function. This is the first demonstration that SLFs measured at rest from functionally-related regions are correlated and detectable by fMRI.

Biswal et al. (1995) used a seed region in the left somatosensory cortex to derive correlation coefficients, which defined the measure of functional connectivity. In this type of analysis, a seed region is selected by the researcher and correlations between the time-course of this seed region and other regions (or voxels) is computed. This approach is straightforward, but is highly susceptible to bias as the results are dependent upon the chosen seed regions. In comparison, independent component analyses (ICAs) are primarily data driven and, therefore, do not require *a priori* hypotheses. In this method, components are produced from the time-courses. Common components across voxels represent regions with common temporal covariation. However, the results from an ICA approach are not as straightforward to interpret at the seed region approach but are less susceptible to bias.

b. Resting-State fMRI Correlates of Tinnitus

FMRI studies indicate that the persistence of this phantom perception is associated with interplay between the auditory and cognitive-emotional brain networks (see Section II.C.1.b above). This disruption causes impariement in subsequent conditioned emotional reactions to tinnitus (Mirz et al., 1999; Wunderlich et al., 2010). The use of a diverse set of networks to perform auditory processing has been shown in normal hearing, healthy adults (Langers & Melcher, 2011). Evidence of these plastic changes suggests the possible functional reorganization of the networks which exist between auditory and cognitive-emotional brain regions, changes which may correlate with the appearance of tinnitus.

i. Assessment of Functional Connectivity from Resting-State fMRI

Subjective tinnitus[2] can easily be studied using resting-state fMRI where it is not necessary to perform task-based modulations, although this is possible (see Section II.C.1.b above). However, it may be plausible that the continuous perception of a chronic internal noise restricts an individual from truly achieving a resting state; they may be in a continuous task-based state. This steady task-based state is thought to be cause detectable alterations in networks, such as the default mode network (DMN), when compared to healthy humans. Contrary to other networks, the DMN shows enhanced activity at rest and reduced activity when individuals enter a task-based state (Shulman et al., 1997). Therefore, it would be expected to observe reduced DMN in tinnitus patients compared to healthy controls.

Kim et al. (2012) conducted one of the first studies to investigate altered functional connectivity in tinnitus patients using fMRI. They compared connectivity of auditory cortices from four patients to six age-matched healthy controls. Using an ICA approach, they found increased connectivity between the auditory cortex and the limbic system in tinnitus patients. This supports Gu et al.'s (2010) postulation that elevated A1 activity may be driven by attention drawn to the auditory. In a ROI analysis, correlations were computed between four seed regions comprised of the left and right primary and secondary auditory cortices. Connectivity scores were computed from each of these regions. They identified a decreased connectivity between left and right

[2] This project will only consider subjective tinnitus, a form of tinnitus where the cause of the tinnitus percept cannot be linked to something physical. In the few cases where the tinnitus percept can be objectively heard by others (*e.g.* through the use of a stethoscope), the phantom sound arises from a physical phenomenon (*e.g.* muscle contractions, blood flow).

auditory cortical regions. Further, they revealed increased connectivity in the left amygdala and the dorsomedial prefrontal cortex in tinnitus patients compared to healthy controls. Their evidence suggests elevated intrinsic brain connectivity between auditory networks and regions involved in emotion processing and cognitive control. Additionally, their evidence supports the hypothesis that tinnitus may be related to a reduction in the balance of excitatory and inhibitory inputs to the central auditory system. This imbalance is observed through the reduced interhemispheric coherence, where equilibrium is important for optimal function (Diesch, Andermann, Flor, & Rupp, 2010).

Maudoux et al. (2012) compared resting-state functional connectivity, measured from fMRI, on two groups. They selected auditory ROIs from the first group of twelve healthy individuals. Data from a second group of thirteen patients with chronic tinnitus was compared to the first group. In the second group, patients with hyperacusis and phonophobia were excluded. The identified auditory network in healthy controls included bilateral primary and associative auditory cortices, insula, prefrontal, sensorimotor, anterior cingulate (ACC), and left occipital cortices. The group of tinnitus patients showed a similar network, excluding the ACC. In this group, the identified auditory network also included regions of the brainstem, thalamus, nucleus accumbens, isthmus of cingulate gyrus, right occipital, parietal, and prefrontal cortices. Further, for the tinnitus patients, increased connectivity was identified in deeper brain structures (brainstem, cerebellum, right basal ganglia/nucleus accumbens), right frontal and parietal, and left sensorimotor and superior temporal regions. Finally, the tinnitus patients showed lower connectivity in the right A1, left fusiform gyrus, and left frontal and bilateral occipital regions.

Davies, Gander, Andrews, & Hall (2014) conducted a comparison of resting-state functional connectivity between twelve tinnitus patients and eleven age-matched healthy controls. Resting-state fMRI were collected and analyzed using ICA to extract auditory components of interest. In an ROI analysis, similar to Kim et al. (2012), when corrected for family-wise error the two groups did not appear to have differences in functional connectivity. This study contradicts earlier reports of disturbed connectivity (Kim et al., 2012; Maudoux et al., 2012), however this may be due to methodological differences. Tinnitus symptoms are variable (*e.g.* lateralized, non-lateralized) and is often accompanied by other disorders such as hearing loss. While Kim et al. (2012) studied patients with lateralized tinnitus, Davies et al. (2014) used a cohort of patients experiencing bilateral tinnitus. Further, Kim et al. (2012) did not account for high frequency hearing loss in their control group while Davies et al. (2014) did.

ii. Summary

Few studies have explored tinnitus physiopathology through resting-state functional connectivity using fMRI. The results from two studies suggested detectable differences in resting-state functional connectivity, aligning with the Neurophysiological Model which suggests non-auditory tinnitus physiopathology. Both of these studies indicated increased input from the limbic system which coincide with postulations made in previous auditory stimulation fMRI studies. This effect is proposed in the Neurophysiological Model, suggesting the limbic system plays a role in negative reinforcement and draws more attention to the auditory system causing the tinnitus signal to be perceived. Furthermore, these studies indicate altered connectivity in the nucleus accumbens and associated paralimbic regions in the medial prefrontal cortex when compared to healthy controls. These regions have been implicated to play a role in an inhibitory feedback loop

which “cancels out” the tinnitus signal in the thalamus (Rauschecker, Leaver, & Mühlau, 2010). If this inhibitory feedback loop is compromised, the tinnitus signal may reach the auditory cortex and give rise to the tinnitus percept. These studies, although limited, suggest tinnitus is related functional reorganization which may be detected using resting-state fMRI.

3. Steady-State Perfusion

Blood flow can provide valuable information for guiding and monitoring therapies. Tissue-specific blood flow, or perfusion, is a physiologic measure of the volume of blood flowing through microvasculature of a mass of tissue in a given amount of time. In most cases, perfusion is measured using a tracer which are used to derive measures of perfusion. In the case of MRI, it is possible to use magnetically-tagged ^{1}H atoms as a tracer to measure perfusion. This is very useful, particularly for the brain as there are no approved MR contrast agents that can cross the intact blood-brain barrier (Alsop, 2006).

a. Arterial Spin Labeling

i. Background

The *in vivo* detection and quantification of cerebral blood flow (CBF) is achievable using Arterial Spin Labeling (ASL). ASL utilizes spatially selective excitation to magnetically-tag 1H contained in arterial blood. This method unique as it does not require the injection of a contrast agent and has a short decay rate (on the order of 1 s). A slab selective inversion is performed prior to imaging. This excitation labels the blood in the arteries contained within that slab. A short delay between labeling and imaging allows blood to perfuse to the imaged slice. The inverted magnetization in the inflowing labeled blood to the imaging slab causes the signal to be reduced. However, the change in the measured signal is quite small so the image must be subtracted from another image acquired without the inversion. This difference is proportional to the blood flow into the imaged slab (Alsop, 2006).

The majority of ASL relies upon labeling magnetization in the z-direction in either a pulsed or continuous manner.[3] Changes in this magnetization return to equilibrium on the order of T1, which is slower than T2 and, therefore, can generate a larger differential signal. The implementation of pulsed inversion can vary, each with different approaches to ensure the differential signals are only affected by perfusion. In one popular method, EPISTAR, an inversion slab is prepared inferior to the imaged brain region to label arterial spins and a superior inversion slab is selected for the control image. This ensures equal magnetization transfer effects between both image acquisitions. In another popular method, FAIR, a nonselective inversion pulse labels the entire imaged region, along with superior and inferior slabs. Prior to the control, a slab

[3] In pulsed labeling, the RF inversion pulse is applied to the inversion slab at a time approximately 1 s prior to imaging. In continuous labeling, a RF inversion pulse is continuously applied throughout imaging to produce a larger signal. Pulsed labeling requires uses traditional RF and gradient strategies, is less susceptible to systematic error, and can produce quality images. Pulsed labeling is analogous to a decaying bolus experiment often utilized in contrast-driven MRI or PET, while continuous labeling can be operated as a steady-state experiment.

selective inversion is applied to only the entire imaged region. In this technique, the spins are always inverted rather than left unaffected in the control as in the EPISTAR method.

ii. Quantification of CBF

The simple subtraction image from ASL is reflective of relative blood flow but quantitative measurements can be very useful, specifically in clinical applications. Magnetization in the z-direction behaves according to the Bloch equation, assuming no flow or RF pulses:

$$\frac{\partial M_z}{\partial t} = -\frac{M_z - M_z^0}{T1}, \quad (4)$$

where M_z represents the net magnetization in the z-direction at time t and M_z^0 represents the net magnetization in the z-direction at time 0. When blood flow occurs, inflowing spins from arteries add their magnetization to the voxel and magnetization from outflowing spins subtract from the voxel. The Bloch equation can be modified to account for flow:

$$\frac{\partial M_z}{\partial t} = -\frac{M_z - M_z^0}{T1} + \rho_b f(M_a - M_v), \quad (5)$$

where f is the blood flow (perfusion), ρ_b is the tissue density, M_a is the magnetization in the inflowing spins, and M_v is the magnetization in outflowing spins. One can assume complete free diffusion into the tissue, meaning M_v equals M_z at the capillary level.

From the flow-modified Bloch equation, it is apparent the ASL signal represents a competition between T1 decay and inflow of labeled spins. Using this modified equation, the image intensity due to ASL is approximately f*T1. The T1 decay of blood is often taken from literature, but attempts have been made to measure it *in vivo*. Also, T1 of tissue can vary from blood and across various types of tissue.

Assuming tissue and blood T1s are the same, an inversion that creates a bolus of labeled spins of duration t_b, and a time TI between labeling and imaging, the labeled signal will be the perfusion times t_b times a decay factor for T1 decay over time TI:

$$M_{label} = 2\rho_b f M_{blood} t_b e^{-\frac{TI}{T1}}, \quad (6)$$

where M_{label} and M_{blood} are the magnetic moments of tissue and blood, respectively. This equation can be rewritten as follows to solve for perfusion (f):

$$f = \frac{M_{label} e^{-\frac{TI}{T1}}}{2\rho_b f M_{blood} t_b}. \quad (7)$$

In pulsed ASL, t_b is unknown as the inversion pulse inverts a thickness of tissue containing arteries. To account for this, a saturation pulse may be applied to the inversion slab to eliminate any labeled blood still remaining within this volume. Using this method, t_b is equal to $TI - T_{sat}$ where T_{sat} is the time delay between the saturation pulse and the inversion pulse.

The above equations are reliant upon measurements of magnetic moments (M) of the tissue, quantities that are not measured directly but through signal intensities in arbitrary units. A proton

density-weighted image can serve to compute magnetic moments, as the signal is proportional to *M*. This image can serve as a voxel-wise reference approach:

$$\frac{M_{label}}{M_{blood}} = \frac{\left(\frac{M_{label}}{M_{voxel}}\right)}{\left(\frac{M_{blood}}{M_{voxel}}\right)} = \frac{\left(\frac{ASL_{signal}}{PD_{signal}}\right)}{\rho_b \lambda_{blood/tissue}}, \quad (8)$$

where ASL_{signal} and PD_{signal} represent the ASL and proton density-weighted image intensities, λ is the blood-brain partition coefficient (usually taken from the literature for gray matter and white matter). Alternatively, a reference intensity could be selected from somewhere in the image such as CSF within a ventricle which has almost the same magnetic moment as pure water.

Adding to the complexity, perfect inversion of labeled blood does not occur in practice. Therefore, a correction factor for imperfect efficiency, α, is included in the quantification equations. The efficiency can either be estimated from simulations or measured *in vivo*.

3D acquisition techniques enable the collection of signals from all slices at exactly the same time after labeling. In 3D scans, motion-related phase errors can cause ghosting and other artifacts, which can be reduced using background suppression techniques.

b. ASL Correlates of Tinnitus

To date, there have not been any studies which have investigated the neural correlates of tinnitus using ASL. However, there have been a limited number of studies that researched steady-state metabolism associated with tinnitus using F^{18}-deoxyglucose (FDG; F^{18}-tagged glucose) PET. Although ASL does not offer a direct measure of metabolism like FDG, perfusion is a correlate of metabolism (see Section II.C.1.a.ii above). In the case of FDG PET imaging, increases in neural activity causes regional increases in blood flow in response to oxygen and glucose consumption (demand). This causes an accumulation of FDG in cells which is proportional to the metabolic rate for glucose. Increased FDG leads to higher signals when imaged in PET.[4]

Wang et al. (2001) conducted one of the first studies to investigate tinnitus using FDG PET. They studied eleven patients with chronic disabling tinnitus, some with unilateral (left or right) and some with bilateral tinnitus, and ten healthy normal individuals. FDG PET was acquired while participants rested in bed, but maintained conscious. Measures were taken to control visual and auditory input. Imaging data was analyzed from circular ROIs placed on the left and right temporal superior and transversal gyri. All eleven tinnitus patients had metabolic hyperactivity in the left temporal superior and transversal gyri. Furthermore, an asymmetry index indicated tinnitus patients had significantly greater asymmetry than healthy controls:

$$\frac{(L-R)\cdot 100}{\frac{L+R}{2}} \quad (9)$$

[4] Photons are emitted when radioactive tracers such as FDG undergo radioactive decay when the tagged molecule is consumed. Specifically, F^{18} decays to O^{18} by electron capture (3%) and positron (β^+; 97%) emission (Cherry, Sorenson, & Phelps, 2012).

where *L* and *R* indicates the hemisphere containing the ROI (left or right, respectively).

Langguth et al. (2006) did not perform a controlled study but instead investigated relationships between steady-state glucose metabolism, measured using FDG PET, and changes in tinnitus symptoms and severity following repetitive transcranial magnetic stimulation (rTMS) of the temporal transversal gyrus. Twenty patients suffering from unilateral or bilateral tinnitus were treated with low-frequency rTMS across a period of five days (2000 stimuli per day at 110% motor threshold). Targeted rTMS was delivered to the area of increased metabolic activity in the temporal transversal gyrus, measured from FDG PET prior to any stimulation. The asymmetry index (modified form of Equation 9), was computed from the FDG PET imaging data of the left and right temporal transversal gyri prior to the rTMS protocol:

$$\frac{(ROI_1 - ROI_2)\cdot 100}{\frac{ROI_1 + ROI_2}{2}} \quad (10)$$

where ROI_1 represents the higher activated area (left or right temporal transversal gyrus) and ROI_2 represents the lesser activated area. ROI_1 was selected as the target for rTMS. Additionally, the activity of ROI_1 was normalized to the activity of the corresponding slice ($ROI_1/slice$). In seventeen patients, the left temporal transversal gyrus was metabolically hyperactive prior to rTMS. For the remaining three patients, the right temporal transversal gyrus was metabolically hyperactive. These results were independent of handedness and tinnitus laterality. Improvement in tinnitus behavior and the metabolic activity of the stimulated area was significantly correlated. No other correlations passed significance, but it was noted that the asymmetry index was significantly more pronounced in left-handed patients.

Schecklmann et al. (2013) studied 91 patients with tinnitus: 30 predominately left, 23 predominately right, and 38 bilateral. FDG PET data were acquired during rest (eyes closed). Tinnitus duration and glucose metabolism in the right inferior frontal cortex were significantly correlated. Tinnitus distress was significantly correlated with the metabolic activity in the bilateral posterior inferior temporal gyrus and posterior parahippocampal-hippocampal interface. A significant main effect of hemisphere was observed in the metabolic activity of A1 with higher activity in the left hemisphere. The asymmetry was independent of tinnitus laterality as there was no significant interaction between hemisphere and laterality was revealed.

Although the work of Schecklmann et al. (2013) included a large number of patients, no control population was used. Geven, de Kleine, Willemsen, & van Dijk (2014) expanded upon the previous work which demonstrated an increase in glucose metabolism in the left A1 when compared to the right (Schecklmann et al., 2013), and that this asymmetry was abnormal when compared to healthy controls (Wang et al., 2001). In their study of twenty right-handed patients suffering from bilateral tinnitus and nineteen healthy right-handed controls. Participants rested in a quiet, dark room during FDG PET acquisition. In a voxel-wise analysis, no areas of significant difference between patients and controls were found when corrected for multiple comparisons; however, two clusters appeared when a correction for multiple comparisons was not applied (left middle frontal gyrus and left STG). It is unclear if this result is due to tinnitus or hearing loss as the patients had significantly more hearing loss than the healthy controls. In a ROI analysis, no difference was found between left or right A1, secondary auditory cortex (A2), Brodmann area (BA) 22, or IC in the patients versus controls. A significant difference in A1 metabolic

asymmetry was not found between patients and controls. Furthermore, significant differences in asymmetry of the other ROIs were not found. These results conflict with the previous reports from Wang et al. (2001), although the asymmetry index varied between the two studies.

c. Summary

To date, no studies have investigated tinnitus using ASL although there have been a handful of studies that have used PET. Only a subset of these studies have explored tinnitus during steady-state, achieved using FDG PET. The results from most of these studies suggest detectable differences in steady-state metabolism in auditory cortices, manifesting mainly as abnormal asymmetry between the left and right hemispheres. Despite these results, only two of the studies presented utilized healthy control groups and most only explored auditory cortices. Regardless, it is unclear if these differences are attributable to tinnitus or other disorders (*e.g.* hearing loss or hyperacusis) and if they can be detected using ASL. However, the physiology between glucose metabolism and CBF would suggest these differences can be measured using ASL.

III. Methods

The purpose of the proposed study is to determine the efficacy of fMRI-NFT for the treatment of tinnitus. We will randomly assign healthy participants to one of two groups. During closed-loop neuromodulation, we will provide the experimental group with real feedback regarding activity in the primary auditory cortex (A1) while the control group will receive sham feedback yoked from a participant in the experimental group. The participants will be blinded to the group assignments. Activity from A1 during closed-loop neuromodulation will be quantified for each individual. Additionally, behavioral measures of attentional control will be assessed prior to and following fMRI-NFT. Neural measures will be collected before and after training to quantify A1 response to auditory stimulation, resting-state networks, and steady-state perfusion in auditory and attentional regions.

A. Participants

Healthy volunteers were recruited from Wright State University and the surrounding community. Prior to being enrolled, each potential participant completed a telephone screening to qualify for the study (Appendix I). Forty-seven (47) participants meeting the inclusion/exclusion criteria (Table 2) were recruited for the study. These participants were selected at random from the qualifying group. The study was approved by Wright State University's Institutional Review Board (IRB) and the Air Force Medical Support Agency Surgeon General's Research Oversight Committee[5], and informed consent was obtained prior to the execution of any experimental procedures. Participants eligible[6] for compensation will receive equal remuneration.

[5] Approval for this study was been obtained by Wright State University's IRB SC #5848 and the Air Force Medical Support Agency Surgeon General's Research Oversight Committee FSG20150041H.

[6] On-duty Federal personnel are ineligible for compensation for research participation (other than blood draws) under DoDI 3216.02, Enclosure 3, Paragraph 11.

Table 2. Inclusion and exclusion criteria establishing participant eligibility for the experiment.

Inclusion Criteria	Exclusion Criteria
• Between the age of 18 and 50 inclusive • Able to read and write in English • Right handed • Able to lay supine for up to an hour • Able to hold still during MRI • Normal or corrected to normal vision • Have signed the consent form for the study • Able to complete all training sessions within three consecutive weeks	• Conditions that would preclude the completion of an MRI such as claustrophobia, pacemaker, metal objects in the body, and/or pregnancy • Serious unstable medical or mental illness • History of brain cancer or other brain disease • Medical contraindication to any element of the study procedure • Have not read and signed the informed consent form, or do not understand its contents • Hearing loss > 40 dB

Participants were randomly assigned to one of two groups and were blinded to the assigned group. The experimental group (EXP) received real feedback regarding activity in A1 during closed-loop neuromodulation. The control group (CON) was supplied with sham feedback yoked from a participant in the experimental group. Activity from A1 during closed-loop neuromodulation will be quantified for everyone. Additionally, behavioral measures of attentional control will be assessed prior to and following neurofeedback training, as well as approximately 2 weeks following the final fMRI-NFT session. Further, neural measures of tinnitus will be collected before and after training. These measures will quantify brain activity, resting-state network activity, and steady-state perfusion. Nineteen (19) participants voluntarily withdrew or were withdrawn from the study due to excessive motion, absenteeism/tardiness, or software/hardware issues limiting the completion of study procedures. The MRI data for a single participant was corrupted. This resulted in a final group of eighteen (18) EXP and nine (9) CON participants. Three (3) EXP participants did not complete follow-up sessions, therefore analysis including the follow-up data represent fifteen (15) EXP and nine (9) CON participants.

B. Experimental Design

An overview of the experimental procedure is shown in Figure 13. A consent visit was completed before the first session of the experimental procedure. At the consent visit and prior to performing any study-related tasks, all participants signed informed consent documents detailing the requirements of participation. At the time of informed consent but after obtaining consent, the participants completed a MRI screening form (Appendix II) and other forms (Appendix III and Appendix IV). Next, a short hearing test was conducted to verify normal hearing (no frequency > 40 dB on a standard audiogram; Shoebox Audiometry, Ontario, Canada). This test is a simple self-applied test that has been clinically validated (Saliba et al., 2017; Thompson, Sladen, Borst, & Still, 2015). Finally, participants received short (< 3 min) training on the CPT-X and Attention to Emotion tasks. Following the consent visit, the subjects completed five fMRI-NFT sessions and a 2 week follow up. The first session will begin with a pre-NFT behavioral assessment

followed by an assessment of neural measures and neurofeedback training. The second, third, and fourth sessions only consisted of fMRI-NFT. The fifth session began with fMRI-NFT, followed by a post-NFT assessment of neural measures and a behavioral assessment. All neural assessments and NFT procedures were performed inside the MRI while the behavioral assessments were completed outside of the MRI. All MRI procedures were conducted on a 3 Tesla (T) MRI (Discovery 750W, GE Healthcare, Madison, WI) using a 24-channel head coil. These five sessions were executed within 21 days with no more than one per day. A follow-up behavioral assessment was performed 12 to 16 days following the final fMRI-NFT session.

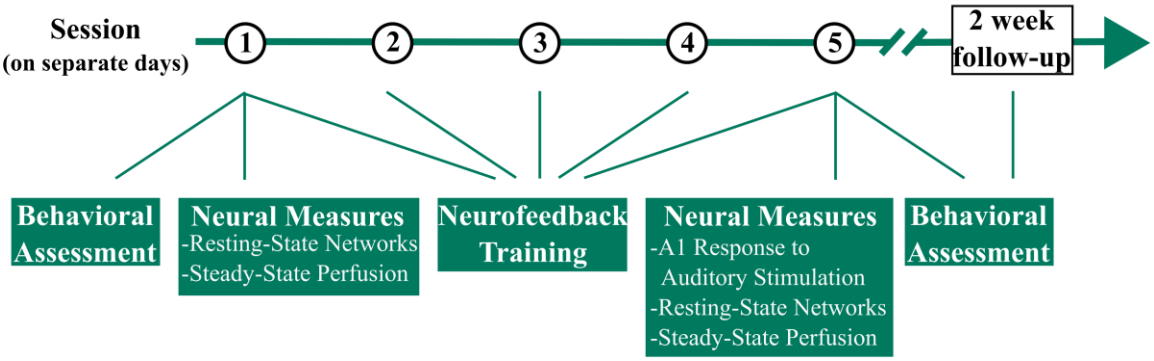

Figure 13. Experimental design overview. The first session began with an initial assessment of behavior and neural measures followed by fMRI-NFT. The second, third, and fourth sessions consisted of only fMRI-NFT. The final session started with fMRI-NFT followed by a second assessment of neural measures and behavior. A follow-up behavioral assessment will be completed approximately 2 weeks after the fifth fMRI-NFT session. Behavioral assessments were conducted outside of the MRI.

1. FMRI-NFT

To achieve the overall objective, fMRI-NFT was performed across five sessions. Prior to entering the MRI environment, MRI screening forms were reviewed by a registered MRI technician. Female participants were required to take a urine dipstick pregnancy test. All participants completed the caffeine consumption and sleep form (Appendix V). Once entering the MRI, the participants first inserted MRI-compatible ear plugs (MagnaCoil, Magnacoustics Inc., Atlantic Beach, NY) capable of providing communication and auditory stimulation (Genesis Ultra, Magnacoustics Inc., Atlantic Beach, NY). Next, the participants were positioned supine on the MRI table, their head was padded to restrict motion, and the upper part of the 24-channel head coil was attached. Using a laser, the nasion was landmarked relative to the MRI. The landmarked position was moved to the center of the MRI bore.

Once positioned, the MRI procedures began. Each fMRI-NFT session consisted of a single run of bilateral auditory stimulation which was used to individually and functionally localize A1. This scan is referred to as the “functional localizer”, followed by two runs of closed-loop neuromodulation (Figure 14). Between the functional localizer and the closed-loop neuromodulation runs, a structural MRI was acquired using an 3D brain volume imaging (BRAVO) pulse sequence which acquires images using an inversion recovery prepared fast spoiled gradient-echo (FSPGR). The structural images were acquired using a 256 x 256 element

matrix, 172 slices oriented in the same plane as the functional scans, 1 mm^3 isotropic voxels, 0.8 phase field of view factor, TI/TE = 450/3.224 ms, a flip angle of 13°, and an auto-calibrated reconstruction for cartesian sampling with a phase acceleration factor of 2.0.

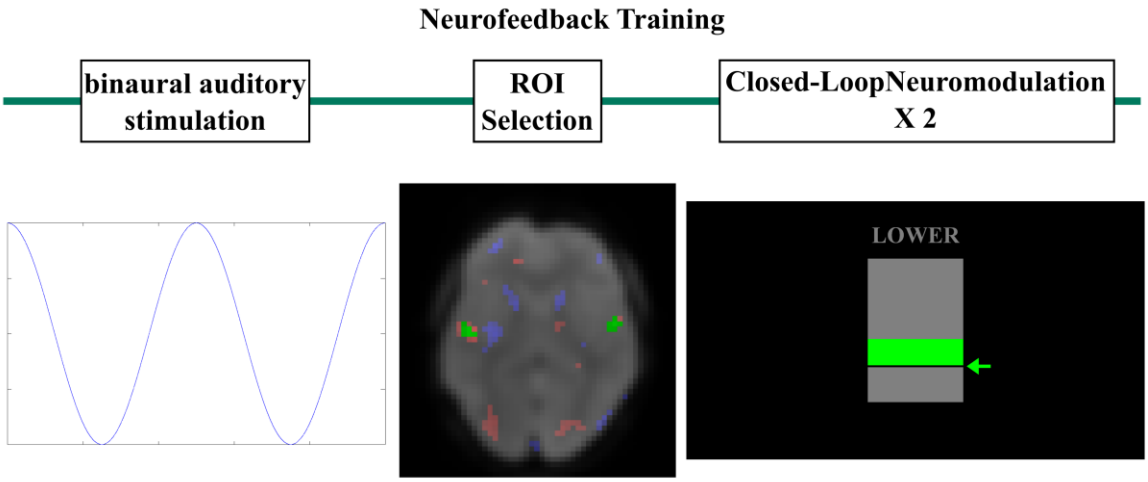

Figure 14. Overview of fMRI-NFT. Each fMRI-NFT session began with binaural continuous noise stimulation. The bilateral A1 was selected from voxels robustly activated during auditory stimulation. Lastly, two runs of closed-loop neuromodulation were completed.

a. Binaural Auditory Stimulation

To identify A1, a single run of standard binaural auditory stimulation was executed in a boxcar design with eight (8) repetitions of OFF and ON blocks. The duration of each block was 20 s, and the first block began after the acquisition of four (4) dummy volumes and one (1) software preparation volume. Binaural auditory stimulation will be delivered via the headphones only during ON blocks and controlled via a stimulus presentation software (Presentation, Neurobehavioral Systems, Inc., Berkeley, CA). Auditory stimulation consisted of 10 kHz lowpass filtered white noise presented at 90 dB, previously shown to be effective at producing a BOLD response (Haller, Birbaumer, & Veit, 2010). The participants were not required to respond in any way during the scan, however they were instructed to remain awake and to focus on a round fixation dot presented in gray with a black background on a MRI-compatible display (SensaVue, Invivo, Gainesville, FL). FMRI data were acquired using a gradient-recalled-echo (GRE) sequence sensitive to the BOLD signal. This sequence acquired data using the following parameters: 64 x 64 element matrix, 41 slices oriented parallel to the AC-PC plane, 3.5 x 3.5 x 3 mm^3 voxels size, 0.5 mm slice gap, TR/TE = 2000/20 ms, and a flip angle of 90° with fat suppression enabled. In previous data collections, these parameters have been shown to reduce susceptibility artifacts which can be significant at high field strengths such as 3T.[7]

[7] In previous data collections, significant susceptibility artifacts were apparent in the majority of cases. Personal communications between Mr. Sherwood and GE Healthcare led Mr. Sherwood to Dr. Glover (Stanford University) who helped greatly in refining the imaging parameters for fMRI data acquisition.

b. ROI Selection

Immediately following acquisition, the BOLD data were pre-processed using custom MATLAB and C++ software. The pre-processing included standard spatial filtering (3D, 5-point Gaussian low-pass kernel, full-width half-maximum of 7 mm), motion correction (corrected to the first volume using a rigid-body 3-parameter model) and temporal filtering (5-point Gaussian low-pass kernel, sigma of 3 s) processing functions (Friston et al., 1995).

An activation map was created by defining a single explanatory variable (EV) by convolving a boxcar model containing 20 s control and task conditions with a pre-defined HRF (Ashby, 2011). Next, the BOLD data at each voxel was fit to the model using a general linear model (GLM) by applying a weight of +1 to the EV, representative of activation (positive correlation to the model). The resulting β parameter maps were converted to *t* statistic maps (activation maps) using standard statistical transforms. The region in A1 in which the feedback signal for the subsequent closed-loop neuromodulation runs was derived from this activation map. Voxels were added to the A1 ROI by first locating the axial slice in which the inferior surface of the anterior ventricle horns are visible. Finally, activation patterns on the left and right hemispheres near the posterior end of the lateral sulci were observed. Voxels within this region responding robustly to binaural auditory stimulation were added to the ROI to complete the determination of the functional localizer.

c. Closed-Loop Neuromodulation

Following the functional localizer, two runs of closed-loop neuromodulation were completed. BOLD data was acquired using the same scan parameters as described for the functional localizer (see Section III.B.1.a above). Four (4) dummy volumes and one (1) software preparation volume were acquired first. Then, eight (8) volumes were acquired to determine a baseline BOLD signal value for the selected A1 ROI. During the acquisition of the baseline volumes, a countdown was displayed on the screen, however there was no auditory stimulation during either the eight baseline volumes or the five preparatory volumes. In the subsequent scanning for the experimental group, a feedback signal was computed and displayed to the participants from real-time analysis of BOLD data. This real-time analysis was implemented in custom MATLAB and C++ software and included standard spatial filtering (3D, 5-point Gaussian low-pass kernel, full-width half-maximum of 7 mm) and motion-correction (corrected to the first volume of the functional localizer using a rigid-body 3-parameter model) processing functions (Friston et al., 1995). This custom software further compared the average BOLD signal in the voxels selected from the functional localizer at baseline to that of the current volume to derive the percent signal change. The current feedback signal was determined by temporally-filtering (5-point Gaussian low-pass kernel consisting of only past components, sigma of 3 s) the percent BOLD signal change with the feedback signals from previous volumes. This feedback signal was presented to the participants using a thermometer-style bar plot. The thermometer plot will contain a running average of the previous four (4) values and a running task minimum. For participants in the control group, the feedback signal was yoked from a random EXP participant with experimental

---

These parameters were used in a previous, unrelated study in which susceptibility artifacts did not impede the results.

progress matched. Both runs from each session were duplicated from the same EXP participant but the EXP participant was selected randomly each session.

After baseline, six repetitions of 30 s relax and lower blocks were completed in a boxcar-design. Both blocks were accompanied with binaural auditory stimulation using the same continuous noise from the functional localizer. During relax, every participant was instructed to relax and clear their mind, resulting in an increase in the feedback signal.[8] They were also instructed to keep their eyes open. Participants were instructed to lower the feedback signal during lower blocks by performing a mindfulness task wherein they should decrease brain activity associated with auditory input. A list of four example mindfulness tasks were provided, giving the participants a few starting points. Through training, participants learned mindfulness tasks that are most successful in regulating A1. Task instructions indicating the current block (rest or task) were supplied above the thermometer plot.

Participants were then removed from the MRI and escorted out of the MRI room. Participants were then informally interviewed by the experimenter (Appendix VI), then escorted to a bathroom to change back into their clothes.

2. Behavioral Assessment

To achieve the overall objective, we collected behavioral measures of attentional control using one questionnaire and two computerized tasks. These tasks were conducted using a laptop outside of the MRI. The participants wore active noise-cancelling headphones (, Samsung Electronics America, Ridgefield Park, NJ) to mitigate distracting sounds during the tasks. The questionnaire provided subjective measures of attentional control while the computerized tasks provide objective measures. The results of these tests were compared across groups to assess Hypothesis 2.

a. Attentional Control Scale

The attentional control scale (ACS; Appendix VII; Derryberry & Reed, 2002) was created to combine attentional focusing and shifting scales to measure attentional control. The ACS is a 20-item self-report questionnaire. Items are scored on a 4-point scale: 1) almost never, 2) sometimes, 3) often, and 4) always; with eleven of the twenty items reverse-scored. The scale was found as a measure of the general capacity for attentional control. Subfactors were found to be related to the abilities to focus attention, shift attention between tasks, and flexibly control thought. The measure is internally consistent ($\alpha = 0.88$), and is positively related to indices of positive emotionality ($r = 0.4$) and inversely proportional to aspects of negative emotionality ($r = -0.55$; Derryberry & Reed, 2002).

The ACS was completed at a computer using a digitized version (Qualtrics, Provo, UT). Written instructions for this test were consistent with the following:

[8] An increase in A1 was anticipated due to the auditory stimulation being provided during the relax condition but not during the baseline acquisition, thereby increasing the BOLD signal relative to baseline.

" The purpose of this questionnaire is to assess your concentration and attention during normal activities. Please select the answer that applies to you for each statement."

b. Attention to Emotion

The attention to emotion (AE; Harris & Pashler, 2004) is a task used to test the impact of emotion on attentional performance. The test was developed from the theory that a person's own name or emotionally-charged stimuli attract attention involuntarily. In this test, participants are asked to make a speedy judgement about the parity of two digits separated by a word. In a limited number of scattered trials, response times are significantly slowed when the word is the participant's own name. This task was implemented to determine the influence of, if any, fMRI-NFT on how emotion impacts attention.

The task contained 130 trials. Each trial began with a gray fixation point presented for 500ms. The stimuli followed the fixation. This consisted of two digits (1-9) in gray flanking a word presented in green. The stimuli were presented for 150ms. 100 trials contained neutral words and 30 contained the participant's name. No neutral words were repeated within a single session. After the stimulus, there was a feedback period with a duration dependent upon the response time. The feedback period was limited to a minimum of 500ms and maximum of 5000ms. Participants were to use this time to indicate using the keyboard whether the digits present were both even or odd (left control button) or mismatched (right control button). Half of the name and half of the neutral trials mismatched, the other half matched. The trials were randomized apart from the first fifteen (15) trials which contained neutral trials. Finally, a 1000ms inter-trial interval (ITI) separated the start of the next trial from the response both of which contained no stimuli. The background for the entire task was black.

c. Continuous Performance Test

The continuous performance test (CPT) was developed to measure deficits in sustained attention (Chen, Hsiao, Hsiao, & Hwu, 1998). The CPT-X was developed as a simultaneous discrimination vigilance task. The CPT-X uses a single character or number as a target. Participants are asked to inhibit responses when the stimulus infrequently matches the target, but respond whenever the stimulus does not match the target. This task was implemented to measure sustained attention and vigilance.

The task contained 300 trials separated even across four (4) continuous blocks. Each block contained fifteen (15) matching trials and 60 non-matching trials. The order of the stimuli was randomized within each block. The stimuli consisted of capitalized letters from the English alphabet with 'X' being the target. Participants were instructed to press the right control button when the stimulus did not match the target and inhibit the response when the stimulus matched the target. The stimulus was presented for 500 ms in gray upon a black background. An ITI randomly sampled from 500, 700, and 900 ms separated each stimulus to prevent participants from predicting the presentation of stimuli. During this period, a gray fixation point was presented on a black background.

3. Neural Measures

We collected neural measures of tinnitus using three MRI sequences. The results of these neural measures were compared across groups to assess Hypotheses 3, 4, and 5.

a. A1 Response to Auditory Stimulation

Measures of brain activity during binaural auditory stimulation will be collected from each neurofeedback training session prior to neurofeedback (*i.e.*, functional localizer). Additionally, a final acquisition will be performed after neurofeedback on the fifth neurofeedback session. FMRI data was acquired during binaural auditory stimulation as described in Section III.B.1.a above.

b. Resting-State Networks

Baseline measures of resting-state network activity will be collected during the first fMRI-NFT session prior to neurofeedback training. FMRI data was be collected using the same parameters described previously (see Section III.B.1.a above) and an initial four (4) dummy volumes. A final measure of resting-state network activity will be acquired during the last fMRI-NFT session after neurofeedback. During the scan which lasted 5 min 8 s, participants were instructed to remain awake and focus on a fixation dot presented on the display. This condition has demonstrated significantly greater reliability across all within-network connections, as well as within default-mode, attention, and auditory networks when compared to eyes open (no specified fixation) and closed methods (Patriat et al., 2013).

c. Steady-State Perfusion

Baseline measures of steady-state perfusion were acquired during the first fMRI-NFT session prior to neurofeedback. A second measure of steady-state perfusion was collected during the last fMRI-NFT session after neurofeedback. CBF was measuring using an ASL pulse sequence implementing a pseudo-continuous labeling technique (Dai, Garcia, de Bazelaire, & Alsop, 2008). T1-weighted images were acquired with a 3D Fast Spin Echo sequence with background suppression and inferior saturation pulses applied to suppress the inflowing arterial blood spins after labeling is completed. A continuous pulse scheme was employed with a labeling duration of 1 s. Other acquisition parameters included 128 x 128 element matrix, 42 slices oriented in true axial plane, 1.875 x 1.875 x 4.0 mm^3, 4 mm slice gap, TR = 4895 ms, TE =10.704 ms, flip angle =111°, post-label delay = 2025 ms, and number of excitations = 3. During the scan, participants was instructed to remain awake and to focus on the focal point placed above their eyes.

C. Data Analysis

1. A1 Control

The BOLD data acquired from each closed-loop neuromodulation run was processed using the FMRIB Software Library (FSL; Smith et al., 2004; Woolrich et al., 2009). First, individual (first-level) analyses were conducted on each of the 4D fMRI data sets. Prior to the individual analyses, t pre-processing was performed using standard techniques. These consisted of applying a high-pass temporal filter (Gaussian-weighted least-squares straight line fitting, cut-off = 60 s) to each voxel, correcting for motion by registering each volume to the center volume of the data set (rigid-body 12-parameter model; Jenkinson, Bannister, Brady, & Smith, 2002), creating a brain mask from the first volume and applying to each subsequent volume (Smith, 2002), spatial filtering on each volume using Gaussian convolution (full-width half-maximum of 5.625 mm), and removing low-frequency trends using a local fit of a straight line across time at each voxel with Gaussian weighting within the line to create a smooth response.

Next, individual analyses were conducted on each of the 4D fMRI data sets. A single EV will be defined by convolving a boxcar model containing 30 s rest and task conditions with a HRF (modeled by a gamma function; phase offset = 0 s, standard deviation = 3 s, mean lag = 6 s). The temporal derivative of the original waveform will be added to the result. The temporal filter used in pre-processing will applied to the model. The data set will be fit to the model using a GLM with prewhitening by applying a weight of -1 to the EV, representative of deactivation during closed-loop neuromodulation (negative correlation with the model). *Z* statistic maps will be created using standard statistical transforms to convert the β parameter maps. A clustering method will allow us to account for false positives due to multiple comparisons. This method considers adjacent voxels with a *z* statistic of 2.3 or greater to be a cluster. The significance of each cluster will be estimated and compared to a threshold of $p < 0.05$ using Gaussian Random Field theory. Voxels that either do not pass the significance level threshold or do not belong to a cluster will be set to zero. A mean image of the data set will be registered to the individual's high-resolution structural image by estimating motion from a boundary-based registration method including a fieldmap-based distortion correction (Greve & Fischl, 2009), then will be further registered to the MNI-152 T1-weighted 2 mm template provided in FSL (Collins, Holmes, Peters, & Evans, 1995; Mazziotta et al., 2001) using a 12-parameter model. The *z* statistic maps will be converted to standard space using the transform responsible for morphing the mean image of each data set to the template to co-register all volumes.

The target ROI coordinates using in each fMRI-NFT session were converted to a binary mask. Since the ROI was determined from the first volume of the functional localizer, motion was corrected in the functional localizer data by registering each volume to the first volume using the method described above and a mean image was created. Next, the mean image of each neuromodulation run was registered to the mean image of the associated functional localizer using a rigid-body 12-parameter model. The transform responsible for morphing the mean image of each neuromodulation run was applied to the associated ROI mask. A1 control was assessed in both groups by masking the deactivation map from above with the registered ROI mask. A mixed-model ANOVA (between-subjects factor: group; within-subjects factors: session and run) was performed on the neuromodulation performance metric using SPSS (IBM SPSS statistics version 24.0, IBM Corp., Amonk, New York).

2. Behavior

    a. ACS

The total score was computed for each participant/session by summing the scores from the responses.[9] A 2x2 mixed-model ANOVA (between-subjects factor: group; within-subjects factor: session) was completed on the ACS total score to assess changes across pre- and post-training assessments. *Post hoc*, Bonferroni-corrected pairwise comparisons will be conducted on significant interaction effects. These analyses were completed using SPSS.

[9] Eleven (11) items were reverse-scored (4-1) while the other nine (9) items were normally scored (1-4).

The mixed-model ANOVA and *post hoc* testing was repeated for the fifteen (15) EXP and nine (9) CON participants which completed the follow-up assessment. This analysis was the same as that described above with the addition of the follow-up data to the session within-subjects factor.

b. AE

Emotionally-charged stimuli can attract attention, distracting individuals from a task. Therefore, the AE was analyzed to measure latency (*i.e.,* response time). Each trial was categorized as correct or incorrect. Mean latency was determined for the correct responses from each type (emotional or neutral) and session. A test statistic to analyze for outliers was performed using the following equation:

$$T1 = \frac{\mathrm{x(n)-x}}{s} \quad (11)$$

where *x(n)* is the latency of a single observation, *x* is the mean latency, and *s* is the standard deviation. The test statistic was compared to a critical value of 3.27 (Lovie, 1986). A final mean latency was recalculated by using the latencies with test statistics less than the critical value. To determine the impact of emotionally-charged stimuli on attention, the difference between the mean emotion and neutral latency was computed as a percent change.

A 2x2 mixed-model ANOVA (between-subjects factor: group; within-subjects factor: session) was completed on ΔAE mean latency to assess changes across pre- and post-training assessments. *Post hoc*, Bonferroni-corrected pairwise comparisons will be conducted on significant interaction effects. These analyses were completed using SPSS.

The mixed-model ANOVA and *post hoc* testing was repeated for the fifteen (15) EXP and nine (9) CON participants which completed the follow-up assessment. This analysis was the same as that described above with the addition of the follow-up data to the session within-subjects factor.

c. CPT-X

Assessment of the CPT-X is founded upon signal detection theory (SDT; Green & Swets, 1966). Each trial was separated each trial into one of four possibilities according to SDT: 1) target was not present and the response was indicated (*i.e.,* correct rejection), 2) target was present and the response was inhibited (*i.e.,* hit), 3) target was not present and the response was inhibited (*i.e.,* false alarm), and 4) target was present and the response was indicated (*i.e.,* miss). Using the hit and false alarm rates from each session, an index of sensitivity (d', *i.e.,* discriminability) was computed using the procedures previously verified (Sorkin, 1999). Sensitivity is desirable as it is free from motivational effects (Swets & Sewall, 1963). In summation, this process finds the *z* scores for which the standard normal cumulative distribution equals the hit and false alarm rates. The *z* score for the false alarm rate became indeterminate when the no false alarms were made, which was the case in several sessions. Therefore, a corrected false alarm rate was calculated when no false alarms were present using the equation:

$$1 - 2^{-1/\mathrm{t}} \quad (12)$$

where *t* is the number of correct rejection trials. Then, d' is calculated as the difference between the *z* score for the hit and false alarm rate ($z_{\mathrm{hit}} - z_{\mathrm{false\_alarm}}$).

A 2x2 mixed-model ANOVA (between-subjects factor: group; within-subjects factor: session) was completed on CPT-X d' to assess changes across pre- and post-training assessments. *Post hoc*, Bonferroni-corrected pairwise comparisons will be conducted on significant interaction effects. These analyses were completed using SPSS.

The mixed-model ANOVA and *post hoc* testing was repeated for the fifteen (15) EXP and nine (9) CON participants which completed the follow-up assessment. This analysis was the same as that described above with the addition of the follow-up data to the session within-subjects factor.

3. Neural Measures

a. A1 Response to Auditory Stimulation

The BOLD data acquired from each functional localizer was processed using FSL. First, individual (first-level) analyses will be conducted on each of the 4D fMRI data sets. Prior to the individual analyses, the data sets will be pre-processed in the same manner as that described in Section III.C.1 above except for the high-pass filter had a cutoff of 40 s. After pre-processing, a single EV will be defined by convolving a boxcar model containing 20 s rest and task conditions with a HRF (modeled by a gamma function; phase offset = 0 s, standard deviation = 3 s, mean lag = 6 s). The temporal derivative of the original waveform will be added to the result, accounting for small shifts in phase potentially improving the model fit. The temporal filter described above will be applied to the model, mimicking the pre-processing conducted on the measured data. The data set will be fit to the model using a GLM with prewhitening by applying a weight of +1 to the EV. This will be representative of activation during the task (positive correlation with the model). *Z* statistic maps will be created using standard statistical transforms to convert the β parameter maps. A clustering method will allow us to account for false positives due to multiple comparisons. This method considers adjacent voxels with a *z* statistic of 2.3 or greater to be a cluster. The significance of each cluster will be estimated and compared to a threshold of $p < 0.05$ using Gaussian Random Field theory. Voxels that either do not pass the significance level threshold or do not belong to a cluster will be set to zero. A mean image of the data set will be registered to the individual's high-resolution structural image by estimating motion from a boundary-based registration method including a fieldmap-based distortion correction (Greve & Fischl, 2009), then will be further registered to the MNI-152 T1-weighted 2 mm template provided in FSL using a 12-parameter model. The *z* statistic maps will be converted to standard space using the transform responsible for morphing the mean image of each data set to the template to co-register all volumes.

ROIs for the left and right A1 will be created from the Talairach atlas (Talairach & Tournoux, 1988). Indices for each region will be extracted and transformed to the Montreal Neurological Institute (MNI) space using the Talairach-to-ICBM transform (Lancaster et al., 2007). Resulting MNI coordinates will be will be translated into image indices (including rounding to the next highest integer). Binary masks representing each ROI will be created by setting the value of each index to 1 and all others to 0. Average activation in each ROI will be computed from the voxels which survived the cluster-based correction for multiple comparisons and whose value are above a threshold of Z = 2.3. A 2x2x2 (between-subjects factor: group, within-subjects factors: session and hemisphere) mixed-model ANOVA will be conducted on the left and right A1 average activity using SPSS. A significant session by group or session by group and hemisphere interaction will indicate differential changes in A1 activity across groups and training, supportive

of Hypothesis 3. Post hoc, pairwise, Bonferroni-corrected comparisons will be conducted in SPSS to compare A1 activity between groups at session 1 and 5 separately. We anticipate similar activity across groups at session 1, while a significant difference at session 5, with the experimental group showing reduced activity which will further support Hypothesis 3.

b. Resting-State Activity

The BOLD data acquired from the pre- and post-training resting-state fMRI was processed using FSL. Prior to the analysis, the data sets were pre-processed in the same manner as that described in Section III.C.1 except for the high-pass filter had a cutoff of 30 s. ICA was conducted on the pre-processed data. The MELODIC software of FSL will conduct a probabilistic ICA (Beckmann & Smith, 2004) using multisession temporal concatenation to create standard-order IC maps (the number of ICs will be approximately 1/4 to 1/6 of the total volumes acquired). Resulting IC maps were thresholded using an alternative hypothesis based on the fit of a Gaussian/gamma mixture model to the distribution of voxel intensities within the spatial maps (Beckmann, DeLuca, Devlin, & Smith, 2005) and a $p < 0.05$.

In a group analysis, voxel-based comparisons were made between groups and sessions using a dual-regression technique (Filippini et al., 2009; Littow et al., 2010; Veer et al., 2010). This technique performs multiple linear regression of the *z* statistic group IC maps against the individual pre-processed BOLD data to produce subject-variance normalized time courses for each component. Multiple linear regression of these time courses was then carried out against the pre-processed individual data sets to create subject-specific spatial maps. Non-parametric statistical differences were determined using permutation testing implemented using FSL Randomize incorporating threshold-free cluster enhancement (TFCE; Smith & Nichols, 2009). Null *t* distributions for a contrasts representative of the main effect of session and the interaction of session by group were derived by performing 1000 random permutations (Nichols & Holmes, 2002). Resultant *z* statistic difference maps were thresholded at $p < 0.05$ (corrected for family-wise error using TFCE) and resampled into standard space. The difference maps from the component representing the auditory network[10] were assessed. In the resulting 1-*p* images, voxels identified in the interaction effect of session by group at session 5 will indicate regions of the auditory network responding to fMRI-NFT[11], supportive of Hypothesis 4.

In an exploratory analysis, the IC maps from the components representing the default mode and executive control networks[12] were assessed in the same manner described above. In the resulting 1-*p* images, voxels identified in the effect of group at session 5 will indicate network nodes responding to fMRI-NFT.

---

[10] The component representing this network was determined from visual inspection of all the IC maps generated from the group multisession temporal concatenation ICA processing.

[11] In the 1-*p* images, voxels with a value between 0.95 and 1.0 (one-tailed) will indicate significant results when assessing only a single component.

[12] The components representing these networks will be determined from visual inspection of all the IC maps generated from the group multisession temporal concatenation ICA processing.

c. Steady-State Perfusion

Steady-state perfusion was assessed from ASL to quantify CBF. CBF was measured in units of mL/100 mg/min. Data was extracted from ROIs encompassing the left and right A1, ACC, medial frontal gyrus (MeFG), and STG using the Talairach atlas (Talairach & Tournoux, 1988). ROIs were generated in the same manner as described in Section **Error! Reference source not found.**. The proton density-weighted images acquired were registered to the individual's high-resolution structural image by estimating motion from a boundary-based registration method including a fieldmap-based distortion correction (Greve & Fischl, 2009), then further registered to the MNI-152 T1-weighted 2 mm template provided in FSL (Collins et al., 1995; Mazziotta et al., 2001) using a 12-parameter model (Jenkinson & Smith, 2001; Jenkinson et al., 2002). The CBF maps were converted to standard space using the transform responsible for morphing the proton density-weighted image of each data set to the template in order to co-register all volumes. Data from two (2) participants (1 CON, 1 EXP) was corrupted, therefore the analysis includes the remaining 8 CON and 17 EXP participants. 2x2x2 (between-subjects factor: group; within-subjects factors: session and hemisphere) mixed-model ANOVAs were carried out for each ROI. A significant session by group interaction, with the experimental group showing a greater reduction in perfusion will provide evidence for Hypothesis 5.

IV. Results

A. A1 Control

A mixed-model ANOVA evaluated the effects of group, session, and run on A1 activity during closed-loop neuromodulation. A1 activity is representative of an individual's ability to self-regulate brain activity of A1 (*i.e.*, A1 control). The descriptive statistics for this data is presented in Table 3. The results of the tests of between-subjects effects (Table 4) revealed a significant main effect of group ($p = 0.029$, one-tailed). One-tailed statistics are reported as the *a priori* hypothesis that A1 control would be greater in the EXP group. The ANOVA analysis included Mauchly's Test of Sphericity (Table 5) which determined that the variances of the differences between all possible pairs of within-subject conditions were not significant for the main effect of session ($p = 0.160$, two-tailed) or the interaction of session and run ($p = 0.776$, two-tailed). This test could not be conducted on the main effect of run because there is only a single difference to compute and, therefore, no comparison to be made. These results validate the assumption of sphericity, which will be used to assess the results of the within-subjects tests henceforth. The results of the within-subjects testing (Table 6) identify a significant main effect of session (Figure 15; $p = 0.0175$, one-tailed). One-tailed statistics are reported as our *a priori* hypothesis that A1 control would increase with training. The main effect of run was not significant ($p > 0.05$). The interaction effects of session by group, run by group, session by run, and session by group and run are not significant ($p > 0.05$).

Table 3. Descriptive statistics for A1 control measures separated by factors session, run, and group.

Session	Run	Group	Mean A1 Control (*z* statistic)	Std. Deviation	N
1	1	CON	-.513575	1.8176834	9
		EXP	-.109704	1.5335134	18
		Total	-.244328	1.6099299	27
	2	CON	-.364050	1.0258848	9
		EXP	1.009057	2.0692044	18
		Total	.551354	1.8863820	27
2	1	CON	.328114	2.5873677	9
		EXP	1.842709	2.7490086	18
		Total	1.337844	2.7441516	27
	2	CON	-.079995	2.7550314	9
		EXP	2.047707	2.1369636	18
		Total	1.338473	2.5230988	27
3	1	CON	.967520	3.1121580	9
		EXP	1.605297	2.7123791	18
		Total	1.392705	2.8079132	27
	2	CON	.203470	2.1023534	9
		EXP	1.971905	3.1324199	18
		Total	1.382427	2.9150025	27
4	1	CON	.587748	2.6300614	9
		EXP	1.979438	2.5839438	18
		Total	1.515541	2.6345602	27
	2	CON	.431830	2.2720221	9
		EXP	1.658697	2.8785080	18
		Total	1.249741	2.7117029	27
5	1	CON	.391666	2.6307519	9
		EXP	3.201307	3.0964049	18
		Total	2.264760	3.1968894	27
	2	CON	-.075156	2.5194464	9
		EXP	2.229866	3.4949272	18
		Total	1.461525	3.3415013	27

Table 4. Results of the between-subjects tests from the mixed-model ANOVA. Power is computed using an alpha of 0.05.

Source	Type III Sum of Squares	df	Mean Square	F	Sig. (one-tailed)	Partial Eta Squared	Observed Power
Intercept	22.381	1	22.381	6.073	.011	.195	.659
Group	14.524	1	14.524	3.941	.029	.136	.480
Error	92.135	25	3.685				

Table 5. The results of Mauchly's test of sphericity.

Within Subjects Effect	Mauchly's W	Approx. Chi-Square	df	Sig. (two-tailed)
Session	.572	13.074	9	.160
Session * Run	.786	5.643	9	.776

Table 6. Results of the within-subjects tests from the mixed-model ANOVA. Power is computed using an alpha of 0.05.

Factor	Type III Sum of Squares	df	Mean Square	F	Sig. (one-tailed)	Partial Eta Squared	Observed Power
Session	59.395	4	14.849	2.702	.0175	.098	.731
Session * Group	20.447	4	5.112	.930	.225	.036	.286
Run	.933	1	.933	.338	.283	.013	.087
Run * Group	2.506	1	2.506	.908	.175	.035	.150
Session * Run	11.377	4	2.844	1.772	.070	.066	.524
Session * Run * Group	6.121	4	1.530	.953	.218	.037	.292

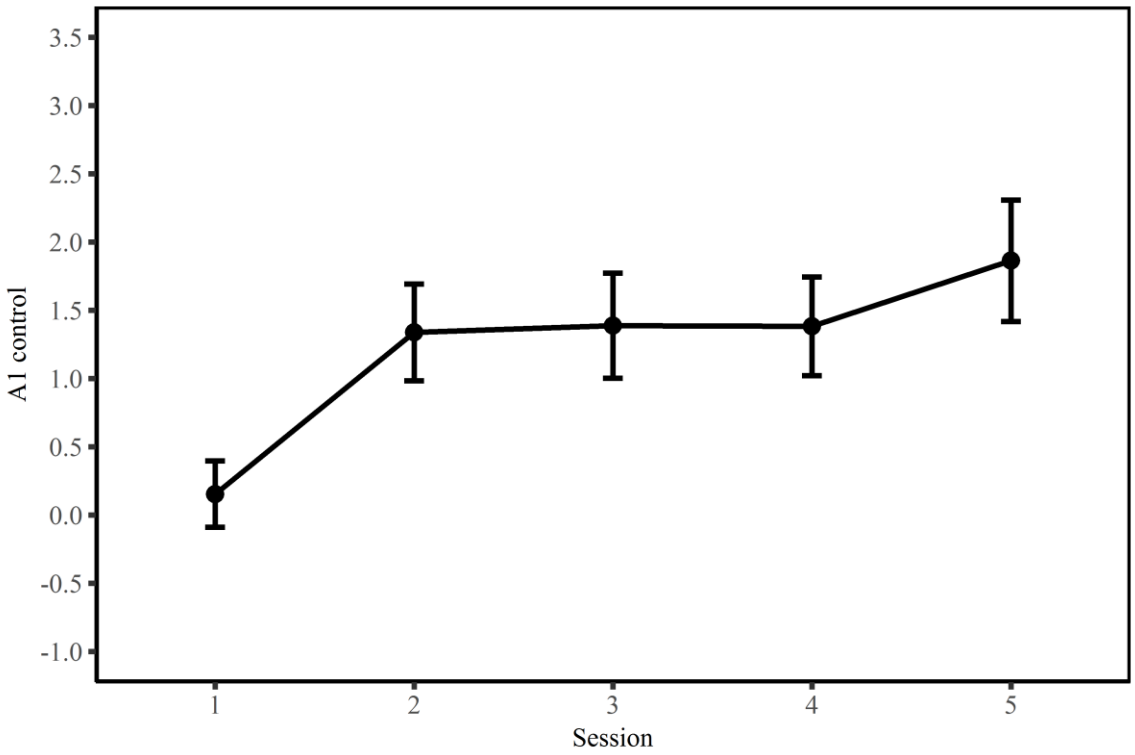

Figure 15. A1 Control averaged across groups and runs for each session. The main effect of session was found to be significant ($p = 0.0175$, one-tailed, sphericity assumed).

Post hoc Bonferroni-corrected pairwise comparisons were conducted on the session by group interaction (Table 7). These results revealed no significant difference between session 1 and 5 for the CON group ($p > 0.05$) however a significant difference between these sessions were identified in the EXP group ($p = 0.0165$, one-tailed). Furthermore, there was a significant difference between sessions 1 and 2 for the EXP group ($p = 0.038$, one-tailed).

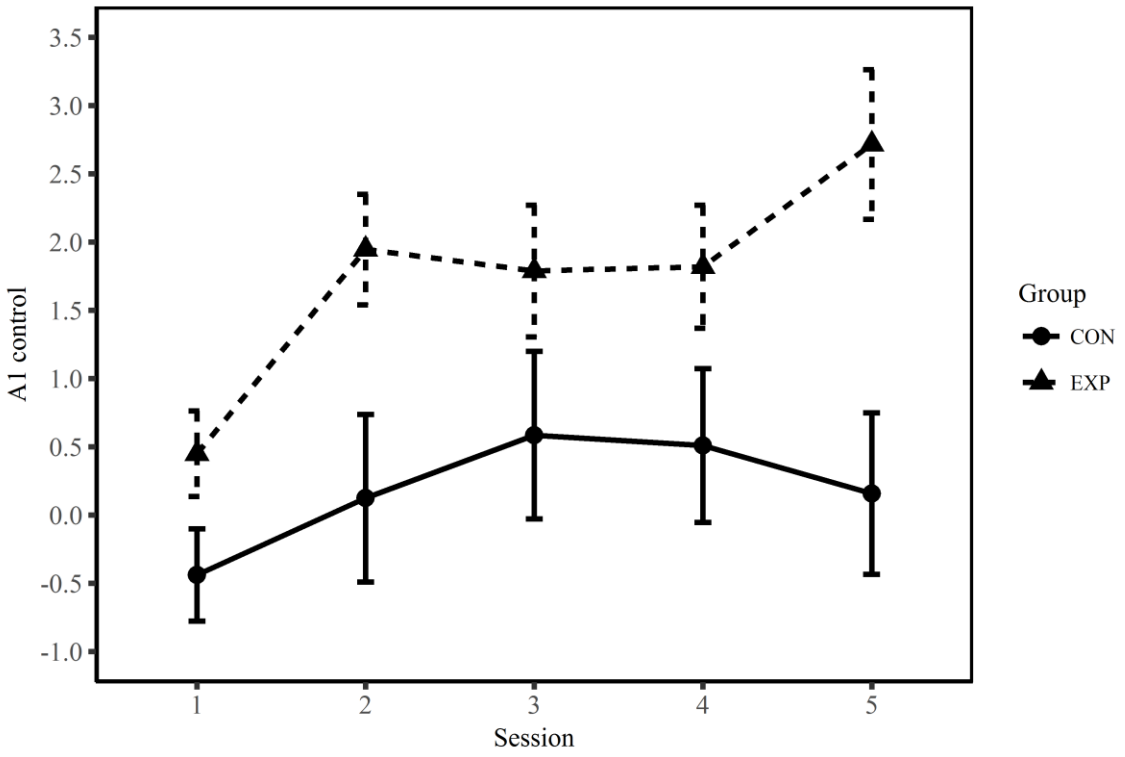

Figure 16. A1 control averaged across runs separated by group and session. The *post hoc* pairwise comparisons did not reveal any significant differences for the CON group, however sessions 2 ($p = 0.038$, one-tailed, Bonferroni-corrected) and 5 ($p = 0.0165$, one-tailed, Bonferroni-corrected) were found to be significantly greater than session 1 for the EXP group.

Table 7. Results of the *post hoc* pairwise comparisons for the session interaction with group. Confidence intervals and statistical significance was computed using Bonferroni correction for multiple comparisons. Statistical significance reported is one-tailed due to the *a priori* hypotheses.

Group	(I) Session	(J) Session	Mean Difference (I-J)	Std. Error	Sig.	95% Confidence Interval for Difference	
						Lower Bound	Upper Bound
CON	1	2	-.563	.730	1.000	-2.808	1.683
		3	-1.024	.802	1.000	-3.494	1.446
		4	-.949	.813	1.000	-3.451	1.554
		5	-.597	.978	1.000	-3.607	2.413
	2	3	-.461	.719	1.000	-2.676	1.753
		4	-.386	.828	1.000	-2.935	2.163
		5	-.034	.829	1.000	-2.586	2.518
	3	4	.076	.742	1.000	-2.208	2.360
		5	.427	.739	1.000	-1.848	2.702
	4	5	.352	.571	1.000	-1.407	2.110
EXP	1	2	-1.496	.516	.038	-3.083	.092
		3	-1.339	.567	.132	-3.086	.408
		4	-1.369	.575	.125	-3.139	.400
		5	-2.266	.692	.0165	-4.395	-.137
	2	3	.157	.509	1.000	-1.409	1.722
		4	.126	.586	1.000	-1.676	1.928
		5	-.770	.586	1.000	-2.575	1.034
	3	4	-.030	.525	1.000	-1.646	1.585
		5	-.927	.523	.441	-2.535	.682
	4	5	-.897	.404	.178	-2.140	.347

B. Behavior

1. ACS

Mixed-model ANOVAs evaluated the effects of group and session on ACS total score. The ACS total score is a subjective measure of attentional control. First are presented the results of the ANOVA which evaluated the ACS scores for sessions 1 and 5 (Table 8). The results of the tests of between-subjects effects revealed main effect of group was not significant (Table 9; $p > 0.05$, one-tailed). One-tailed statistics are reported as the *a priori* hypothesis that ACS total score would be greater in the EXP group. Mauchly's Test of Sphericity could not be conducted on the within-subjects factors because there is only a single difference to compute and, therefore, no comparison to be made. However, this test was conducted and significant on the 2x3 ANOVA (analysis and results below), therefore the assumption of sphericity is not validated and Greenhouse-Geisser correction will be applied. The results of the within-subjects testing (Table 10) identified the main effect of session was not significant (Figure 17; $p > 0.05$, one-tailed). One-tailed statistics are reported as our *a priori* hypothesis that ACS total score would increase with training. The interaction effect of session and group was not significant ($p > 0.05$), therefore no *post hoc* testing was performed.

Table 8. Descriptive statistics for ACS total score for sessions 1 and 5 separated by group.

Session	Group	Mean ACS total score	Std. Deviation	N
1	CON	49.3333	8.70345	9
	EXP	49.6667	9.39336	18
	Total	49.5556	9.00142	27
5	CON	48.8889	8.63777	9
	EXP	49.8889	11.51924	18
	Total	49.5556	10.48564	27

Table 9. Results of the between-subjects tests from the 2x2 mixed-model ANOVA. Power is computed using an alpha of 0.05.

Source	Type III Sum of Squares	df	Mean Square	F	Sig. (one-tailed)	Partial Eta Squared	Observed Power
Intercept	58674.074	1	58674.074	632.536	< .001	.962	1.000
Group	2.667	1	2.667	.029	.433	.001	.053
Error	2319.000	25	92.760				

Table 10. Results of the within-subjects tests from the 2x2 mixed-model ANOVA. Power is computed using an alpha of 0.05.

Factor	Type III Sum of Squares	df	Mean Square	F	Sig. (one-tailed)	Partial Eta Squared	Observed Power
Session	.148	1	.148	.012	.457	.000	.051
Session * Group	1.333	1	1.333	.104	.375	.004	.061

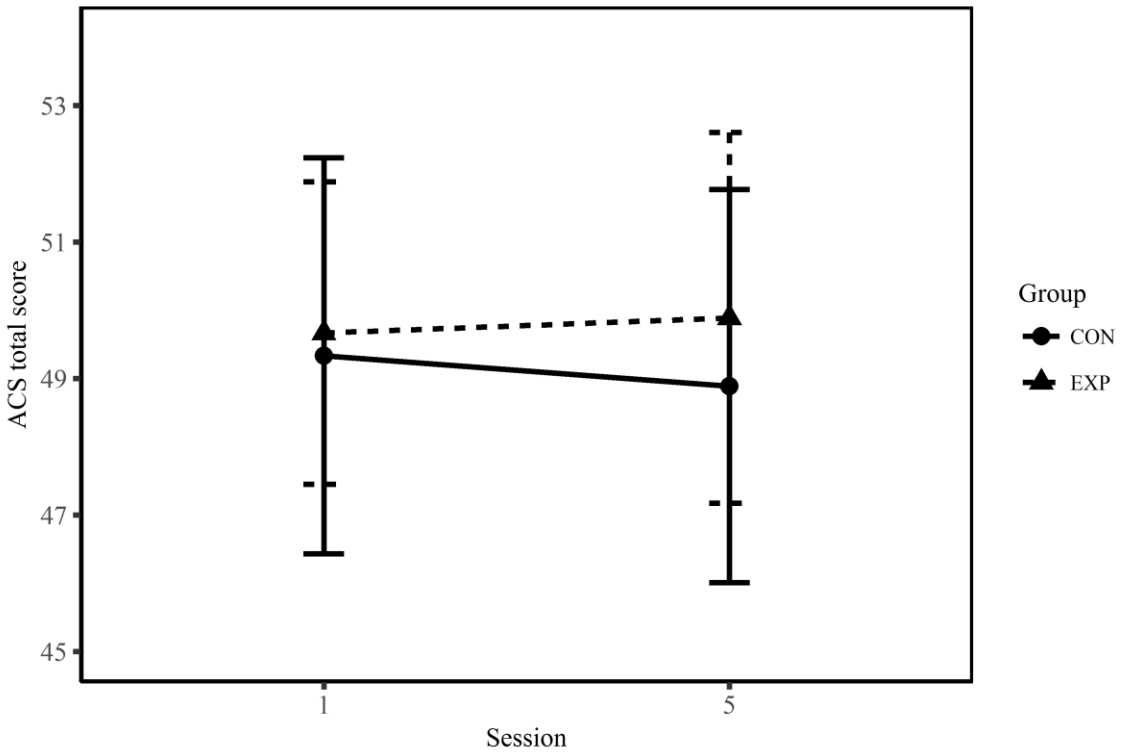

Figure 17. ACS total score averaged across participants for each group and session. No significant main effects or interactions were found.

Next are the results from the 2x3 mixed-model ANOVA which evaluated the ACS scores for sessions 1, 5, and the follow-up (Table 11). The results of the tests of between-subjects effects revealed main effect of group was not significant (Table 12; $p > 0.05$, one-tailed). One-tailed statistics are reported as the *a priori* hypothesis that ACS total score would be greater in the EXP group. Mauchly's Test of Sphericity was significant (Table 13; $p = 0.02$, two-tailed), therefore the assumption of sphericity is not validated and Greenhouse-Geisser correction will be applied. The results of the within-subjects testing (Table 14) identified the main effect of session was not significant (Figure 18; $p > 0.05$, one-tailed). One-tailed statistics are reported as our *a priori* hypothesis that ACS total score would increase with training. The interaction effect of session and group was not significant ($p > 0.05$), therefore no *post hoc* testing was performed.

Table 11. Descriptive statistics for ACS total score for sessions 1, 5, and the follow-up separated group.

Session	Group	Mean ACS total score	Std. Deviation	N
1	CON	49.3333	8.70345	9
	EXP	49.5333	9.73115	15
	Total	49.4583	9.16505	24
5	CON	48.8889	8.63777	9
	EXP	50.2000	12.07832	15
	Total	49.7083	10.73183	24
Follow-Up	CON	49.3333	11.55422	9
	EXP	49.8667	12.64836	15
	Total	49.6667	11.99517	24

Table 12. Results of the between-subjects tests from the 2x3 mixed-model ANOVA. Power is computed using an alpha of 0.05.

Source	Type III Sum of Squares	df	Mean Square	F	Sig. (one-tailed)	Partial Eta Squared	Observed Power
Intercept	55188.390	1	55188.390	516.320	< .001	.959	1.000
Group	2.612	1	2.612	.024	.438	.001	.053
Error	2351.536	22	106.888				

Table 13. The results of Mauchly's test of sphericity.

Within-Subjects Effect	Mauchly's W	Approx. Chi-Square	df	Sig. (two-tailed)
Session	.689	7.836	2	.020

Table 14. Results of the within-subjects tests from the 2x3 mixed-model ANOVA. Power is computed using an alpha of 0.05.

Factor	Type III Sum of Squares	df	Mean Square	F	Sig. (one-tailed)	Partial Eta Squared	Observed Power
Session	.324	1.525	.212	.009	.488	.000	.051
Session * Group	3.657	1.525	2.398	.098	.428	.004	.062

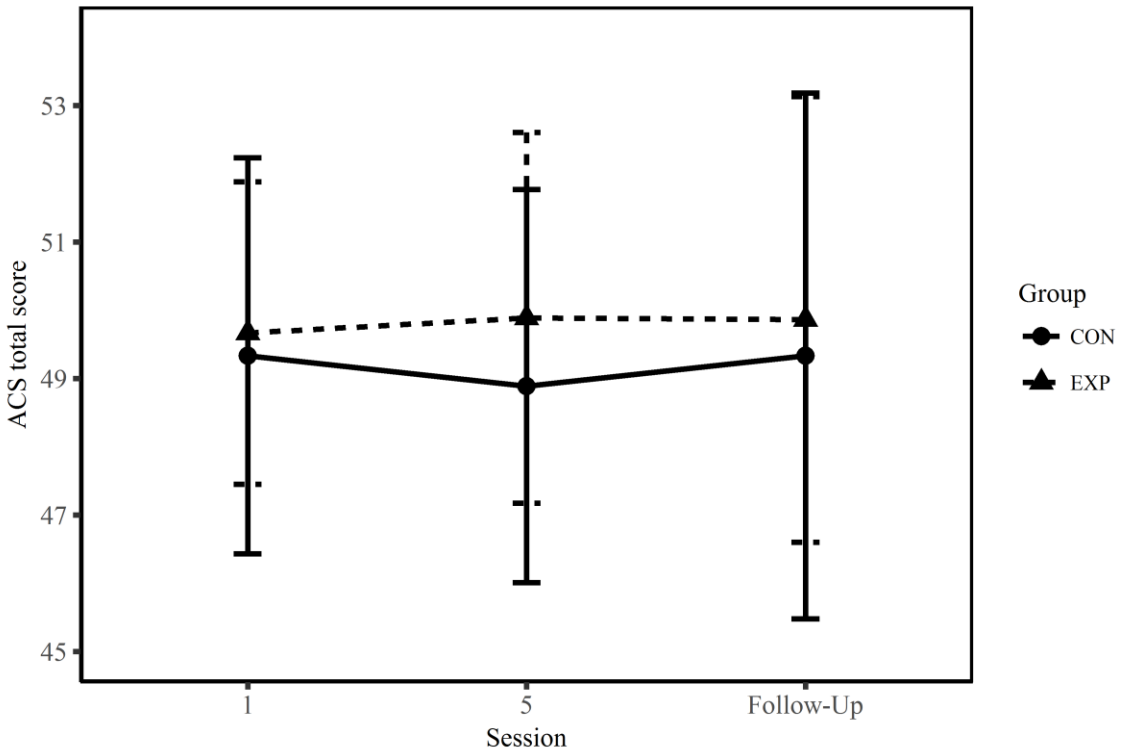

Figure 18. ACS total score averaged across participants for each group and session. No significant main effects or interactions were found.

2. AE

Mixed-model ANOVAs evaluated the effects of group and session on ΔAE mean latency. First are the results of the ANOVA which evaluated sessions 1 and 5 (Table 15). The results of the tests of between-subjects effects (Table 16) revealed the main effect of group was significant ($p = 0.042$, one-tailed), with a larger impact of emotionally-charged stimuli on attention in the EXP group. Mauchly's Test of Sphericity could not be conducted on the within-subjects factors because there is only a single difference to compute and, therefore, no comparison to be made. However, this test was conducted on the 2x3 ANOVA (analysis and results below) but was not significant for the main effect of session ($p > 0.05$). Therefore, the assumption of sphericity is valid. The results of the within-subjects testing (Table 17) identified the main effect of session and the session by group interaction effect were not significant (Figure 19; $p > 0.05$). One-tailed statistics are reported as our *a priori* hypothesis that the impact of emotionally-charged stimuli would decrease with training.

Table 15. Descriptive statistics for ΔAE mean latency for sessions 1 and 5 separated by group and emotion.

Session	Group	ΔAE Mean Latency (%)	Std. Deviation (ms)	N
1	CON	.3178	5.07895	9
	EXP	3.5611	6.42796	18
	Total	2.4800	6.11397	27
5	CON	1.0833	6.68607	9
	EXP	3.9639	4.94246	18
	Total	3.0037	5.62511	27

Table 16. Results of the between-subjects tests from the 2x2 mixed-model ANOVA. Power is computed using an alpha of 0.05.

Source	Type III Sum of Squares	df	Mean Square	F	Sig. (one-tailed)	Partial Eta Squared	Observed Power
Intercept	119.513	1	119.513	6.940	.007	.217	.716
Group	56.253	1	56.253	3.267	.042	.116	.412
Error	430.527	25	17.221				

Table 17. Results of the within-subjects tests from the 2x2 mixed-model ANOVA. Power is computed using an alpha of 0.05.

Factor	Type III Sum of Squares	df	Mean Square	F	Sig. (one-tailed)	Partial Eta Squared	Observed Power
Session	4.095	1	4.095	.125	.364	.005	.063
Session * Group	.395	1	.395	.012	.457	.000	.051

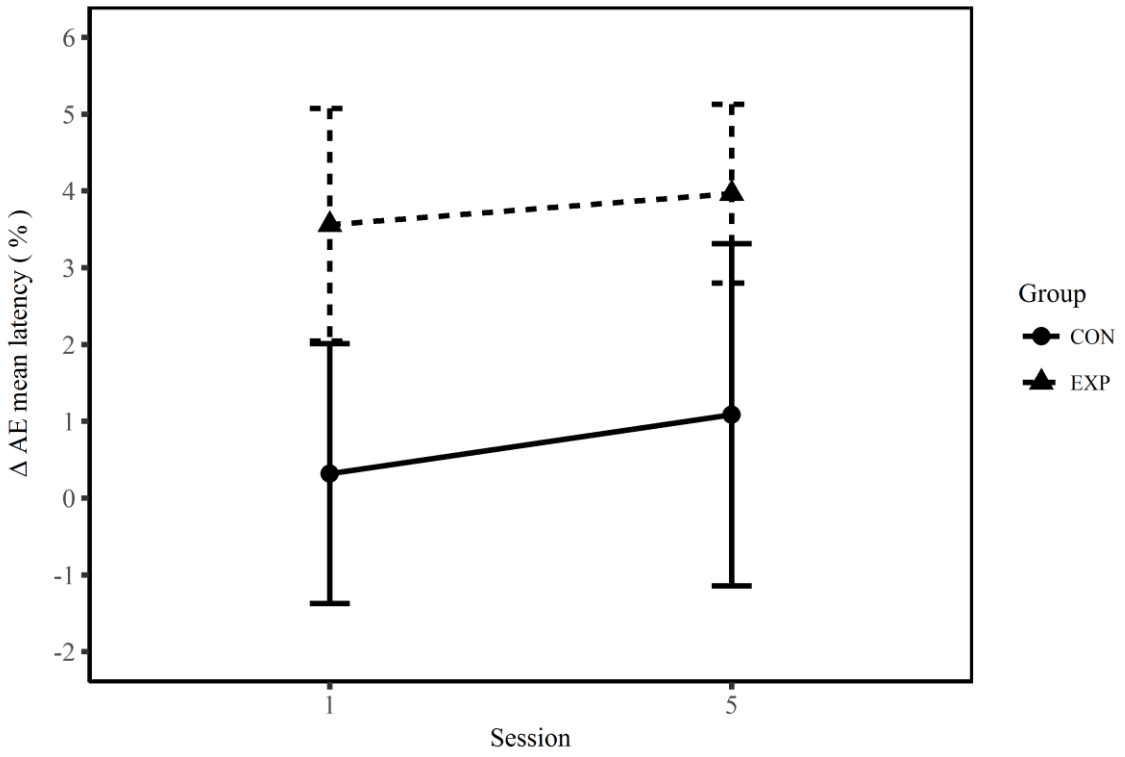

Figure 19. ΔAE mean latency averaged across participants for each session and group. ΔAE mean latency was found to be significantly greater in the EXP group.

Next are the results from the 2x3 mixed-model ANOVA which evaluated the ΔAE mean latency for sessions 1, 5, and the follow-up (Table 18). The results of the tests of between-subjects effects (Table 19) revealed the main effect of group was not significant ($p > 0.05$, one-tailed). One-tailed statistics are reported as the *a priori* hypothesis that AE latency would be lower in the EXP group. Mauchly's Test of Sphericity was not significant for the main effect of session (Table 21; $p > 0.05$, two-tailed), therefore the assumption of sphericity was validated. The results of the within-subjects testing (Table 21) identified the main effect of session and the session by group interaction were not significant (Figure 20; $p > 0.05$, one-tailed). One-tailed statistics are reported as our *a priori* hypothesis that the impact of emotionally-charged stimuli would decrease with training.

Table 18. Descriptive statistics for ΔAE mean latency for sessions 1, 5, and the follow-up separated by group and emotion.

Session	Group	ΔAE Mean Latency (%)	Std. Deviation (ms)	N
1	CON	.3178	5.07895	9
	EXP	2.9673	6.57527	15
	Total	1.9738	6.08323	24
5	CON	1.0833	6.68607	9
	EXP	3.9313	5.32265	15
	Total	2.8633	5.89724	24
Follow-Up	CON	2.9371	4.57266	9
	EXP	1.1399	5.81798	15
	Total	1.8138	5.35410	24

Table 19. Results of the between-subjects tests from the 2x3 ANOVA. Power is computed using an alpha of 0.05.

Source	Type III Sum of Squares	df	Mean Square	F	Sig. (one-tailed)	Partial Eta Squared	Observed Power
Intercept	95.740	1	95.740	7.626	.006	.257	.752
Group	8.558	1	8.558	.682	.209	.030	.124
Error	276.182	22	12.554				

Table 20. The results of Mauchly's test of sphericity for the 2x3 ANOVA.

Within-Subjects Effect	Mauchly's W	Approx. Chi-Square	df	Sig. (two-tailed)
Session	.911	1.964	2	.375

Table 21. Results of the within-subjects tests from the 2x3 ANOVA. Power is computed using an alpha of 0.05.

Factor	Type III Sum of Squares	df	Mean Square	F	Sig. (one-tailed)	Partial Eta Squared	Observed Power
Session	8.433	2	4.217	.135	.437	.006	.069
Session * Group	77.609	2	38.804	1.239	.150	.053	.256

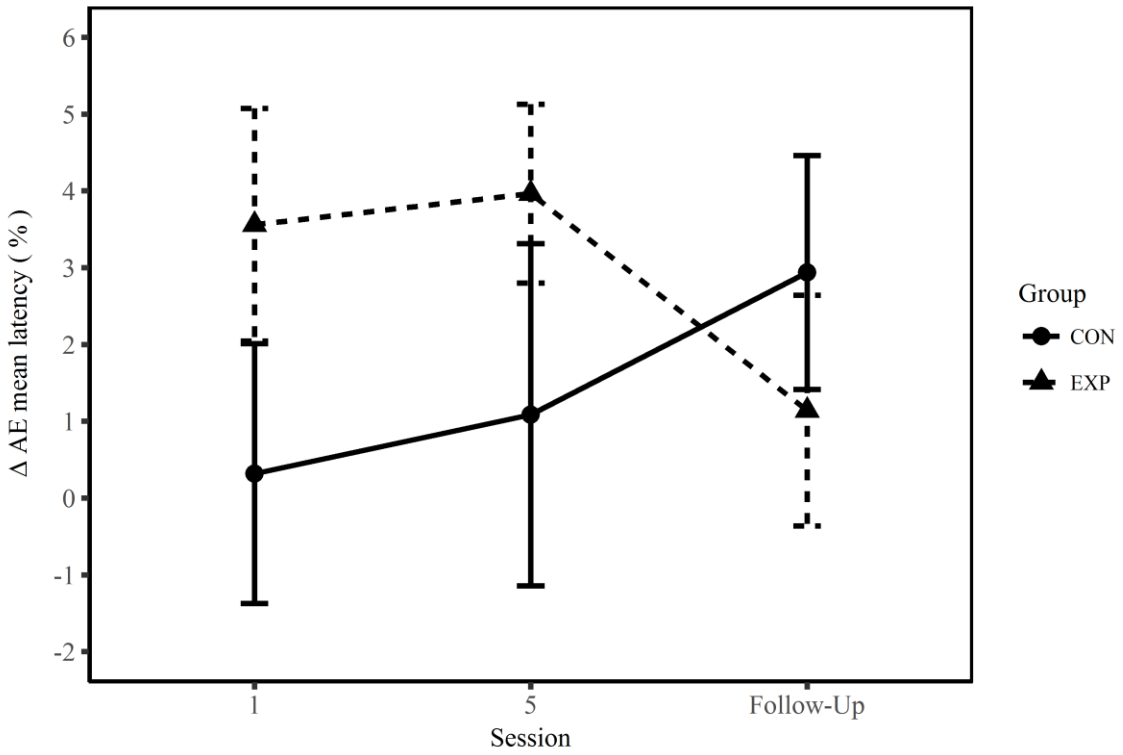

Figure 20. ΔAE mean latency averaged across participants for each session and group.

3. CPT-X

Mixed-model ANOVAs evaluated the effects of group and session on CPT-X sensitivity (d'). First the results of the ANOVA which evaluated the d' for sessions 1 and 2 (Table 22). The results of the tests of between-subjects effects revealed main effect of group was not significant (Table 23; $p > 0.05$, one-tailed). One-tailed statistics are reported as the *a priori* hypothesis that CPT-X sensitivity would be greater in the EXP group. Mauchly's Test of Sphericity could not be conducted on the within-subjects factors because there is only a single difference to compute and, therefore, no comparison to be made. However, this test was conducted and not significant on the 2x3 ANOVA (analysis and results below), therefore the assumption of sphericity is valid. The results of the within-subjects testing (Table 24) identified the main effect of session was not significant (Figure 21; $p > 0.05$, one-tailed). One-tailed statistics are reported as our *a priori* hypothesis that CPT-X sensitivity would increase with training. The interaction effect of session and group was not significant ($p > 0.05$), therefore no *post hoc* testing was performed.

Table 22. Descriptive statistics for CPT-X d' for sessions 1 and 5 separated by group.

Session	Group	Mean CPT-X d'	Std. Deviation	N
1	CON	3.5175	.44068	9
	EXP	3.4090	.37979	18
	Total	3.4452	.39596	27
5	CON	3.6271	.57090	9
	EXP	3.4995	.50729	18
	Total	3.5420	.52183	27

Table 23. Results of the between-subjects tests from the 2x2 mixed-model ANOVA. Power is computed using an alpha of 0.05.

Source	Type III Sum of Squares	df	Mean Square	F	Sig. (one-tailed)	Partial Eta Squared	Observed Power
Intercept	296.233	1	296.233	1795.844	< .001	.986	1.000
Group	.084	1	.084	.507	.242	.020	.105
Error	4.124	25	.165				

Table 24. Results of the within-subjects tests from the 2x2 mixed-model ANOVA. Power is computed using an alpha of 0.05.

Factor	Type III Sum of Squares	df	Mean Square	F	Sig. (one-tailed)	Partial Eta Squared	Observed Power
Session	.120	1	.120	1.095	.153	.042	.172
Session * Group	.001	1	.001	.010	.461	.000	.051

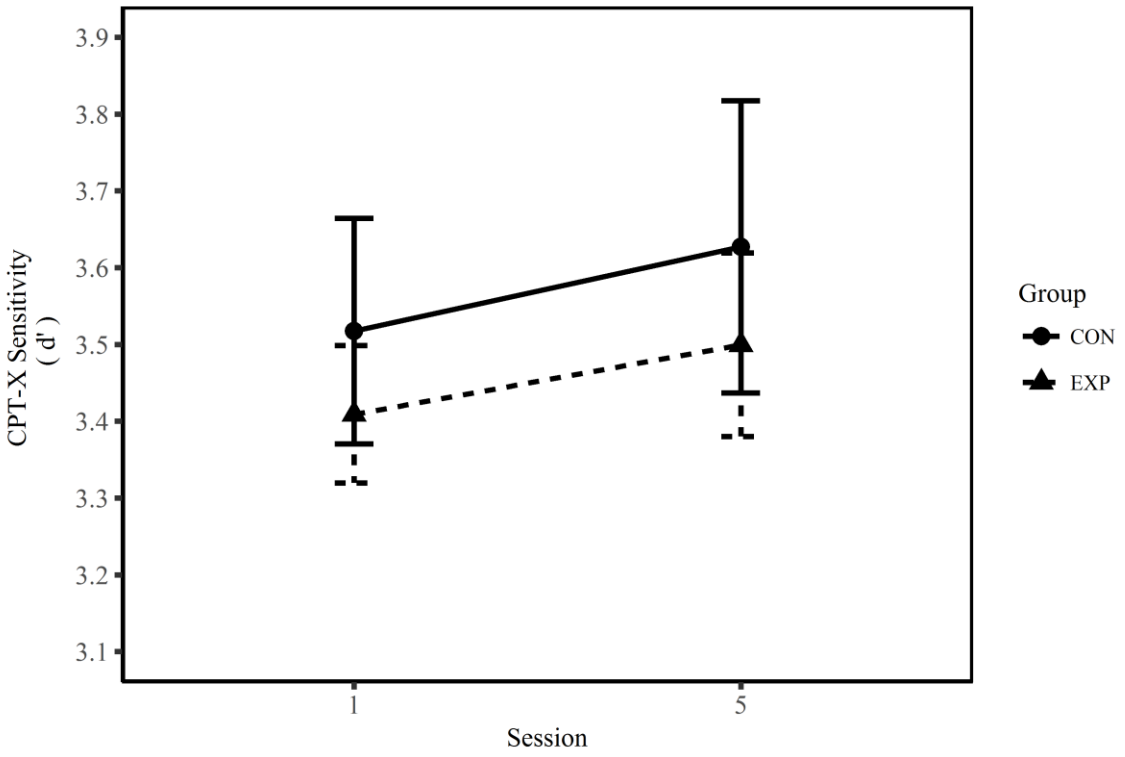

Figure 21. CPT-X sensitivity (d') averaged across participants for each group and session. No significant main effects or interactions were found.

The data from the 2x3 mixed-model ANOVA analysis of the CPT-X sensitivity are presented in (Table 25). The results of the tests of between-subjects effects revealed main effect of group was not significant (Table 26; $p > 0.05$, one-tailed). One-tailed statistics are reported as the *a priori* hypothesis that CPT-X sensitivity would be greater in the EXP group. Mauchly's Test of Sphericity was significant (Table 27; $p = 0.02$, two-tailed), therefore the assumption of sphericity is valid and utilized for the within-subject tests. The results of the within-subjects testing (Table 28) identified the main effect of session was not significant (Figure 22; $p > 0.05$, one-tailed). One-tailed statistics are reported as our *a priori* hypothesis that ACS total score would increase with training. The interaction effect of session and group was not significant ($p > 0.05$), therefore no *post hoc* testing was performed.

Table 25. Descriptive statistics for CPT-X sensitivity for sessions 1, 5, and the follow-up separated group.

Session	Group	Mean CPT-X d’	Std. Deviation	N
1	CON	3.5175	.44068	9
	EXP	3.3937	.40907	15
	Total	3.4402	.41612	24
5	CON	3.6271	.57090	9
	EXP	3.4806	.47020	15
	Total	3.5356	.50318	24
Follow-Up	CON	3.4909	.47909	9
	EXP	3.3489	.63650	15
	Total	3.4022	.57565	24

Table 26. Results of the between-subjects tests from the 2x3 mixed-model ANOVA. Power is computed using an alpha of 0.05.

Source	Type III Sum of Squares	df	Mean Square	F	Sig. (one-tailed)	Partial Eta Squared	Observed Power
Intercept	271.931	1	271.931	1375.944	< .001	.984	1.000
Group	.106	1	.106	.538	.236	.024	.108
Error	4.348	22	.198				

Table 27. The results of Mauchly's test of sphericity.

Within-Subjects Effect	Mauchly's W	Approx. Chi-Square	df	Sig. (two-tailed)
Session	.794	4.836	2	.089

Table 28. Results of the within-subjects tests from the 2x3 mixed-model ANOVA. Power is computed using an alpha of 0.05.

Factor	Type III Sum of Squares	df	Mean Square	F	Sig. (one-tailed)	Partial Eta Squared	Observed Power
Session	.217	2	.108	1.172	.159	.051	.244
Session * Group	.002	2	.001	.009	.496	.000	.051

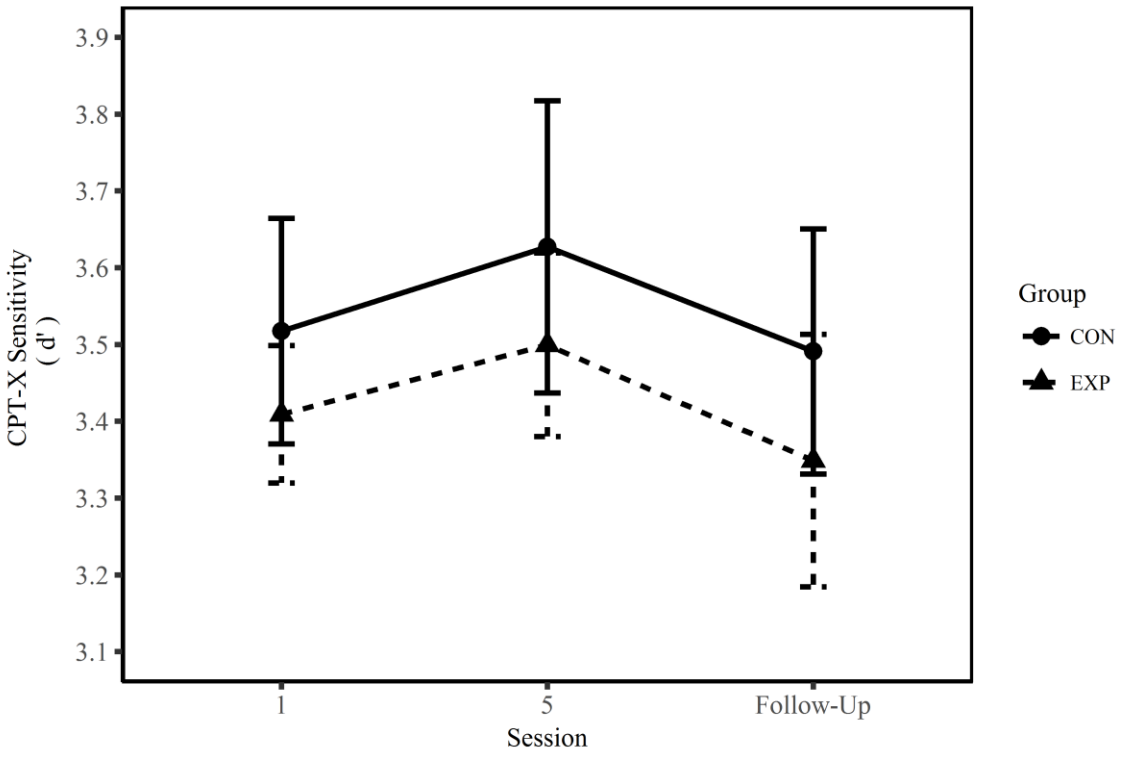

Figure 22. CPT-X sensitivity averaged across participants for each group and session. No significant main effects or interactions were found.

C. Neural Measures

1. A1 Response to Auditory Stimulation

A mixed-model ANOVA evaluated the effects of group, session, and hemisphere on A1 activity during continuous noise stimulation. The results of the test of between-subjects effects revealed the main effect of group was not significant (Table 29; $p > 0.05$, one-tailed). One-tailed statistics are reported as the *a priori* hypothesis that A1 activity would be lower in the EXP group. Mauchly's Test of Sphericity could not be conducted on the within-subjects factors because there is only a single difference to compute and, therefore, no comparison to be made and sphericity was assumed. The results of the within-subjects testing (Table 30) identified the main effect of session was significant ($p = 0.0115$, one-tailed), with decreased activation in session 5 (Figure 23). One-tailed statistics are reported as our *a priori* hypothesis that A1 activity induced from continuous noise stimulation would decrease with training. All other main effects and interactions were not significant ($p > 0.05$), therefore no *post hoc* testing was performed.

Table 29. Results of the between-subjects tests from the 2x2x2 mixed-model ANOVA for A1 activity during continuous noise stimulation. Power is computed using an alpha of 0.05.

Source	Type III Sum of Squares	df	Mean Square	F	Sig. (one-tailed)	Partial Eta Squared	Observed Power
Intercept	60.390	1	60.390	60.158	.000	.706	1.000
Group	.003	1	.003	.003	.478	.000	.050
Error	25.096	25	1.004				

Table 30. Results of the within-subjects tests from the 2x2 mixed-model ANOVA. Power is computed using an alpha of 0.05.

Factor	Type III Sum of Squares	df	Mean Square	F	Sig. (one-tailed)	Partial Eta Squared	Observed Power
Session	14.184	1	14.184	5.844	0.0115	.189	.642
Session * Group	2.907	1	2.907	1.198	0.142	.046	.183
Hemisphere	.550	1	.550	.612	0.2205	.024	.117
Hemisphere * Group	.899	1	.899	.999	0.1635	.038	.161
Session * Hemisphere	.626	1	.626	1.774	0.0975	.066	.249
Session * Hemisphere * Group	.223	1	.223	.632	0.217	.025	.119

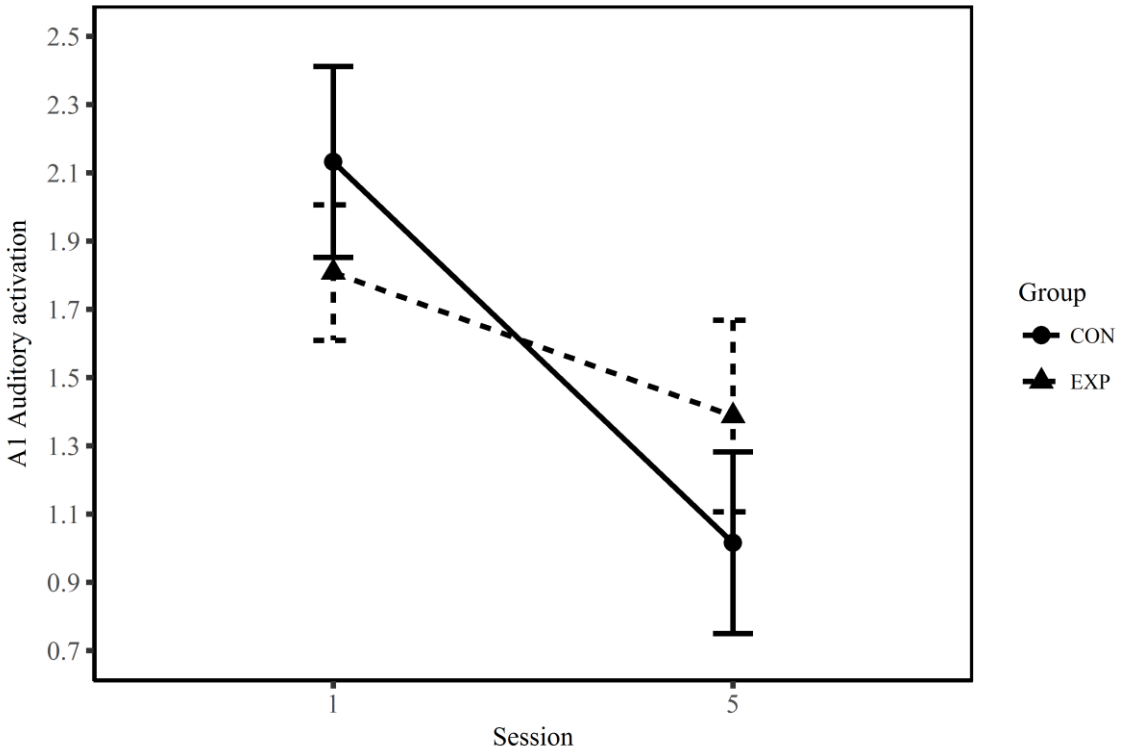

Figure 23. A1 activity in response to continuous noise stimulation. Averaged across groups and hemispheres, activity during session 5 was significantly lower than session 1.

2. Resting-State Activity

Probabilistic ICA resulted in 63 components identified automatically, approximately 1/5 of the total volumes acquired). From these components, three (3) components were identified each representing the auditory network (Figure 24), DMN (Figure 25), or the executive control network (Figure 26).

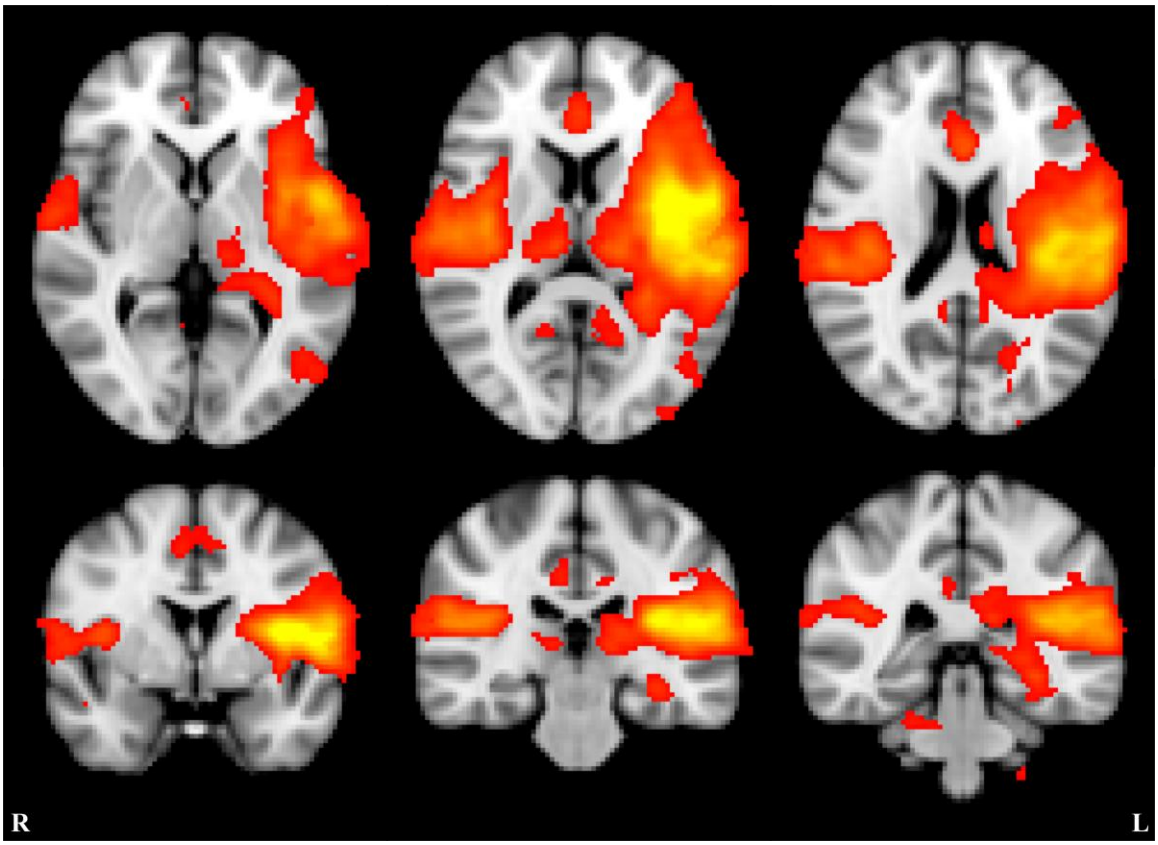

Figure 24. Resting auditory network. Axial slices are displayed at MNI coordinates z = 2, 10 and 20 mm (left to right). Coronal slices are displayed at MNI coordinates y = 0, 26, and 34 mm (left to right).

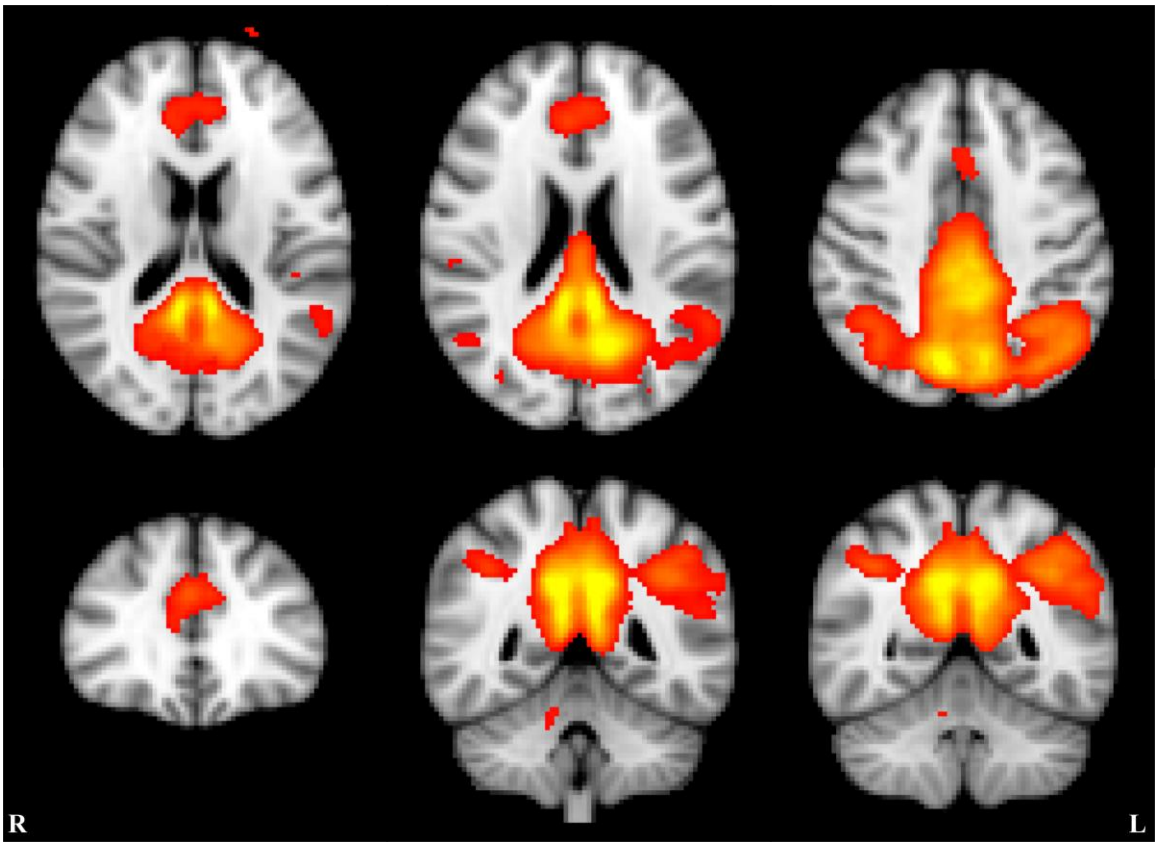

Figure 25. Default mode network. Axial slices are displayed at MNI coordinates z = 18, 22, and 42 mm (left to right). Coronal slices are displayed at MNI coordinates y = 32, 48, and 52 mm (left to right).

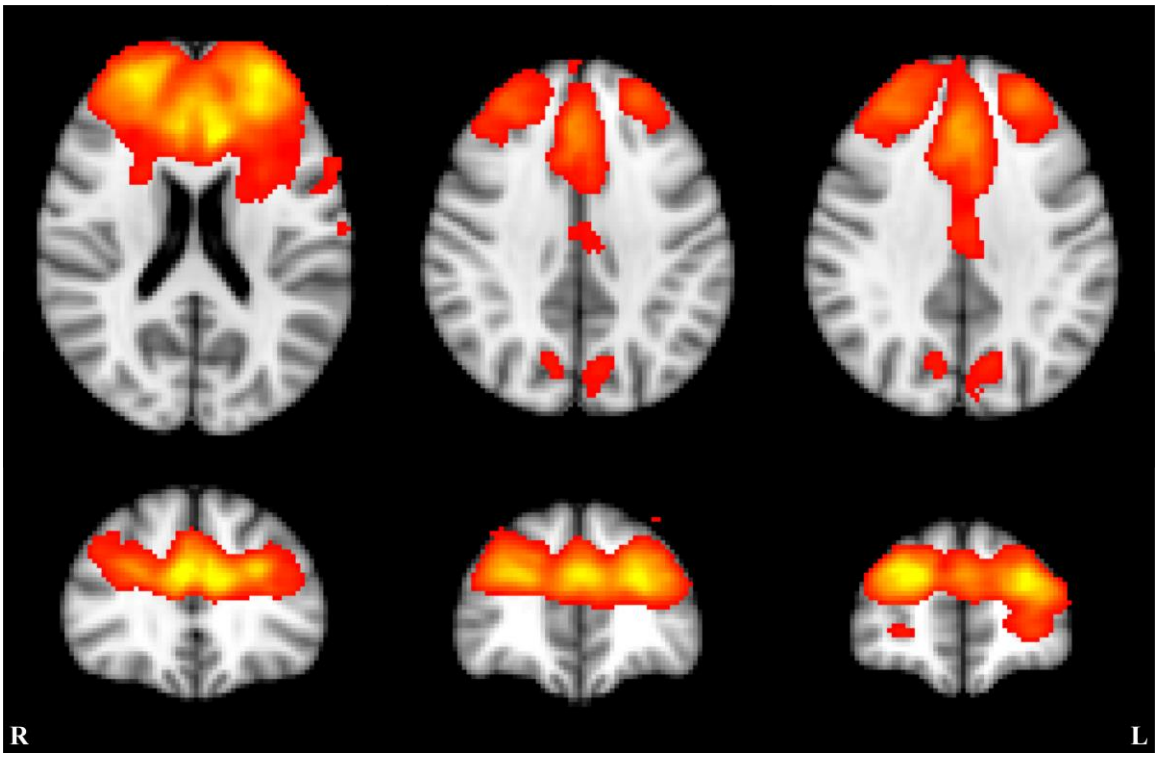

Figure 26. Resting executive control network. Axial slices are displayed at MNI coordinates z = 0, 4, and 6 mm (left to right). Coronal slices are displayed at MNI coordinates y = 32, 42, and 52 mm (left to right).

A voxel-wise dual-regression technique was carried out to assess the effect of session and session by group on these three networks. There was no main effect of session within the executive control network ($p > 0.05$), however there was a significant main effect of session in the auditory network and DMN ($p < 0.05$, one-tailed). Regions in the auditory network were found to have significantly enhanced connectivity over the course of training were identified as the left STG, transverse temporal gyrus, and postcentral gyrus (Figure 27). For the DMN, enhanced connectivity (Figure 28) over training were found predominately in the left hemisphere: BA19, precuneus, middle frontal gyrus, supramarginal gyrus, and the inferior parietal lobule; but bilateral effects were observed in the superior frontal gyrus. Additionally, increased connectivity was observed in the right transverse temporal gyrus. No significant session by group interaction was found in any of the three networks ($p > 0.05$, one-tailed).

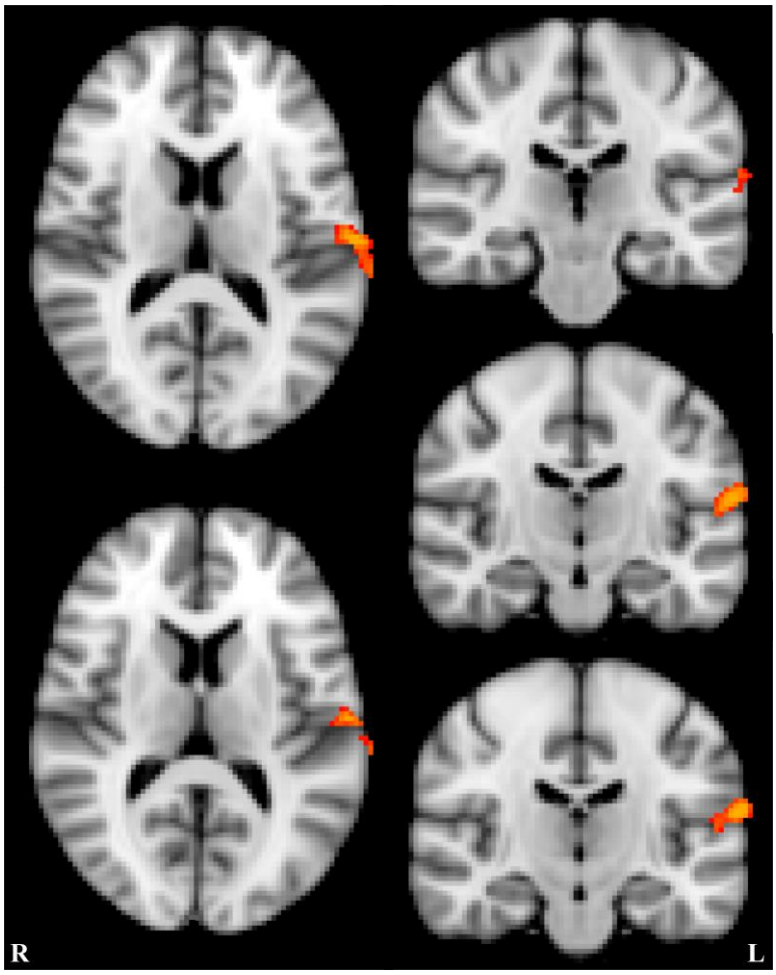

Figure 27. Effect of session in the resting auditory network. The left STG, transverse temporal gyrus, and postcentral gyrus had significantly enhanced connectivity over the course of training. Axial slices are displayed at MNI coordinates z = 12 and 14 mm (top to bottom). Coronal slices are displayed at MNI coordinates y = -24, -18, and -16 mm (top to bottom).

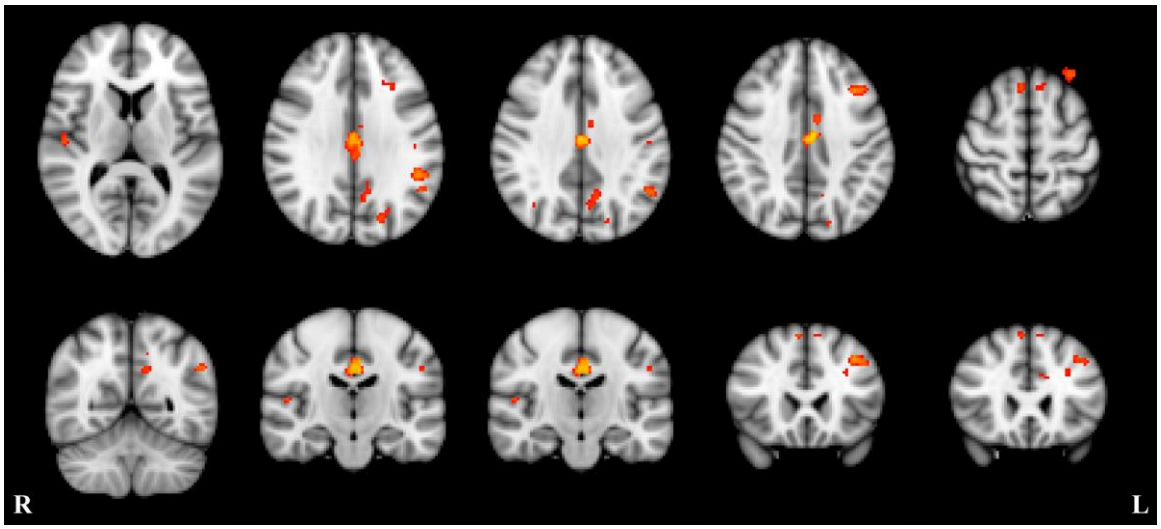

Figure 28. Effect of session in the DMN. Enhanced connectivity was observed only in the left hemisphere include BA19, precuneus, middle frontal gyrus, supramarginal gyrus, and the inferior parietal lobule; while the right transverse temporal gyrus demonstrated increased connectivity. Bilateral increased connectivity was observed in the superior frontal gyrus. Axial slices are displayed at MNI coordinates z = 10, 30, 34, 38, and 58 mm (left to right). Coronal slices are displayed at MNI coordinates y = -56, -40, -18, 22, and 24 mm (top to bottom).

3. Steady-State Perfusion

Mixed-model ANOVAs evaluated the effects of group, session, and hemisphere on CBF from four ROIs (Appendix I). The results of the tests of between-subjects effects revealed main effect of group was not significant for all four ROIs (Table 31; $p > 0.05$, one-tailed). One-tailed statistics are reported as the *a priori* hypothesis that resting CBF would be lower in the EXP group. Mauchly's Test of Sphericity could not be conducted on the within-subjects factors because there is only a single difference to compute and, therefore, no comparison to be made and sphericity was assumed. The results of the within-subjects testing identified the main effect of hemisphere was significant for all four ROIs (Table 32; $p < 0.05$, one-tailed). One-tailed statistics are reported as our *a priori* hypothesis that resting CBF would decrease with training. Interestingly, the right hemisphere had greater resting CBF than the left for regions associated with auditory processing (A1 and STG) while the opposite was found for regions involved in attentional processes (ACC, MeFG). All other main effects and interactions were not significant ($p > 0.05$), therefore no *post hoc* testing was performed.

Table 31. Results of the between-subjects tests from the 2x2x2 mixed-model ANOVAs for each ROI. Power is computed using an alpha of 0.05.

ROI	Source	Type III Sum of Squares	df	Mean Square	F	Sig. (one-tailed)	Partial Eta Squared	Observed Power
A1	Intercept	80669.702	1	80669.7	1294.546	< .001	.983	1.000
	Group	60.661	1	60.661	.973	.167	.041	0.157
	Error	1433.246	23	62.315				
STG	Intercept	67839.499	1	67839.4	1487.024	< .001	.985	1.000
	Group	42.684	1	42.684	.936	.172	.039	.153
	Error	1049.282	23	45.621				
ACC	Intercept	48951.536	1	48951.5	1376.936	< .001	.984	1.000
	Group	40.794	1	40.794	1.147	.148	.048	.177
	Error	817.675	23	35.551				
MeFG	Intercept	57576.836	1	57576.8	1250.924	< .001	.982	1.000
	Group	10.228	1	10.228	.222	.321	.010	.074
	Error	1058.632	23	46.027				

Table 32. Results of the within-subjects tests from the 2x2x2 mixed-model ANOVAs for each ROI. Power is computed using an alpha of 0.05.

ROI	Factor	Type III Sum of Squares	df	Mean Square	F	Sig. (one-tailed)	Partial Eta Squared	Observed Power
A1	Session	6.498	1	6.498	.169	.3425	.007	.068
	Session * Group	3.845	1	3.845	.100	.3775	.004	.061
	Hemisphere	457.388	1	457.388	31.631	< .001	.579	1.000
	Hemisphere * Group	.031	1	.031	.002	.4815	.000	.050
	Session * Hemisphere	7.253E-5	1	7.253E-5	.000	.4985	.000	.050
	Session * Hemisphere * Group	.002	1	.002	.000	.493	.000	.050
STG	Session	1.540	1	1.540	.052	.411	.002	.055
	Session * Group	11.472	1	11.472	.386	.27	.017	.092
	Hemisphere	270.734	1	270.734	34.566	< .001	.600	1.000
	Hemisphere * Group	.085	1	.085	.011	.459	.000	.051
	Session * Hemisphere	2.160	1	2.160	.732	.2005	.031	.130
	Session * Hemisphere * Group	7.530	1	7.530	2.551	.062	.100	.334
ACC	Session	21.120	1	21.120	.960	.1685	.040	.156
	Session * Group	11.858	1	11.858	.539	.235	.023	.108
	Hemisphere	3693.343	1	3693.34	224.74	< .001	.907	1.000
	Hemisphere * Group	5.433	1	5.433	.331	.2855	.014	.085
	Session * Hemisphere	3.208	1	3.208	.884	.1785	.037	.147
	Session * Hemisphere * Group	.965	1	.965	.266	.3055	.011	.078
MeFG	Session	3.449	1	3.449	.118	.367	.005	.063
	Session * Group	12.837	1	12.837	.440	.257	.019	.097
	Hemisphere	2289.514	1	2289.51	292.96	< .001	.927	1.000
	Hemisphere * Group	10.120	1	10.120	1.295	.1335	.053	.194
	Session * Hemisphere	1.519	1	1.519	.703	.205	.030	.127
	Session * Hemisphere * Group	1.115	1	1.115	.516	.24	.022	.106

D. Bivariate Correlation

Changes across training in behavior (session 5 minus session 1) and A1 control (session 5, run 2 minus session 1 run 1) were computed. Bivariate correlations (Table 33) were carried out in SPSS to evaluate the relationship between these changes in behavior and A1 control under the

hypothesis that those individuals with the greatest change in A1 control will have more profound changes in behavior. The change in A1 control was found to have a significant negative correlation with the change in ΔAE mean latency (Pearson's r = -0.323, p = 0.05). The change in ACS total score and CPT-X sensitivity were not significantly correlated to A1 control.

Table 33. Results of the bivariate correlation analysis.

		ACS Total Score	CPT-X Sensitivity (d')	ΔAE Mean Latency (%)
A1 control	Pearson's r	.244	.119	-.323
	Significance (one-tailed)	.110	.277	.050
	n	27	27	27

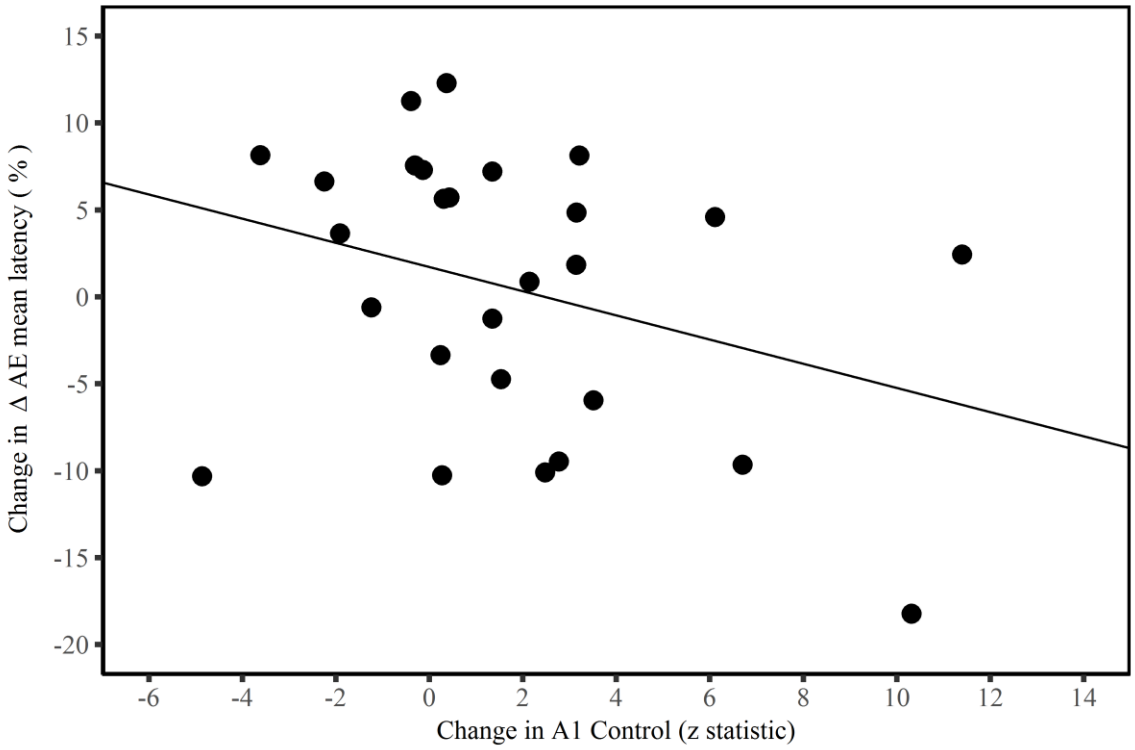

Figure 29. Bivariate correlation revealed a significant negative relationship between the change in A1 control and the change in ΔAE mean latency.

V. Discussion

The ability to induce and/or control neural plasticity holds the promise of enhancing recovery from brain injury (Johnston et al., 2011; Veit et al., 2012) and combating brain disorders and diseases (Hamilton, Glover, Hsu, Johnson, & Gotlib, 2011; Vaughan et al., 2006), as well as improving human performance in healthy subjects (deCharms et al., 2005; Haller et al., 2010; Logothetis, Pauls, Augath, Trinath, & Oeltermann, 2001; Sherwood, Kane, Weisend, & Parker, 2016). Of the techniques currently being explored, endogenous neuromodulation techniques (Mak

& Wolpaw, 2009; Smith et al., 2004; Sulzer et al., 2013) have the advantages of no known side effects and may be translated to exercises that could be performed at home without the use of sophisticated equipment and trained professionals (Caria et al., 2007; Linden et al., 2012). Real-time functional magnetic resonance imaging (Cox, Jesmanowicz, & Hyde, 1995; Weiskopf et al., 2007) has seen a dramatic rise in interest since its advent in 1995, with a large portion of research dedicated to its application for training endogenous neuromodulation. In this technique, termed closed-loop neuromodulation, the fMRI signal is measured from a specific region of the brain, processed, and presented to the subject in real-time. Through training, subjects develop self-directed mental processing techniques that regulate this signal.

The study presented in this work trained self-regulation of A1 using fMRI-NFT. The experimental group attempted self-regulation with the aid of real information regarding the current BOLD signals in A1 while the control group was supplied sham feedback yoked from a random participant in the experimental group and matched for training progress. In both groups, the bilateral A1 was identified both anatomically and functionally using an activation map produced during binaural continuous noise stimulation at each of the five training sessions. The results indicate an overall increase in the ability to volitionally decrease A1 activity across training (Figure 15), a region known to be hyperactive in chronic tinnitus. Furthermore, self-control over A1 deactivation between the first and last training session was significantly increased in the experimental group. There was also a significant increase between the first and second training session signifying a rapid effect of neurofeedback training on A1 control. These effects were not observed in the control group.

These results add to a growing body of research that demonstrates the success of fMRI-NFT in teaching individuals to self-regulate localized brain activity. A previous controlled study indicates healthy individuals can learn to control the activated cortical volume in the primary and secondary auditory cortex using fMRI-NFT (Yoo et al., 2006). A second previous study indicated that control over the magnitude of A1 activation is also achievable however not necessarily attributable to fMRI-NFT (Haller et al., 2010). The results above add to these previous studies by indicating fMRI-NFT aids control over the magnitude of A1 activation. In addition, this result shows that 60 min of distributed fMRI-NFT is adequate to train A1 self-regulation, but significant observable effects are prevalent after only 24 min of training.

Training self-regulation of brain activity from fMRI-NFT has shown promise in a broad range of applications such as the improvement of human performance (Scharnowski, Hutton, Josephs, Weiskopf, & Rees, 2012; Sherwood et al., 2016; Zhang, Yao, Zhang, Long, & Zhao, 2013) and a variety of medical applications including recovery from stroke (Chiew, LaConte, & Graham, 2012), major depression (Linden et al., 2012; Young et al., 2014), Parkinson's disease (Subramanian et al., 2011), and chronic pain (deCharms et al., 2005). However, only one previous study has investigated fMRI-NFT as a possible treatment for tinnitus (Haller et al., 2010). In this study, four 4 min closed-loop neuromodulation runs were completed in a single training session. The behavioral assessments were conducted before and after the single fMRI-NFT session. This study indicates the promise of fMRI-NFT in treating tinnitus, but they only studied six participants and did not offer a control group. Furthermore, the researchers did not perform any statistics on the behavioral data.

This research evaluated possible implications for the treatment of tinnitus by utilizing healthy participants and assessing the impact of fMRI-NFT on attentional processes. It has been suggested that auditory activity may be elevated by increased attention to the auditory system in tinnitus patients (Gu et al., 2010). The results of the work presented do not suggest an overall effect of fMRI-NFT on attentional processes. However, the improved control over auditory activity did lead to a decreased effect of emotionally-charged stimuli on attention. This suggests that when successful control over auditory activity is achieved emotional distraction can be minimized. This may be a useful coping mechanism in the tinnitus population to drive attention away from the tinnitus percept and to reduce the enhanced emotional response to auditory stimulation that has been associated with tinnitus patients (Golm et al., 2013; Wunderlich et al., 2010).

This research also evaluated neural effects of fMRI-NFT. FMRI-NFT has been associated with long-term potentiation (LTP), plastic changes occurring during associative learning, with some opinions indicating spike timing-dependent plasticity (Sulzer et al., 2013). Others have indicated LTP from synaptic plasticity resulting in enhanced synaptic efficiency (Sherwood et al., 2016). Yet another postulation suggests cellular mechanisms of learning may involve changes in voltage-dependent membrane conductance which is expressed as a change in neural excitability (Mozzachiodi & Byrne, 2010). The results presented herein identified a significant reduction in auditory activity in response to binaural continuous noise stimulation. Due to this effect being prevalent in across experimental and control groups, it may be a training effect however it is also plausible that this effect is from attempted control over auditory activity. Unfortunately, this research lacks the ability to differentiate these effects. Similarly, enhanced connectivity in the auditory network was observed across the entire participant sample within the left STG, transverse temporal gyrus, regions implicated in the processing of auditory stimuli (Upadhyay et al., 2008) and sensory mirror neurons (Cheng, Yang, Lin, Lee, & Decety, 2008; Ebisch et al., 2008). Moreover, enhanced connectivity in the DMN was found across the participant sample in the left hemisphere: BA19, precuneus, middle frontal gyrus, supramarginal gyrus, and the inferior parietal lobule; and bilaterally in the superior frontal gyrus. These regions are indicated in sustained attention (Le, Pardo, & Hu, 1998), visual mental imagery (Knauff, Mulack, Kassubek, Salih, & Greenlee, 2002; Platel et al., 1997), recollection of events (Tulving et al., 1994), and executive function (Rama et al., 2001). Despite these results, changes in resting CBF were not found. Taken together, these results suggest changes in the response to auditory stimulation and resting connectivity, but not in steady-state metabolism, which support spike timing-dependent plasticity and not changes in synaptic efficiency. These results showcase a reduction in the auditory response to noise stimulation which may be useful in the treatment of tinnitus as increase auditory activation is a common finding (Gu et al., 2010; Seydell-Greenwald et al., 2012; Smits et al., 2007), however these effects were found across both groups suggesting these effects may be generally produced by attempting control of the auditory cortex and not aided by fMRI-NFT. The efficacy of attempting control over the auditory cortex in the treatment of tinnitus may be aided by the functional reorganization apparent in both the auditory and default mode networks.

VI. Conclusion

Tinnitus can cause sever impairments and can even limit the ability to perform daily functions. The financial burden associated with tinnitus is insurmountable. For U.S. veterans alone, the

annual cost of service-connected tinnitus disability payments in 2014 was estimated at $3.9 billion while the cost of tinnitus-related healthcare services to these individuals is estimated to be much higher. The number of individuals receiving service-connected disability for tinnitus exceeded all other disorders including post-traumatic stress disorder, hearing loss, and major depression. The tinnitus percept is attributed to a central mechanism as it remains following complete dissection of the auditory nerve. Furthermore, tinnitus has been associated with hyperactivity in the auditory cortex which is theorized to cause to the tinnitus percept. Tinnitus is also associated with reduced attentional control leading to increased attention directed towards the auditory system. This is exacerbated by enhanced emotional responses to auditory stimuli. The results presented here suggest attempting control over the auditory cortex may be a possible treatment for tinnitus by decreasing the emotional response to auditory stimuli. Although fMRI-NFT aided the ability to control the auditory cortex, the findings were not limited to the group which received real neurofeedback. These findings support the transition of such a treatment outside of the MRI to possible home-based therapies which may be provided through mobile applications or simple to use device. Moreover, these findings support a possible treatment for other neurologic disorders such as chronic pain which also have reported enhanced emotional responses and abnormal attentional states.

VII. Acknowledgements

This material is based on research sponsored by the U.S. Air Force under agreement number FA8650-16-2-6702. The views expressed are those of the authors and do not reflect the official views or policy of the Department of Defense and its Components. The U.S. Government is authorized to reproduce and distribute reprints for Governmental purposes notwithstanding any copyright notation thereon. The voluntary, fully informed consent of the subjects used in this research was obtained as required by 32 CFR 219 and DODI 3216.02_AFI 40-402.

VIII. References

Alsop, D. (2006). Perfusion imaging of the brain: Contribution to clinical MRI. In R. R. Edelman, J. R. Hesselink, M. B. Zlatkin & J. V. Crues III (Eds.), *Clinical magnetic resonance imaging* (3rd ed., pp. 333-357). Philadelphia, PA: Saunders Elsevier.

American Tinnitus Association. (2015). The economic impact of tinnitus. Retrieved from https://www.ata.org/understanding-facts/impact-tinnitus

Andersson, G., & Kaldo, V. (2004). Internet-based cognitive behavioral therapy for tinnitus. *Journal of Clinical Psychology, 60*(2), 171-178. doi:10.1002/jclp.10243

Ashby, F. G. (2011). *Statistical analysis of fMRI data* MIT press.

Axelsson, A., & Ringdahl, A. (1989). Tinnitus - A study of its prevalence and characteristics. *British Journal of Audiology, 23*(1), 53-62. doi:10.3109/03005368909077819

Baguley, D. M. (2002). Mechanisms of tinnitus. *British Medical Bulletin, 63*(1), 195-212. doi:10.1093/bmb/63.1.195

Beckmann, C. F., & Smith, S. M. (2004). Probabilistic independent component analysis for functional magnetic resonance imaging. *Medical Imaging, IEEE Transactions On, 23*(2), 137-152. doi:10.1109/TMI.2003.822821

Beckmann, C. F., DeLuca, M., Devlin, J. T., & Smith, S. M. (2005). Investigations into resting-state connectivity using independent component analysis. *Philosophical Transactions of the Royal Society of London B: Biological Sciences, 360*(1457), 1001-1013. doi:10.1098/rstb.2005.1634

Biswal, B., Zerrin Yetkin, F., Haughton, V. M., & Hyde, J. S. (1995). Functional connectivity in the motor cortex of resting human brain using echo-planar mri. *Magnetic Resonance in Medicine, 34*(4), 537-541. doi:10.1002/mrm.1910340409

Buxton, R. B. (2009). *Introduction to functional magnetic resonance imaging: Principles and techniques* (2nd ed.). United Kingdom: Cambridge university press.

Caria, A., Veit, R., Sitaram, R., Lotze, M., Weiskopf, N., Grodd, W., & Birbaumer, N. (2007). Regulation of anterior insular cortex activity using real-time fMRI. *NeuroImage, 35*(3), 1238-1246. doi:10.1016/j.neuroimage.2007.01.018

Chen, W. J., Hsiao, C. K., Hsiao, L., & Hwu, H. (1998). Performance of the continuous performance test among community samples. *Schizophrenia Bulletin, 24*(1), 163-174.

Cheng, Y., Yang, C. Y., Lin, C. P., Lee, P. L., & Decety, J. (2008). The perception of pain in others suppresses somatosensory oscillations: A magnetoencephalography study. *NeuroImage, 40*(4), 1833-1840. doi:10.1016/j.neuroimage.2008.01.064 [doi]

Cherry, S. R., Sorenson, J. A., & Phelps, M. E. (2012). Chapter 3 - modes of radioactive decay. In S. R. Cherry, J. A. Sorenson & M. E. Phelps (Eds.), *Physics in nuclear medicine (fourth edition)* (pp. 19-30). Philadelphia: W.B. Saunders. doi:10.1016/B978-1-4160-5198-5.00003-4

Chiew, M., LaConte, S. M., & Graham, S. J. (2012). Investigation of fMRI neurofeedback of differential primary motor cortex activity using kinesthetic motor imagery. *NeuroImage, 61*(1), 21-31. doi:10.1016/j.neuroimage.2012.02.053

Coles, R. R. A. (1984). Epidemiology of tinnitus: (1) prevalence. *The Journal of Laryngology & Otology, 98*(Supplement S9), 7-15. doi:10.1017/S1755146300090041

Collins, D. L., Holmes, C. J., Peters, T. M., & Evans, A. C. (1995). Automatic 3-D model-based neuroanatomical segmentation. *Human Brain Mapping, 3*(3), 190-208. doi:10.1002/hbm.460030304

Cox, R. W., Jesmanowicz, A., & Hyde, J. S. (1995). Real-time functional magnetic resonance imaging. *Magnetic Resonance in Medicine, 33*(2), 230-236. doi:10.1002/mrm.1910330213

Dai, W., Garcia, D., de Bazelaire, C., & Alsop, D. C. (2008). Continuous flow-driven inversion for arterial spin labeling using pulsed radio frequency and gradient fields. *Magnetic Resonance in Medicine, 60*(6), 1488-1497. doi:10.1002/mrm.21790

Davies, J., Gander, P. E., Andrews, M., & Hall, D. A. (2014). Auditory network connectivity in tinnitus patients: A resting-state fMRI study. *International Journal of Audiology, 53*(3), 192-198. doi:10.3109/14992027.2013.846482

Davis, A., & Rafaie, E. A. (2000). Epidemiology of tinnitus. In R. S. Tyler (Ed.), *Tinnitus handbook* (pp. 1-23). San Diego: Singular Publishing Group.

de Ridder, D., de Mulder, G., Verstraeten, E., Seidman, M., Elisevich, K., Sunaert, S., . . . Moller, A. (2007). Auditory cortex stimulation for tinnitus. In D. Sakas, & B. Simpson (Eds.), (pp. 451-462) Springer Vienna. doi:10.1007/978-3-211-33081-4_52

de Ridder, D., Ryu, H., Moller, A. R., Nowe, V., Van de Heyning, & Verlooy, J. (2004). Functional anatomy of the human cochlear nerve and its role in microvascular decompressions for tinnitus. *Neurosurgery, 54*(2)

deCharms, R. C., Maeda, F., Glover, G. H., Ludlow, D., Pauly, J. M., Soneji, D., . . . Mackey, S. C. (2005). Control over brain activation and pain learned by using real-time functional MRI. *Proceedings of the National Academy of Sciences of the United States of America, 102*(51), 18626-18631. doi:10.1073/pnas.0505210102

Derryberry, D., & Reed, M. A. (2002). Anxiety-related attentional biases and their regulation by attentional control. *Journal of Abnormal Psychology, 111*(2), 225-236. doi:10.1037/0021-843X.111.2.225

Diesch, E., Andermann, M., Flor, H., & Rupp, A. (2010). Functional and structural aspects of tinnitus-related enhancement and suppression of auditory cortex activity. *NeuroImage, 50*(4), 1545-1559. doi:10.1016/j.neuroimage.2010.01.067

Ebisch, S. J., Perrucci, M. G., Ferretti, A., Del Gratta, C., Romani, G. L., & Gallese, V. (2008). The sense of touch: Embodied simulation in a visuotactile mirroring mechanism for observed animate or inanimate touch. *Journal of Cognitive Neuroscience, 20*(9), 1611-1623. doi:10.1162/jocn.2008.20111 [doi]

Eggermont, J. J., & Roberts, L. E. (2004). The neuroscience of tinnitus. *Trends in Neurosciences, 27*(11), 676-682. doi:10.1016/j.tins.2004.08.010

Fabijanska, A., Rogowski, M., Bartnik, G., & Skarzynski, H. (1999). Epidemiology of tinnitus and hyperacusis in poland. *Proceedings of the Sixth International Tinnitus Seminar*, Cambridge, UK. 569-571.

Feldmann, H. (1971). Homolateral and contralateral masking of tinnitus by noise-bands and by pure tones. *Audiology, 10*(3), 138-144. doi:10.3109/00206097109072551

Filippini, N., MacIntosh, B. J., Hough, M. G., Goodwin, G. M., Frisoni, G. B., Smith, S. M., . . . Mackay, C. E. (2009). Distinct patterns of brain activity in young carriers of the APOE-e4 allele. *Proceedings of the National Academy of Sciences, 106*(17), 7209-7214. doi:10.1073/pnas.0811879106

Folmer, R. L., Griest, S. E., & Martin, W. H. (2001). Chronic tinnitus as phantom auditory pain. *Otolaryngology -- Head and Neck Surgery, 124*(4), 394-400. doi:10.1067/mhn.2001.114673

Fowler, E. (1944). Head noises in normal and in disordered ears: Significance, measurement, differentiation and treatment. *Archives of Otolaryngology, 39*(6), 498-503.

Friston, K. J., Holmes, A. P., Poline, J., Grasby, P. J., Williams, S. C. R., Frackowiak, R. S. J., & Turner, R. (1995). Analysis of fMRI time-series revisited. *NeuroImage, 2*(1), 45-53. doi:10.1006/nimg.1995.1007

Geven, L. I., de Kleine, E., Willemsen, A. T. M., & van Dijk, P. (2014). Asymmetry in primary auditory cortex activity in tinnitus patients and controls. *Neuroscience, 256*, 117-125. doi:10.1016/j.neuroscience.2013.10.015

Giraud, A. L., Chery-Croze, S., Fischer, G., Fischer, C., Vighetto, A., Gregoire, M. C., . . . Collet, L. (1999). A selective imaging of tinnitus. *Neuroreport, 10*(1)

Golm, D., Schmidt-Samoa, C., Dechent, P., & Kröner-Herwig, B. (2013). Neural correlates of tinnitus related distress: An fMRI-study. *Hearing Research, 295*, 87-99. doi:10.1016/j.heares.2012.03.003

Green, D., & Swets, J. (1966). Signal detectability and psychophysics.

Greve, D. N., & Fischl, B. (2009). Accurate and robust brain image alignment using boundary-based registration. *NeuroImage, 48*(1), 63-72. doi:10.1016/j.neuroimage.2009.06.060

Gu, J. W., Halpin, C. F., Nam, E., Levine, R. A., & Melcher, J. R. (2010). Tinnitus, diminished sound-level tolerance, and elevated auditory activity in humans with clinically normal hearing sensitivity. *Journal of Neurophysiology, 104*(6), 3361-3370.

Guo, J. N., & Blumenfeld, H. (2014). Chapter 6 - network imaging. In C. L. F. Blumenfeld (Ed.), *Neuronal networks in brain function, CNS disorders, and therapeutics* (pp. 77-89). San Diego: Academic Press. doi:10.1016/B978-0-12-415804-7.00006-X

Haller, S., Birbaumer, N., & Veit, R. (2010). Real-time fMRI feedback training may improve chronic tinnitus. *European Radiology, 20*(3), 696-703. doi:10.1007/s00330-009-1595-z

Hamilton, J. P., Glover, G. H., Hsu, J., Johnson, R. F., & Gotlib, I. H. (2011). Modulation of subgenual anterior cingulate cortex activity with real-time neurofeedback. *Human Brain Mapping, 32*(1), 22-31. doi:10.1002/hbm.20997

Harris, C. R., & Pashler, H. (2004). Attention and the processing of emotional words and names. *Psychological Science, 15*(3), 171-178. doi:10.1111/j.0956-7976.2004.01503005.x

Hearing Center of Excellence. (2013). Hearing loss 101: Stats & figures. Retrieved from http://hearing.health.mil/HearingLoss101/StatsandFigures.aspx#foot02

Heller, A. J. (2003). Classification and epidemiology of tinnitus. *Otolaryngologic Clinics of North America, 36*(2), 239-248. doi:10.1016/S0030-6665(02)00160-3

Hendee, W. R., & Ritenour, E. R. (2002). *Medical imaging physics* (4th ed.). New York: Wiley-Liss.

Henry, J. A., Dennis, K. C., & Schechter, M. A. (2005). General review of TinnitusPrevalence, mechanisms, effects, and management. *Journal of Speech, Language, and Hearing Research, 48*(5), 1204-1235.

Huettel, S. A., Song, A. W., & McCarthy, G. (2004). *Functional magnetic resonance imaging* Sinauer Associates Sunderland, MA.

Jastreboff, P. J. (1990). Phantom auditory perception (tinnitus): Mechanisms of generation and perception. *Neuroscience Research, 8*(4), 221-254. doi:10.1016/0168-0102(90)90031-9

Jastreboff, P. J., Gray, W. C., & Gold, S. L. (1996). Neurophysiological approach to tinnitus patients. *Otology & Neurotology, 17*(2), 236-240.

Jenkinson, M., Bannister, P., Brady, M., & Smith, S. (2002). Improved optimization for the robust and accurate linear registration and motion correction of brain images. *NeuroImage, 17*(2), 825-841. doi:10.1006/nimg.2002.1132

Jenkinson, M., & Smith, S. (2001). A global optimisation method for robust affine registration of brain images. *Medical Image Analysis, 5*(2), 143-156. doi:10.1016/S1361-8415(01)00036-6

Johnston, S., Linden, D. E. J., Healy, D., Goebel, R., Habes, I., & Boehm, S. G. (2011). Upregulation of emotion areas through neurofeedback with a focus on positive mood.

Cognitive, Affective, & Behavioral Neuroscience, 11(1), 44-51. doi:10.3758/s13415-010-0010-1

Kaltenbach, J. A. (2000). Neurophysiologic mechanisms of tinnitus. *Journal of the American Academy of Audiology, 11*, 125-137.

Kandel, E. R., Schwartz, J. H., & Jessell, T. M. (1991). Part V. sensory systems of the brain: Sensation and perception. In E. R. Kandel, J. H. Schwartz & T. M. Jessell (Eds.), *Principles of neural science* (Third ed., pp. 326-328). New York: Elsevier.

Kelly, J. P. (1991). Hearing. In E. R. Kandel, J. H. Schwartz & T. M. Jessell (Eds.), *Principles of neural science* (Third ed., pp. 481-499). New York: Elsevier.

Kim, J., Kim, Y., Lee, S., Seo, J., Song, H., Cho, J. H., & Chang, Y. (2012). Alteration of functional connectivity in tinnitus brain revealed by resting-state fMRI?: A pilot study. *International Journal of Audiology, 51*(5), 413-417. doi:10.3109/14992027.2011.652677

Knauff, M., Mulack, T., Kassubek, J., Salih, H. R., & Greenlee, M. W. (2002). *Spatial imagery in deductive reasoning: A functional MRI study* doi:http://dx.doi.org/10.1016/S0926-6410(01)00116-1

Lancaster, J. L., Tordesillas-Gutiérrez, D., Martinez, M., Salinas, F., Evans, A., Zilles, K., . . . Fox, P. T. (2007). Bias between MNI and talairach coordinates analyzed using the ICBM-152 brain template. *Human Brain Mapping, 28*(11), 1194-1205. doi:10.1002/hbm.20345

Langers, D. R. M., & Melcher, J. R. (2011). Hearing without listening: Functional connectivity reveals the engagement of multiple nonauditory networks during basic sound processing. *Brain Connectivity, 1*(3), 233-244. doi:10.1089/brain.2011.0023

Langguth, B., Eichhammer, P., Kreutzer, A., Maenner, P., Marienhagen, J., Kleinjung, T., . . . Hajak, G. (2006). The impact of auditory cortex activity on characterizing and treating patients with chronic tinnitus – first results from a PET study. *Acta Oto-Laryngologica, 126*, 84-88. doi:10.1080/03655230600895317

Lanting, C. P., de Kleine, E., & van Dijk, P. (2009). Neural activity underlying tinnitus generation: Results from PET and fMRI. *Hearing Research, 255*(1–2), 1-13. doi:10.1016/j.heares.2009.06.009

Le, T. H., Pardo, J. V., & Hu, X. (1998). 4 T-fMRI study of nonspatial shifting of selective attention: Cerebellar and parietal contributions. *Journal of Neurophysiology, 79*(3), 1535-1548.

Leske, M. C. (1981). Prevalence estimates of communicative disorders in the U.S. language, hearing and vestibular disorders. *Asha, 23*(3), 229-237.

Levine, R. A., & Kiang, N. Y. S. (1995). A conversation about tinnitus. In J. A. Vernon, & A. R. Møller (Eds.), *Mechanisms of tinnitus* (pp. 149-161). Boston: Allyn and Bacon.

Linden, D. E. J., Habes, I., Johnston, S. J., Linden, S., Tatineni, R., Subramanian, L., . . . Goebel, R. (2012). Real-time self-regulation of emotion networks in patients with depression. *PLoS ONE, 7*(6), e38115.

Littow, H., Abou Elseoud, A., Haapea, M., Isohanni, M., Moilanen, I., Mankinen, K., . . . Kiviniemi, V. J. (2010). Age-related differences in functional nodes of the brain cortex - a high model order group ICA study. *Frontiers in Systems Neuroscience, 4*(32), 89-99. doi:10.3389/fnsys.2010.00032

Logothetis, N. K., Pauls, J., Augath, M., Trinath, T., & Oeltermann, A. (2001). Neurophysiological investigation of the basis of the fMRI signal. *Nature, 412*(6843), 150-157.

Lovie, P. (1986). Identifying outliers. In A. D. Lovie (Ed.), *New developments in statistics for psychology and the social sciences* (1st ed., pp. 44-69). London, UK: The British Psychological Society and Methuen.

Mak, J. N., & Wolpaw, J. R. (2009). Clinical applications of brain-computer interfaces: Current state and future prospects. *Biomedical Engineering, IEEE Reviews In, 2*, 187-199. doi:10.1109/RBME.2009.2035356

Maudoux, A., Lefebvre, P., Cabay, J., Demertzi, A., Vanhaudenhuyse, A., Laureys, S., & Soddu, A. (2012). Auditory resting-state network connectivity in tinnitus: A functional MRI study. *PLoS ONE, 7*(5), e36222.

Mazziotta, J., Toga, A., Evans, A., Fox, P., Lancaster, J., Zilles, K., . . . Mazoyer, B. (2001). A probabilistic atlas and reference system for the human brain: International consortium for brain mapping (ICBM). *Philosophical Transactions of the Royal Society of London.Series B: Biological Sciences, 356*(1412), 1293-1322. doi:10.1098/rstb.2001.0915

Melcher, J. R., Sigalovsky, I. S., Guinan, J. J., & Levine, R. A. (2000). Lateralized tinnitus studied with functional magnetic resonance imaging: Abnormal inferior colliculus activation. *Journal of Neurophysiology, 83*(2), 1058-1072.

Meyershoff, W. (1992). Tinnitus. In W. Meyershoff, & D. Ria (Eds.), *Otolaryngology head and neck surgery* (pp. 435-446). Philadelphia: WB Saunders.

Mirz, F., Brahe Pedersen, C., Ishizu, K., Johannsen, P., Ovesen, T., Stødkilde-Jørgensen, H., & Gjedde, A. (1999). Positron emission tomography of cortical centers of tinnitus. *Hearing Research, 134*(1–2), 133-144. doi:10.1016/S0378-5955(99)00075-1

Mozzachiodi, R., & Byrne, J. H. (2010). More than synaptic plasticity: Role of nonsynaptic plasticity in learning and memory. *Trends in Neurosciences, 33*(1), 17-26. doi:http://dx.doi.org.ezproxy.libraries.wright.edu/10.1016/j.tins.2009.10.001

Mühlnickel, W., Lutzenberger, W., & Flor, H. (1999). Localization of somatosensory evoked potentials in primary somatosensory cortex: A comparison between PCA and MUSIC. *Brain Topography, 11*(3), 185-191. doi:10.1023/A:1022277611252

Mühlnickel, W., Elbert, T., Taub, E., & Flor, H. (1998). Reorganization of auditory cortex in tinnitus. *Proceedings of the National Academy of Sciences, 95*(17), 10340-10343. doi:10.1073/pnas.95.17.10340

Nichols, T. E., & Holmes, A. P. (2002). Nonparametric permutation tests for functional neuroimaging: A primer with examples. *Human Brain Mapping, 15*(1), 1-25. doi:10.1002/hbm.1058

Patriat, R., Molloy, E. K., Meier, T. B., Kirk, G. R., Nair, V. A., Meyerand, M. E., . . . Birn, R. M. (2013). The effect of resting condition on resting-state fMRI reliability and consistency: A comparison between resting with eyes open, closed, and fixated. *NeuroImage, 78*, 463-473. doi:10.1016/j.neuroimage.2013.04.013

Penner, M. J. (1990). AN estimate of the prevalence of tinnitus caused by spontaneous otoacoustic emissions. *Archives of OtolaryngologyΓÇôHead & Neck Surgery, 116*(4), 418-423.

Penner, M. J., Brauth, S., & Hood, L. (1981). The temporal course of the masking of tinnitus as a basis for inferring its origin. *Journal of Speech, Language, and Hearing Research, 24*(2), 257-261.

Platel, H., Price, C., Baron, J. C., Wise, R., Lambert, J., Frackowiak, R. S., . . . Eustache, F. (1997). The structural components of music perception. A functional anatomical study. *Brain : A Journal of Neurology, 120 (Pt 2)*(Pt 2), 229-243.

Rama, P., Martinkauppi, S., Linnankoski, I., Koivisto, J., Aronen, H. J., & Carlson, S. (2001). Working memory of identification of emotional vocal expressions: An fMRI study. *NeuroImage, 13*(6 Pt 1), 1090-1101. doi:10.1006/nimg.2001.0777 [doi]

Rauschecker, J. P., Leaver, A. M., & Mühlau, M. (2010). Tuning out the noise: Limbic-auditory interactions in tinnitus. *Neuron, 66*(6), 819-826. doi:10.1016/j.neuron.2010.04.032

Richter, W., & Richter, M. (2003). The shape of the fMRI BOLD response in children and adults changes systematically with age. *NeuroImage, 20*(2), 1122-1131. doi:10.1016/S1053-8119(03)00347-1

Saliba, J., Al-Reefi, M., Carriere, J. S., Verma, N., Provencal, C., & Rappaport, J. M. (2017). Accuracy of mobile-based audiometry in the evaluation of hearing loss in quiet and noisy environments. *Otolaryngol Head Neck Surg, 156*(4), 706-711. doi:10.1177/0194599816683663

Salvi, R. J., Wang, J., & Ding, D. (2000). Auditory plasticity and hyperactivity following cochlear damage. *Hearing Research, 147*(1–2), 261-274. doi:10.1016/S0378-5955(00)00136-2

Scharnowski, F., Hutton, C., Josephs, O., Weiskopf, N., & Rees, G. (2012). Improving visual perception through neurofeedback. *The Journal of Neuroscience, 32*(49), 17830-17841. doi:10.1523/JNEUROSCI.6334-11.2012

Schecklmann, M., Landgrebe, M., Poeppl, T. B., Kreuzer, P., Männer, P., Marienhagen, J., . . . Langguth, B. (2013). Neural correlates of tinnitus duration and distress: A positron emission tomography study. *Human Brain Mapping, 34*(1), 233-240. doi:10.1002/hbm.21426

Schlee, W., Lorenz, I., Hartmann, T., Müller, N., Schulz, H., & Weisz, N. (2011). A global brain model of tinnitus. In A. Møller, B. Langguth, D. de Ridder & T. Kleinjung (Eds.), *Textbook of tinnitus* (pp. 161-169). Heidelberg: Springer.

Seydell-Greenwald, A., Leaver, A. M., Turesky, T. K., Morgan, S., Kim, H. J., & Rauschecker, J. P. (2012). Functional MRI evidence for a role of ventral prefrontal cortex in tinnitus. *Brain Research, 1485*, 22-39. doi:10.1016/j.brainres.2012.08.052

Sherwood, M. S., Kane, J. H., Weisend, M. P., & Parker, J. G. (2016). Enhanced control of dorsolateral prefrontal cortex neurophysiology with real-time functional magnetic resonance imaging (rt-fMRI) neurofeedback training and working memory practice. *NeuroImage, 124, Part A*, 214-223. doi:10.1016/j.neuroimage.2015.08.074

Shulman, G. L., Fiez, J. A., Corbetta, M., Buckner, R. L., Miezin, F. M., Raichle, M. E., & Petersen, S. E. (1997). Common blood flow changes across visual tasks: II. decreases in cerebral cortex. *Journal of Cognitive Neuroscience, 9*(5), 648-663. doi:10.1162/jocn.1997.9.5.648

Sismanis, A., & Smoker, W. R. K. (1994). Pulsatile tinnitus: Recent advances in diagnosis. *The Laryngoscope, 104*(6), 681-688. doi:10.1288/00005537-199406000-00007

Smith, S. M. (2002). Fast robust automated brain extraction. *Human Brain Mapping, 17*(3), 143-155. doi:10.1002/hbm.10062

Smith, S. M., Jenkinson, M., Woolrich, M. W., Beckmann, C. F., Behrens, T. E. J., Johansen-Berg, H., . . . Matthews, P. M. (2004). Advances in functional and structural MR image analysis and implementation as FSL. *NeuroImage, 23, Supplement 1*(0), S208-S219. doi:10.1016/j.neuroimage.2004.07.051

Smith, S. M., & Nichols, T. E. (2009). Threshold-free cluster enhancement: Addressing problems of smoothing, threshold dependence and localisation in cluster inference. *NeuroImage, 44*(1), 83-98. doi:10.1016/j.neuroimage.2008.03.061

Smits, M., Kovacs, S., de Ridder, D., Peeters, R., van Hecke, P., & Sunaert, S. (2007). Lateralization of functional magnetic resonance imaging (fMRI) activation in the auditory pathway of patients with lateralized tinnitus. *Neuroradiology, 49*(8), 669-679. doi:10.1007/s00234-007-0231-3

Sorkin, R. D. (1999). Spreadsheet signal detection. *Behavior Research Methods, Instruments, & Computers, 31*(1), 46-54. doi:10.3758/BF03207691

Subramanian, L., Hindle, J. V., Johnston, S., Roberts, M. V., Husain, M., Goebel, R., & Linden, D. (2011). Real-time functional magnetic resonance imaging neurofeedback for treatment of parkinson's disease. *The Journal of Neuroscience, 31*(45), 16309-16317. doi:10.1523/JNEUROSCI.3498-11.2011

Sulzer, J., Haller, S., Scharnowski, F., Weiskopf, N., Birbaumer, N., Blefari, M. L., . . . Sitaram, R. (2013). Real-time fMRI neurofeedback: Progress and challenges. *NeuroImage, 76*(0), 386-399. doi:10.1016/j.neuroimage.2013.03.033

Swets, J. A., & Sewall, S. T. (1963). Invariance of signal detectability over stages of practice and levels of motivation. *Journal of Experimental Psychology, 66*(2), 120-126. doi:10.1037/h0049098

Talairach, J., & Tournoux, P. (1988). *Co-planar stereotaxic atlas of the human brain*. New York: Thieme Medical Publishers.

Thompson, G. P., Sladen, D. P., Borst, B. J. H., & Still, O. L. (2015). Accuracy of a tablet audiometer for measuring behavioral hearing thresholds in a clinical population. *Otolaryngol Head Neck Surg, 153*(5), 838-842. doi:10.1177/0194599815593737

Tulving, E., Kapur, S., Markowitsch, H. J., Craik, F. I., Habib, R., & Houle, S. (1994). Neuroanatomical correlates of retrieval in episodic memory: Auditory sentence recognition. *Proceedings of the National Academy of Sciences of the United States of America, 91*(6), 2012-2015.

U.S. Centers for Disease Control. (2013). *2011-2012 national health and nutrition examination survey: Audiometry.* Unpublished manuscript.

U.S. Department of Veterans Affairs. (2014). *Annual benefits report fiscal year 2014.* Unpublished manuscript.

Upadhyay, J., Silver, A., Knaus, T. A., Lindgren, K. A., Ducros, M., Kim, D. S., & Tager-Flusberg, H. (2008). Effective and structural connectivity in the human auditory cortex. *The Journal of Neuroscience : The Official Journal of the Society for Neuroscience, 28*(13), 3341-3349. doi:10.1523/JNEUROSCI.4434-07.2008 [doi]

Vanneste, S., Plazier, M., der Loo, E. v., de Heyning, P. V., Congedo, M., & De Ridder, D. (2010). The neural correlates of tinnitus-related distress. *NeuroImage, 52*(2), 470-480. doi:10.1016/j.neuroimage.2010.04.029

Vaughan, T. M., McFarland, D. J., Schalk, G., Sarnacki, W. A., Krusienski, D. J., Sellers, E. W., & Wolpaw, J. R. (2006). The wadsworth BCI research and development program: At home with BCI. *Neural Systems and Rehabilitation Engineering, IEEE Transactions On, 14*(2), 229-233. doi:10.1109/TNSRE.2006.875577

Veer, I. M., Beckmann, C., Van Tol, M., Ferrarini, L., Milles, J., Veltman, D., . . . Rombouts, S. A. R. (2010). Whole brain resting-state analysis reveals decreased functional connectivity in major depression. *Frontiers in Systems Neuroscience, 4*(41), 1-10. doi:10.3389/fnsys.2010.00041

Veit, R., Singh, V., Sitaram, R., Caria, A., Rauss, K., & Birbaumer, N. (2012). Using real-time fMRI to learn voluntary regulation of the anterior insula in the presence of threat-related stimuli. *Social Cognitive and Affective Neuroscience, 7*(6), 623-634. doi:10.1093/scan/nsr061

Vio, M. M., & Holme, R. H. (2005). Hearing loss and tinnitus: 250 million people and a US$10 billion potential market. *Drug Discovery Today, 10*(19), 1263-1265. doi:10.1016/S1359-6446(05)03594-4

Wang, H., Tian, J., Yin, D., Jiang, S., Yang, W., Han, D., . . . Shao, M. (2001). Regional glucose metabolic increases in left auditory cortex in tinnitus patients: A preliminary study with positron emission tomography. *Chinese Medical Journal, 114*(8), 848-851.

Weiskopf, N., Sitaram, R., Josephs, O., Veit, R., Scharnowski, F., Goebel, R., . . . Mathiak, K. (2007). Real-time functional magnetic resonance imaging: Methods and applications. *Magnetic Resonance Imaging, 25*(6), 989-1003. doi:10.1016/j.mri.2007.02.007

Weissman, J. L., & Hirsch, B. E. (2000). Imaging of tinnitus: A review. *Radiology, 216*(2), 342-349. doi:10.1148/radiology.216.2.r00au45342

Woolrich, M. W., Jbabdi, S., Patenaude, B., Chappell, M., Makni, S., Behrens, T., . . . Smith, S. M. (2009). Bayesian analysis of neuroimaging data in FSL. *NeuroImage, 45*(1, Supplement 1), S173-S186. doi:10.1016/j.neuroimage.2008.10.055

World Health Organization. (2012). *WHO global estimates on prevalence of hearing loss.* Unpublished manuscript.

Wunderlich, A. P., Schönfeldt-Lecuona, C., Wolf, R. C., Dorn, K., Bachor, E., & Freund, W. (2010). Cortical activation during a pitch discrimination task in tinnitus patients and controls - an fMRI study. *Audiology and Neurotology, 15*(3), 137-148.

Yoo, S., O'Leary, H. M., Fairneny, T., Chen, N., Panych, L. P., Park, H., & Jolesz, F. A. (2006). Increasing cortical activity in auditory areas through neurofeedback functional magnetic resonance imaging. *Neuroreport, 17*(12), 1273-1278.

Young, K. D., Zotev, V., Phillips, R., Misaki, M., Yuan, H., Drevets, W. C., & Bodurka, J. (2014). Real-time fMRI neurofeedback training of amygdala activity in patients with major depressive disorder. *PLoS ONE, 9*(2), e88785.

Zhang, G., Yao, L., Zhang, H., Long, Z., & Zhao, X. (2013). Improved working memory performance through self-regulation of dorsal lateral prefrontal cortex activation using real-time fMRI. *PLoS ONE, 8*(8), e73735.

Appendix I. Telephone Screening Form

Alternative Tinnitus Management Techniques – Study #1
Telephone Screen Form

Reference ID#:_____

Thank you for calling about the study.

What I would like to do first is to ask you about 20 screening questions that all persons receiving an MRI in this study must complete. I will record the answers you give. But, to ensure your privacy, I won't record your name at this time. If you choose not to answer the questions, your decision will not impact any future health care options, these questions will strictly be used to qualify you for this study.

If you qualify for the study, I'll provide you with a reference ID number we will use to help protect your identity.

Would you like to continue with the screening questions? Yes _____ No _____
(if no, do not ask any further questions. Thank the person for his/her interest and hang up)

Inclusion criteria	
Are you between 18 and 50 years of age?	□ yes □ no
Are you right handed?	□ yes □ no
Are you able to read and write in English?	□ yes □ no
Able to lay supine for up to an hour.	□ yes □ no
Able to hold still during MRI.	□ yes □ no
Normal or corrected to normal vision.	□ yes □ no
Are you able to participate in five 2 hour training sessions over a 3 week period?	□ yes □ no
Exclusion criteria	
Do you have hearing loss above 40dB at any sound frequency?	□ yes □ no
Have you ever had complications during a MRI scan?	□ yes □ no
If so, please explain:	
Are you claustrophobic?	□ yes □ no
Do you have an aneurysm clip?	□ yes □ no
Do you have a cardiac pacemaker?	□ yes □ no
Do you have an implanted defibrillator?	□ yes □ no
Do you have an electronic implant or device?	□ yes □ no
Do you have a magnetically-activated implant?	□ yes □ no
Do you have a neurostimulator?	□ yes □ no
Do you have a bone stimulator?	□ yes □ no
Do you have hearing aids?	□ yes □ no
Do you have an implanted drug infusion device?	□ yes □ no
Do you have any type of prosthesis or implant?	□ yes □ no
Do you have an artificial or prosthetic limb?	□ yes □ no
Do you have a cochlear implant?	□ yes □ no
Do you have a bladder stimulator?	□ yes □ no
Have you had recent surgery or a GI procedure?	□ yes □ no
If so, please explain:	

Have you had an injury to the eye involving a metallic object or fragment?	□ yes □ no
If so, please explain:	
Have you ever been injured by a metallic object or foreign body (bullet, shrapnel, etc)?	□ yes □ no
If so, please explain:	
If female: Are you pregnant?	□ yes □ no

Does caller meet entry criteria for study? Yes _____ No _____

*If caller is **not** eligible:*
It appears you don't qualify to take part in this study so the information you've provided will be destroyed.
Thank them for their interest and then hang up.

*If caller **is** eligible:*
It appears you may qualify to take part in this study. Could we schedule an appointment for you?

*If caller **is** able to schedule appointment:*
(provide reference ID# to caller).
Visit Scheduled for: Date_____Time:_____

*If caller **is not** able to schedule appointment:*
Please call back to schedule an appointment. When calling back, please identify yourself as (provide reference ID#).

(Thank them for their interest and time and then hang up.)

_____ _____
Screener's signature Date

Appendix II. MRI Screening Form

Dayton Children's **NON-MRI PERSONNEL SCREENING FORM**

NAME: _____

Patient_____

Birthdate_____

Medical Record#_____

All individuals requesting to enter MRI control area (Zone III) must complete the form. It does not guarantee access to the MRI suite (Zone IV).

The following items may be harmful to you in the MR suite or may interfere with MR examination:

YES	NO	
____	____	Body Piercing
____	____	Jewelry
____	____	Tattoo/ Permanent Makeup
____	____	Nail Polish
____	____	Hairpiece/ Hair Implants / Hairclips, barrettes or pins – please remove
____	____	Hearing Aid – please remove
____	____	Cochlear Implants
____	____	Stapes Implant/ Any type of ear implant If YES, type_____
____	____	Dentures/ Removable Dental Work
____	____	Retinal Tack/ Eyelid Wire
____	____	Artificial Eye?
____	____	Metal Fragments/ Shrapnel/ Bullets
____	____	Has patient worked with metal lathe, grinder, etc.?
____	____	Has the patient ever had metal fragments removed from the eye(s)?
		If yes, how was it removed? _____
____	____	Neurostimulator Unit (Tens Unit)/ Neurocybernetic Prosthesis System (VNS)
____	____	Shunt (Programmable/ Nonprogrammable)
____	____	Halo Vest
____	____	Surgical Mesh (Location) _____
____	____	Tissue Expander (e.g., breast)
____	____	Artificial Limb or Joint (Location) _____
____	____	Bone/ Joint Pins/ Rods/ Implants
____	____	Spinal Fixation Device/ Spinal Fusion Procedure
____	____	Any Implanted items, e.g., pins, rods, screws, nails, plates, wires (Manufacturer: _____ Model# :_____)
____	____	Implanted drug pump (e.g., Insulin, Baclofen, Chemotherapy, pain medicine)
____	____	Medication pump/ Epidural Catheter
____	____	Medication Patches
____	____	IV access port (Broviac, Hickman, Infusaport)
____	____	Cardiac Pacemaker/ Defibrillator
____	____	Intravascular Coils/ Filters/ Stents If YES, Date of surgery: _____
____	____	Heart Bypass Surgery/ Valves If YES, Type: _____
____	____	Aneurysm or Artery Clip If YES, type: _____
____	____	Are you pregnant?
____	____	Breast Feeding
____	____	Intrauterine Device (IUD), Diaphragm, Pessary If YES, type: _____
____	____	Penile Prosthesis If YES, type: _____
____	____	Radiation Seeds (e.g., cancer treatment)

Signature: _____Relationship to patient: _____ Date:_____ Time: _____

Reviewed by MRI Personnel: _____ Date:_____ Time: _____

RAD9043:7/13

Appendix III. Subject Demographic Form

Alternative Tinnitus Management Techniques – Study #1
Subject Demographic Form

Subject ID# _____
Name: _____ DOB: _____
Address: _____
City: _____ State: _____ Zip: _____
Phone: _____
E-mail: _____
Primary Care Physician: _____ Phone: _____

Please list the family members or significant others, if any, we may contact ONLY IN AN EMERGENCY:

Name: _____
Relationship: _____
Phone: _____

Date of Tinnitus Diagnosis: _____
If not known, approximately when were you diagnosed with Tinnitus: _____

Current Treatment Received

Are you currently in a treatment program: _____
When did you begin this program: _____
What does this program consist of: _____
_____
_____
_____
_____

Appendix IV. Medication and Tobacco Screener

Alternative Tinnitus Management Techniques – Study #1
Medication and Tobacco Use Questionnaire

Subject ID:_____ Date:_____

Please answer the following questions as completely and honestly as you can. Do not write your name anywhere on this page.

1. Are you currently taking any medications?

☐ Yes ☐ No

If yes, please list medications.

_____
_____
_____
_____
_____
_____
_____

2. Do you now smoke cigarettes?

☐ Yes ☐ No

If yes, how many cigarettes do you smoke per day?

_____ cigarettes

3. Do you use any of these tobacco products?

☐ Pipe ☐ Snuff ☐ Chewing Tobacco ☐ Cigars

If yes, how many times per day?

_____ times per day

Appendix V. Caffeine Consumption and Sleep Form

Alternative Tinnitus Management Techniques - Study #1
Caffeine Consumption and Sleep

Subject ID:_____ Date:_____

Please answer the following questions as completely and honestly as you can. Do not write your name anywhere on this page.

1. Log all items that you consumed since waking up this morning. Pay close attention to the size (ounces) of each product. For example, if you drank 10 oz of coffe this would count for 2 servings.

	Morning Waking time – 12pm	Afternoon 12pm-Bed time
Coffee and Tea (5oz)		
Soft Drinks (12oz)		
Over the counter drugs (tablets) (NoDoz, etc.)		

2. On average how many hours of sleep do you get each night? _____

3. How many hours of sleep did you get last night? _____

Appendix VI. Field Notes

Alternative Tinnitus Management Techniques – Study #1
Field Notes

Subject ID:_____ Date:_____

1. How well did you understand the instructions and procedures?

2. How well do you think you performed in the training?

3. What mental/cognitive strategies did you use during neurofeedback training? What worked best?

4. What was your level of comfort during the procedure?

5. Additional Notes

Appendix VII. Attentional Control Scale

Instruct The purpose of this questionnaire is to assess your concentration and attention during normal activities. Please select the answer that applies to you for each statement.

Q1 It's very hard for me to concentrate on a difficult task when there are noises around.

- almost never (1)
- sometimes (2)
- often (3)
- always (4)

Q2 When I need to concentrate and solve a problem, I have trouble focusing my attention.

- almost never (1)
- sometimes (2)
- often (3)
- always (4)

Q3 When I am working hard on something, I still get distracted by events around me.

- almost never (1)
- sometimes (2)
- often (3)
- always (4)

Q4 My concentration is good even if there is music in the room around me.

- almost never (1)
- sometimes (2)
- often (3)
- always (4)

Q5 When concentrating, I can focus my attention so that I become unaware of what's going on in the room around me.

- almost never (1)
- sometimes (2)
- often (3)
- always (4)

Q6 When I am reading or studying, I am easily distracted if there are people talking in the same room.

- ❍ almost never (1)
- ❍ sometimes (2)
- ❍ often (3)
- ❍ always (4)

Q7 When trying to focus my attention on something, I have difficulty blocking out distracting thoughts.

- ❍ almost never (1)
- ❍ sometimes (2)
- ❍ often (3)
- ❍ always (4)

The purpose of this questionnaire is to assess your concentration and attention during normal activities. Please select the answer that applies to you for each statement.

Q8 I have a hard time concentrating when I'm excited about something.

- ❍ almost never (1)
- ❍ sometimes (2)
- ❍ often (3)
- ❍ always (4)

Q9 When concentrating I ignore feelings of hunger or thirst

- ❍ almost never (1)
- ❍ sometimes (2)
- ❍ often (3)
- ❍ always (4)

Q10 I can quickly switch from one task to another

- ❍ almost never (1)
- ❍ sometimes (2)
- ❍ often (3)
- ❍ always (4)

Q11 It takes me a while to get really involved in a new task.

- ❍ almost never (1)
- ❍ sometimes (2)
- ❍ often (3)
- ❍ always (4)

Q12 It is difficult for me to coordinate my attention between the listening and writing required when taking notes during lectures.

- ❍ almost never (1)
- ❍ sometimes (2)
- ❍ often (3)
- ❍ always (4)

Q13 I can become interested in a new topic very quickly when I need to.

- ❍ almost never (1)
- ❍ sometimes (2)
- ❍ often (3)
- ❍ always (4)

Q14 It is easy for me to read or write while I'm also talking on the phone.

- ❍ almost never (1)
- ❍ sometimes (2)
- ❍ often (3)
- ❍ always (4)

Q15 I have trouble carrying on two conversations at once.

- ❍ almost never (1)
- ❍ sometimes (2)
- ❍ often (3)
- ❍ always (4)

Q16 I have a hard time coming up with new ideas quickly.

- ❍ almost never (1)
- ❍ sometimes (2)
- ❍ often (3)
- ❍ always (4)

The purpose of this questionnaire is to assess your concentration and attention during normal activities. Please select the answer that applies to you for each statement.

Q17 After being interrupted or distracted, I can easily shift my attention back to what I was doing before.

- ❍ almost never (1)
- ❍ sometimes (2)
- ❍ often (3)
- ❍ always (4)

Q18 When a distracting thought comes to mind, it is easy for me to shift my attention away from it.

- ❍ almost never (1)
- ❍ sometimes (2)
- ❍ often (3)
- ❍ always (4)

Q19 It is easy for me to alternate between two different tasks.

- ❍ almost never (1)
- ❍ sometimes (2)
- ❍ often (3)
- ❍ always (4)

Q20 It is hard for me to break from one way of thinking about something and look at it from another point of view.

- ❍ almost never (1)
- ❍ sometimes (2)
- ❍ often (3)
- ❍ always (4)

Appendix VIII. Resting CBF Descriptive Statistics

	Session	Hemisphere	Group	Mean CBF (mL/100 mg/min)	Std. Deviation	N
A1	1	left	CON	56.8482	6.09332	8
			EXP	59.7967	8.51757	17
			Total	58.8532	7.82085	25
		right	CON	61.4607	7.16953	8
			EXP	64.3501	10.58058	17
			Total	63.4255	9.56645	25
	5	left	CON	56.9642	7.55288	8
			EXP	60.7701	7.83788	17
			Total	59.5522	7.80234	25
		right	CON	61.5969	7.90868	8
			EXP	65.3104	10.20988	17
			Total	64.1221	9.53221	25
STG	1	left	CON	52.4185	4.69392	8
			EXP	55.1444	8.27895	17
			Total	54.2721	7.33515	25
		right	CON	56.9118	5.80711	8
			EXP	58.3360	9.12146	17
			Total	57.8802	8.10943	25
	5	left	CON	52.8618	6.09991	8
			EXP	55.8634	6.48648	17
			Total	54.9029	6.39877	25
		right	CON	55.5483	6.62111	8
			EXP	59.6013	8.17554	17
			Total	58.3043	7.81468	25
ACC	1	left	CON	52.6145	6.47894	8
			EXP	53.9045	8.06151	17
			Total	53.4917	7.47968	25
		right	CON	39.2602	4.37010	8
			EXP	41.9706	6.13240	17
			Total	41.1033	5.68386	25
	5	left	CON	53.0349	8.42309	8
			EXP	56.2224	8.04637	17
			Total	55.2024	8.13382	25
		right	CON	39.3337	4.09576	8
			EXP	43.0995	5.69721	17
			Total	41.8945	5.45398	25
MeFG	1	left	CON	56.6536	8.11149	8
			EXP	56.3484	8.57901	17
			Total	56.4461	8.26305	25
		right	CON	45.2236	6.19257	8
			EXP	46.7350	7.70576	17
			Total	46.2514	7.16160	25
	5	left	CON	55.7931	7.79285	8
			EXP	57.4768	7.50541	17
			Total	56.9380	7.47724	25
		right	CON	45.3442	6.29771	8
			EXP	47.9390	6.49131	17
			Total	47.1087	6.41759	25